Laboratoire de Mécanique, Matériaux et Structure

Laboratory of Mechanics, Materials and Structure

ON THE WAVE TRANSMISSION IN TRANSVERSELY CONNECTED NONLINEAR PENDULUM PAIRS

Thesis submitted in partial fulfillment of the requirements for the award
of the degree of Doctor of Philosophy (PhD) in Physics,

Specialty: Fundamental Mechanics and Complex Systems

By

KAMDOUM KUITCHE Alex

Registration number : 14U2361

Master of Science in Physics

Under the supervision of

TCHAWOUA Clément

Professor

University of Yaoundé 1

©Year 2024

DEPARTEMENT DE PHYSIQUE
DEPARTMENT OF PHYSICS

ATTESTATION DE CORRECTION DE LA THESE DE DOCTORAT/Ph.D

Nous, Professeurs **NDJAKA Jean Marie Bienvenu et BODO Bertrand**, respectivement Président du jury et Examinateur de la thèse de Doctorat/Ph.D de Monsieur **KAMDOUM KUITCHE Alex** Matricule 14U2361, préparée sous la direction du Professeur **TCHAWOUA Clément**, intitulée : « **On the wave transmission in transversely connected nonlinear pendulum pairs**», soutenue le **Mercredi, 05 Juin 2024**, en vue de l'obtention du grade de Docteur/Ph.D en Physique, option **Mécanique, Matériaux et Structure**, Spécialité **Mécanique fondamentale et systèmes complexes**, attestons que toutes les corrections demandées par le Jury de soutenance ont été effectuées.

En foi de quoi, la présente attestation lui est délivrée pour servir et valoir ce que de droit.

Fait à Yaoundé le **18 JUIN 2024**

Examinateur

Pr. BODO Bertrand

Le Président du Jury
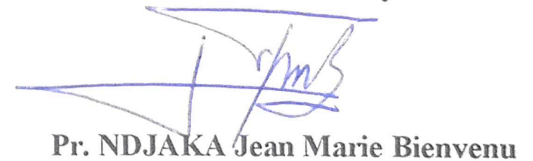
Pr. NDJAKA Jean Marie Bienvenu

Le Chef de Département de Physique

Ndjaka Jean-Marie Bienvenu
Professeur

On the wave transmission in transversely connected nonlinear pendulum pairs

Thesis Submitted in Partial Fulfillment of the

Requirements for the Degree of Doctor of Philosophy in physics

Specialty: Mechanics, materials and structure

Option: Fundamental mechanics and complex systems

Department of Physics, Faculty of Science

Presented by

KAMDOUM KUITCHE Alex

Registration Number: **14U2361**

Master degree in Physics

Under the supervision of

TCHAWOUA Clément

Professor

Contents

List of Figures

Dedications

To my lovely parents **KUITCHE** and **MAKAM Philomène**, who have never given up in the face of difficulties of life and who have been able to infuse in me the sense of perseverance and patience.

To my siblings **TESSO KUITCHE Francky, and MAWE Laura Audrey**, who have understood and accepted my absence during the years of preparation of this document.

To my great Grandmother **MABAH**, for her encouragement.

To my Grandmothers **KENGNE Régine**, and **NGANKAM Marie**, for their unconditional love, encouragement, support and prayers.

And to my late Grandfathers **KAMDOUM Michel** and **NGNECHE Maurice** who were a great support for me.

This thesis is for you...

Acknowledgements

In all humility and simplicity, this thesis would have never seen the light of day without the immense moral and intellectual support and the advice of some special people to whom I would like to express my gratitude.

- My kind gratitude to Pr. **TCHAWOUA Clément**, director of this thesis, whose vigor in work, know-how and cordiality have inspired me throughout this work. I am grateful for his multiform support, scientifically, materially and morally. Dear Professor, receive the expression of my deep and sincere gratitude and proof that your efforts have not been in vain since Master's degree up to now.

- I am exceptionally grateful to Pr. **NDJAKA Jean-Marie Bienvenu**, the Head of Department of Physics. I am very grateful for his administrative contribution and encouragement.

- I also express my gratitude to each and every member of jury who has accepted to evaluate this present work.

- I am eternally indebted to Dr. **TOGUEU MOTCHEYO Alain Bertrand** for his urging follow-up during my research studies with this other work as fruit that adds to Master's degree of few years ago. He has been as a mentor who imparted a lot of knowledge in me. My vision of the field has been deeply shaped through

our interactions. This work would not have been possible without the long hours he spent discussing with me regularly.

- I am also indebted to all the teaching staff and personnel of the Department of Physics, Faculty of Science, University of Yaoundé I, for their teachings, advice, encouragement and support since my Master's degree in this institution. A special thought to Pr. **Timoléon Crépin KOFANE**, Pr. **WOAFO Paul**, Pr. **DJUIDJE KENMOE epse ALOYEM KAZE Germaine.**

- I also owe a lot to all the teaching staff and personnel of the Department of Physics, Higher Teacher Training College, University of Bamenda, for their teachings, and support during my DIPES II diploma in that institution. I am particularly grateful to Pr. **YAMGOUE Serge Bruno** for many fruitful discussions on different aspects of nonlinear physics. I cannot forget his sense of availability and help.

- I also extend my thanks to all the teaching staff and personnel of the Department of Physics, Faculty of Science, University of Dschang, for their teachings and help during my Bachelor's degree in that institution.

- I appreciate the relentless effort of Pr. **KANAA Thomas** for his help during the preparation of different papers of this thesis.

- I also thank Pr. **Dmitry PELINOVSKY** for providing the model.

- On the other hand, I wish to express my deepest gratitude to Pr. **JUAN Archilla** and all the organizers of "Localisation in Condensed Matter" (LCM 2021) CMD 29 online series, for the opportunity given to me to present a part of this work.

- My sincere thanks go to the official editors and referees of Chaos, Solitons and Fractals, The European Physical Journal Plus, and Modern Physics Letters B for their

detailed review, constructive criticism and excellent advice during the preparation of our different publications.

- My deep gratitude is addressed to my elders in the lab Dr. **TCHINANG Joel**, Dr. **NGNINZALONG Carlos** and Dr. **NKENDJI KENKEU Enriqué** for the multiple exchanges and helps.

- My immeasurable gratitude to all my friends for their encouragement and the various supports which enhanced the realization of this thesis. A special thought to Dr. **KAMGA FOUALENG Anauld**, Dr. **NGOUNOU Armel**, Dr. **HAMADOU ALIDOU**, **FOKA Freddy, NGOU Loic, and TATSITSA Guy.**

- I am also indebted to my whole family, especially, **CHEDJOU Victor, KOLLA Roger, MAMBE Brigitte, PENKA KUITCHE Romuald, MABAH KUITCHE Larissa, KAMGANG KUITCHE Aubin, TCHINDA KUITCHE Jospin,** for their moral and financial supports and for all their prayers.

I thank the Almighty God, for all the strength and mercy he has been giving to me. These have led me into the true path toward the realization of this thesis. Thank you Lord for every inspiration I had in the course of this project.

List of abbreviations

2D: **T**wo **D**imensional

DNLSE: **D**iscrete **N**onlinear **S**chrödinger **E**quation

IM: **I**nstabilité **M**odulationnelle

MATLAB: **MAT**rix **LAB**oratory

MI: **M**odulational **I**nstability

NLS: **N**onlinear **S**chrödinger

NST: **N**onlinear **S**upra**T**ransmission

NLSE: **N**onlinear **S**chrödinger **E**quation

PDE(s): **P**artial **D**ifferential **E**quation(s)

$\mathbb{R}$: Set of **R**eal numbers

RK4: **F**ourth-Order **R**unge-**K**utta

$\mathbb{Z}$: Set of **I**ntegers

Abstract

In this Thesis, we study the dynamics of waves propagation in a dynamical system modelled by a chain of coupled pendulum pairs, where each pendulum is connected to the nearest neighbours in the longitudinal and transverse directions.

Firstly, we generate a nonlinear supratransmission phenomenon in the model. By considering the angular displacement of one chain proportional to the other, we derive the homoclinic supratransmission threshold amplitude using the two-dimensional map approach which is in agreement with the numerical one, in the case where only one chain is driven. We also consider the case where both chains are driven and perform numerically the supratransmission threshold amplitude of the two chains in the case of the same driven frequency while the phonon amplification is obtained when both lattices are driven with frequencies in different bands. The actual work extends the deep understanding of supratransmission phenomenon in discrete coupled pendulum systems.

Secondly, we investigate the MI phenomenon in the same model. Based on the obtained equation describing the dynamics of the model, we derive the coupled discrete nonlinear Schrödinger equation using the multiple scale method. We use the obtained coupled discrete nonlinear Schrödinger equation to study the possibility of modulational instability. The linear stability analysis leads us to obtain the growth rate of the MI. It reveals that the instability growth rate and MI band are dramatically affected by the transverse coupling parameter. Finally, we use the MI analysis to study the dynamics of

the generated unstable pane wave solutions numerically. This confirms that the existence of MI in the lattice leads to the break up of wave into periodic localized pulses which have the shape of soliton-like objects.

Finally, we investigate the wave propagation phenomenon in the model. Based on the obtained equation describing the dynamics of the model, we derive the linear dispersion relation which helps us to identify fast-mode as the mode on which we will be focused. Since the obtained discrete simultaneous equation has not been extensively studied in the literature, we assume that the two lines of the model are proportional to each other. We use the rotating wave approximation method to derive a NLS equation governing the propagation of waves in the network. Depending on the choice of wave number, we deduce that the system supports bright and hole soliton solutions. We use the obtained bright soliton as the initial condition for numerical computation which demonstrates the significant role of the transverse coupling parameter in the system. That is, it affects the behaviour of the forward bright soliton generated in the system. The lattice allows generated gain and loss phenomena during the propagation of the waves.

Keywords: Nonlinear supratransmission, Coupled pendulum pairs, Solitons, Rotating wave approximation, NLS equation, Multiple scale method, Modulational instability, Transverse coupling term, Coupled discrete nonlinear Schrödinger equation.

Résumé

Dans cette thèse, nous étudions la dynamique de la propagation des ondes dans un système dynamique modélisé par une chaîne de pendules couplés reliée par des ressorts de torsion, où chaque paire est accrochée sur une chaîne horizontale commune.

Tout d'abord, nous générons le phénomène de supratransmission nonlinéaire dans le modèle. En tenant compte que le déplacement angulaire d'une chaîne est proportionnel à l'autre, nous déduisons l'amplitude seuil de supratransmission homoclinique en utilisant le "2D map" qui est en accord avec les résolutions numériques; dans le cas où une seule chaîne est excitée. Nous considérons aussi le cas où les deux chaînes sont excitées et trouvons numériquement l'amplitude seuil de supratransmission des deux chaînes pour la même fréquence d'excitation tandis qu'une amplification du phonon est obtenue lorsque les deux chaînes sont excitées avec des fréquences prises dans différentes bandes. Le présent travail étend une compréhension du phénomène de supratransmission dans les systèmes couplés discrets.

Deuxièmement, nous étudions le phénomène d'instabilité modulationnelle(IM) dans le même modèle. Se servant de l'équation obtenue en décrivant la dynamique du modèle, nous déduisons une équation couplée discrète de Schrödinger nonlinéaire en utilisant la méthode des échelles à pas multiple. Nous utilisons l'équation couplée obtenue pour étudier le phénomène d'instabilité modulationnelle. L'analyse de la stabilité linéaire nous permet d'obtenir le spectre de gain de l'IM. Il révèle que le spectre de gain de l'instabilité et les

bandes de l'IM sont considérablement affectées par le paramètre de couplage transversal. Enfin, nous utilisons l'analyse de l'IM pour étudier la dynamique des solutions d'ondes planes instables générées numériquement. Ceci confirme que l'existence de l'IM dans le réseau conduit à la génération des trains d'impulsion périodiques localisés qui ont la forme d'un soliton.

Enfin, nous étudions le phénomène de propagation des ondes dans le modèle. Utilisant l'équation décrivant la dynamique du modèle, nous déduisons la relation de dispersion linéaire qui nous aide à identifier le "mode rapide" comme le mode dans lequel nous serons focalisés. Puisque le système d'équation discret obtenu n'a pas été suffisamment étudié dans la littérature, nous supposons que les deux lignes du modèle sont proportionnelles. Nous utilisons la méthode d'approximation des ondes rotatives pour déduire une équation de Schrödinger nonlinéaire qui régit la propagation des ondes dans le réseau. Selon le choix du nombre d'onde, nous déduisons que le système génère des solitons "brillants" et "sombres". Nous utilisons le soliton brillant obtenu comme condition initiale pour le calcul numérique; Ce qui démontre le rôle important du paramètre de couplage transversal dans le système. C'est-à-dire qu'il affecte le comportement du soliton brillant généré dans le système. La chaine génère un phénomène de perte et de gain au cours de la propagation des ondes.

Mots-clés: Supratransmission nonlinéaire, Paire de Pendule couplé, Solitons, Approximation d'onde rotative, Equation discrète de Schrödinger nonlinéaire, Méthode des échelles à pas multiple, Instabilité modulationnelle, Paramètre de couplage transversal, Equation couplée discrète de Schrödinger nonlinéaire.

General introduction

Within the past three decades, wave transmission in dispersive nonlinear media has become an increasingly important research field. The concept of soliton discovered by Zabusky Krustal [1] and the recurrence observation of wave propagation in the dynamics of a medium designed by Fermi-Pasta-Ulam [2] play a great role in understanding the phenomenon. The phenomenon has been studied in many dispersive discrete nonlinear media such as in nonlinear magnetic meta materials [3], in nonlinear transmission line [4], in nonlinear electrical network [5–8], in nonlinear acoustic meta material [9], in dusty plasma crystals [10, 11], in molecular chains [12]. These systems bear many interesting features whose applications extend to different aspect of life [13–15], nonlinear optics [16–19], plasma physics [20], biophysics [21]. One of the mostly used model was the chain of coupled pendulum.

Coupled pendulum models and their properties are fundamental in theoretical physics and can be used to model many interesting phenomena such as intrinsic localized modes in lattices [22, 23], solitons in Josephson junctions [24] and fluid mechanics [25–27], DNA in dynamics to crystal structure of solid states [28], among many other [29, 30]. From different point of view, the chain of coupled pendula has been studied for more than three decades. The majority of research has focused on the chains of single coupled pendula. Stabilization of solitons in coupled nonlinear pendula with simultaneous external and parametric excitations was studied numerically [31]. Numerical approximations were

employed in this paper in order to demonstrate that the use of external and parametric excitations simultaneously enables the transformation of a zero attractor soliton solution to a periodically stable one. In [32] the authors show that, the pinning of the soliton on a "long" impurity expands dramatically its stability region whereas "short" defects simply repel solitons producing effective partition in arrays of parametrically driven pendulum chains. Another example of recent studies can be found in [33–35] where existence and stability of discrete breathers have been addressed numerically.

The previous underlying studies were interesting and worth investigating. However, the authors considered in majority single coupled pendulum chains, which limit the usability of their obtained results to only one-dimensional phenomena, whereas there are many physical phenomena which cannot be properly understood within the one dimensional framework. Nevertheless, many interesting coupled ladders have been studied up to now from different points of view. For example, in continuous limit, spatial and temporal soliton [36], and breathers [37] were realized in the PT-symmetric coupler with gain in one waveguide and loss. Also, discrete solitons were generated in a PT-symmetric ladder-shaped optical array consisting of a chain of waveguides with gain coupled to a parallel chain of waveguides with loss in [38]. Moreover, a novel multicomponent discrete system which is PT-symmetric as the previous has only quite recently appeared in the literature [39–41]. In [39] coupled pendulum chains under parametric PT-symmetric driving force were studied. Here, the authors consider a chain of coupled pendulum pairs, where each pendulum is connected to the nearest neighbors in the longitudinal and transverse directions. The common strings in each pair are modulated periodically by an external force. In the limit of small coupling and near the parametric resonance, they derived a novel system of coupled PT-symmetric discrete nonlinear Schrödinger equations, which has Hamiltonian symmetry but no phase invariance. By using the conserved energy, they

found the parameter range for the linear and nonlinear stability of the zero equilibrium. Numerical experiments illustrated how the destabilization of the zero equilibrium takes place when the stability constraints are not satisfied. Compared to the works in [36, 37], the authors considered different couplings between the two pendulums in a pair and that the model is Hamiltonian but not phase invariant. This coupling describes interactions between the two pendulums connected to each other by a common horizontal string. **We have been inspired by the model proposed in [39] and this model lead us to many interesting physical phenomena.**

Moreover, at the beginning of the $21st$ century, it appeared in the literature an exotic phenomenon called nonlinear supratransmission. The pioneers of this phenomenon namely; Geniet and Leon discovered that a nonlinear system possessing a naturally forbidden bandgap can transmit the energy of a signal with a frequency lying in that forbidden band [42]. They named the process nonlinear supratransmission. The fact that the driving frequency was taken in the forbidden band was not sufficient, the process occurred at a well-defined predictable amplitude called a threshold amplitude. For more than two decades, the NST phenomenon has been studied up to now from different points of view in various physical systems, such as, in sine-Gordon chains [43–46], in Josephson junction [47, 48], in Bragg media [49], in discrete nonlinear electrical transmission lines [50–54], in the Fermi-Pasta-Ulam model [55–58], among many other [59–67]. The majority of research on this phenomenon was done on single chains or single-component systems. Even when studied on a multicomponent system, it was rarely a discrete Sine-Gordon one. For example, in [68], supratransmission phenomenon was studied in multicomponent nonintegrable nonlinear systems. Nevertheless, despite all these studies, to the best of our knowledge, no attention was paid to the gap transmission in transversely connected nonlinear pendulum pairs. **Therefore, the first purpose of this thesis is to address a way to**

generate a gap transmission in a novel multicomponent discrete system that is the chain of coupled pendulum pairs, where each pendulum is connected to the nearest neighbours in the longitudinal and transverse directions.

Also, the examination of the development of MI has been found in a horizontally shaken pendulum chain [69]. The destructive interference of MI has been studied in [70]. It is important to point out that, discrete MI attracted attention in diverse branches of physical and biological science due to its numerous applications [71–73]. In the domain of MI on discrete systems, the majority of research has been devoted to single-component systems. But, discrete MI analysis has not yet been used in the context of transversely connected nonlinear pendulum pairs. **Thus, the second goal of this thesis is to investigate analytically and numerically the discrete MI which leads to the generation of localized solitary waves in the Model.**

Additionally, up to now, the investigations that deal with the direction in which the wave envelope will evolve in the lattice have not yet shown. **Then, we lastly aim to broaden the understanding of two dimensional coupled pendulum networks as propagating media**. Specifically, we investigate the dynamics of the transverse coupling parameter in the model.

The outline of this thesis is structured as follow :

• In the first chapter, an overview on pendulum chains, supratransmission phenomenon, and MI is presented.

• The second chapter consists on the mathematical description of the network and the setting up of nonlinear equation governing the evolution of wave. we also present some numerical and analytical technics used to analyze and solve the problematic of the thesis.

• It follows with the third chapter in which we summarize the findings of this thesis through characterization of analytical results and direct simulations.

• It ends by a general conclusion which summarizes the main results obtained and gives perspectives for future investigations.

LITERATURE REVIEW

1.1 Introduction

The study of oscillatory or vibrational processes is of paramount importance in the analysis and understanding of many natural phenomena. This study has great interest in the most varied branches of physics, engineering, biology, etc. Thus, a system that can present certain natural phenomena is the chain of nonlinear pendulums. This chapter is devoted to generalities which bring out the main concepts that are encountered in our thesis. It is organized as follows: Section 1.2 deals with the overview on pendulum chains, Section 1.3 is devoted to the overview on supratransmission phenomenon, also, in Section 1.4 the generalities on MI are provided. Finally, the last section concludes this chapter.

1.2 Overview on pendulum chains

1.2.1 Pendulum: Definition and history

In physics, a pendulum is a solid body that can oscillate around a fixed point or axis and which, removed from its equilibrium position, returns to it by oscillating under the effect of a force, for example, gravity. The word pendulum given by Huygens (1629-1695) comes from the Latin "pendere", which means "to hang".

There are many types of pendulum, each having a particular interest. They have

been or are used in experiments aimed at highlighting a physical phenomenon (such as isochronism) or for metrological purposes. Thus pendulums were the first gravimeters, that is, the first physical systems capable of measuring the acceleration due to gravity g (1659). They were also used to measure time and were at the origin of the first modern clocks. There are also some famous pendulums such as Foucault's pendulum (1851), which highlighted the daily rotation of the Earth. All pendulums are subjected to the laws of mechanics. However, it is necessary to distinguish the simple pendulum, which is an ideal representation of the possible simplest pendulum, and the physical pendulum which is a more real representation.

1.2.2   Array of coupled pendulums

In the past few years, there were several studies focused on the dynamic behavior of coupled nonlinear oscillators and the most used model is the array of coupled pendulums. This model and its properties are used to investigate many physical phenomena like the propagation of solitons. The soliton is a wave that has an energy localized in space or time and that is extremely stable in the presence of disturbances. It generally moves without changing its form or its characteristics. In the field of hydrodynamics for example, tsunamis and rogue waves are well known as manifestations of solitons. Solitons are caused by an association of nonlinear and dispersive effects in the propagating medium. Coupled pendulum models are typical examples of these dispersive nonlinear media and have been studied for more than thirty years and from different points of view. In what follow, we present a model of coupled pendulums chain.

The experimental device of a chain of pendulums represented on Fig. 1.1 was carried out to experimentally analyze the propagation of a soliton. Let us consider the chain of coupled pendulums depicted in Fig. 1.2, where only pendulums numbers $n-1$, n and

$n+1$ are represented. The pendulums oscillate around a common axis and two consecutive pendulums are connected by a torsional spring.

Figure 1.1: Experimental representation of a chain of coupled pendulums [74].
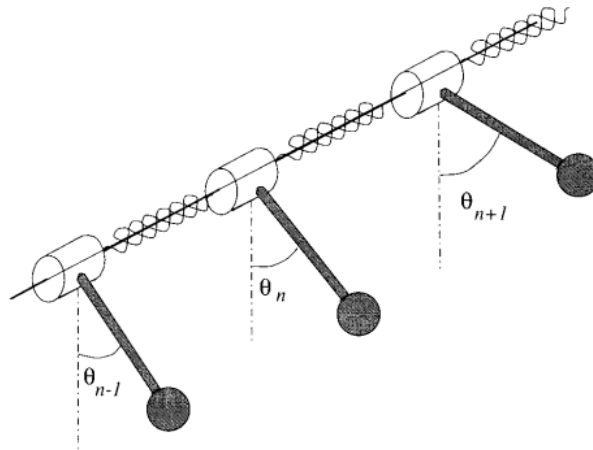
Figure 1.2: Chain of pendulums with common axis, coupled by torsional springs [75].

Note θ_n the angular deviation of the pendulum n from its equilibrium position. The Hamiltonian of the system is the sum, on all the loops of the chain, of three contributions :

$$H = \sum_{n=1}^{N} \frac{I}{2}\left(\frac{d\theta_n}{dt}\right)^2 + \frac{C}{2}(\theta_n - \theta_{n-1})^2 + mgl\left(1 - \cos\theta_n\right). \qquad (1.1)$$

In this equation, The first term corresponds to the kinetic energy of rotation of the

pendulums, where I is the moment of inertia of the pendulum with respect to the axis. The second term represents the elastic potential energy of the coupling between two neighbouring pendulums provided by the torsional springs of stiffness constant C, while the last term describes the gravitational potential energy of the pendulum. Noting l the distance to the axis of its center of gravity, m its mass and g the acceleration due to gravity.

From Halmiton's equations, the equation governing the motion of the nth pendulum is

$$\frac{d^2\theta_n}{dt^2} - \omega_1^2 \left(\theta_{n+1} + \theta_{n-1} - 2\theta_n\right) + \omega_0^2 \sin\theta_n = 0, \tag{1.2}$$

where, $\omega_1^2 = \frac{C}{I}$ and $\omega_0^2 = \frac{mgl}{I}$. The solution of the latter equation depends on the boundary conditions. For large amplitudes, Eq. 1.2 exhibits soliton solutions. These solitons can be of "Kink" type visualized in Fig. 1.3 or "Breather" type visualized in Fig. 1.4.
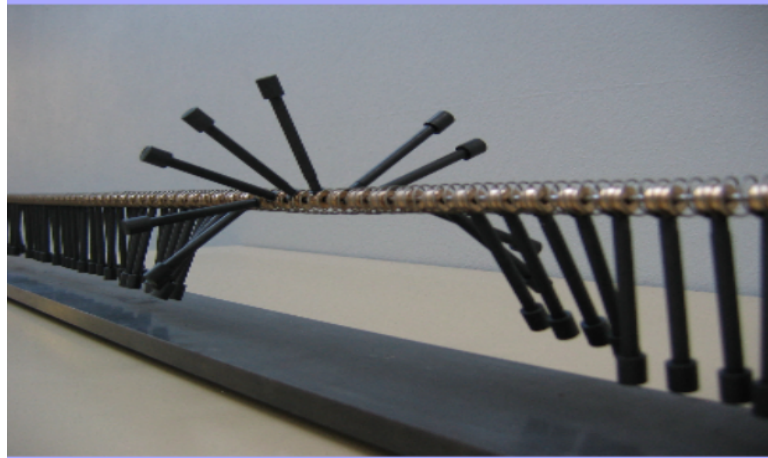
Figure 1.3: Image of a moving Kink soliton in a chain of coupled pendulums [76].

By decreasing the coupling constant C, we could observe a soliton of "Breather" type which is not very frequent.

Additionally, the chain of coupled pendulums has been studied by many seekers and seems to describe numerous interesting physical phenomena. namely;
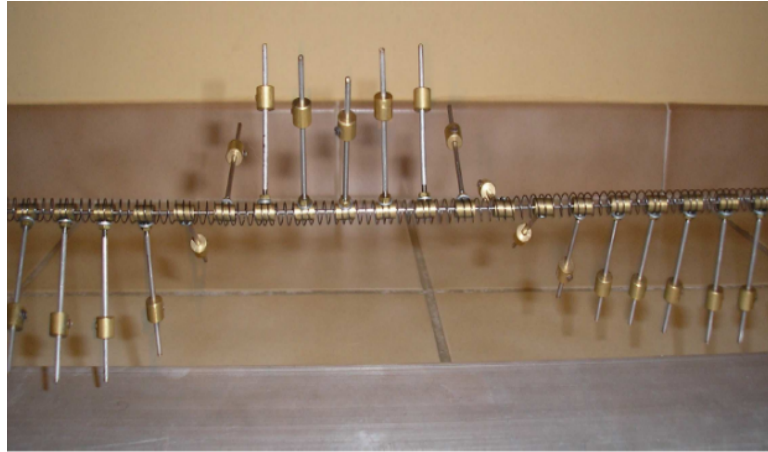
Figure 1.4: Image of a moving Breather soliton in a chain of coupled pendulums [77].

⋆ The stabilization of solitons in coupled nonlinear pendulums with simultaneous external and parametric excitations has been studied in [31] where the authors show how the existence and stability domains of solitons are modified when the coupled pendulums are simultaneously subjected to external and parametric excitations.

⋆ The notion of impurity was also tested numerically [78] on an array of 128 pendulums. The parametric excitation was studied numerically by Alexeeva et al. [32] and experimentally by Chen et al. [79]. The authors showed that "long" impurities can extend the region of stability of the system and "short" impurities are responsible of oscillatory instabilities.

⋆ Alexander et al in [69] consider theoretically the behavior of a chain of planar rigid pendulums suspended in a uniform gravitational field and subjected to a horizontal periodic driving force applied to the pendulum pivots, characterize the motion of a single pendulum, by finding bistability near the fundamental resonance and near the period-3 subharmonic resonance. they examine the development of modulational instability in a driven pendulum chain and find both a critical chain length and a critical frequency for the appearance of the instability. they study the breather solutions and show their connec-

tion to the single-pendulum dynamics and extend their analysis to consider multifrequency breathers connected to the period-3 periodic solution, showing also the possibility of stability in these breather states. And Finally they examine the problem of breather generation and demonstrate a robust scheme for generation of on-site and off-site breathers.

⋆ It has been realized in [80, 81] that the parametrically driven coupled pendula can be analytically studied by using Hamiltonian systems of the dNLS type in the presence of gains and losses. Such systems are simultaneously Hamiltonian and PT-symmetric, where the parity (P) and time-reversal (T) symmetries were used first to characterize the non-Hermitian Hamiltonians [82] and have now been widely observed in many physical experiments [83, 84].

Our purpose in this thesis is to study any additional phenomena beyond the findings presented up to now on the chains of coupled pendula pairs connected to the nearest neighbors in the longitudinal and transverse directions.

1.3 Overview on supratransmission phenomenon

The behavior of a nonlinear system excited by an external sinusoidal driving and the bifurcation of the energy transmission into the system were deeply studied by Geniet and Leon [42, 43]. The Floquet theorem [85] states that, for linear waves in a periodic structure, a forbidden gap of frequency exists. The frequency gap between acoustic and optical branches in the vibration modes of a diatomic chain well embodies this picture. Waves with frequency within this forbidden range exponentially vanish in the medium (evanescent waves). It is not the case in discrete nonlinear lattices if the amplitude exceeds a threshold value. In nonlinear systems excited by plane waves, the appearance of gap solitons [98] and the localization of energy due to nonlinear instability are matter of many

systems [87]. If the nonlinear medium, characterized by a forbidden band gap, is irradiated to one end by a sinusoidal drive, with frequency within the gap, the energy transmission can be supported. This phenomenon is called nonlinear supratransmission and is nowadays reported in several other contexts, from Bragg media (coupled mode equations in Kerr regime) [49,88], coupled-wave-guide arrays (nonlinear Schrödinger model) [89], optical waves guide arrays [60], Fermi-Pasta-Ulam model [55], Klein-Gordon (KG) electronic network [90], chains of coupled oscillators [24], discrete inductance-capacitance electrical line [51] to generic multicomponent nonintegrable nonlinear systems [68]. NLS results from an instability of the evanescent wave profile created by the driving that manifests itself above a threshold amplitude. Today this threshold has been obtained in single component systems by making use of the explicit solution of the model equation and seeking its maximum allowed amplitude at the boundary. Each of the above systems can be modelled by a nonlinear equation in which a supratransmission threshold amplitude has been obtained. In the following, we present some nonlinear equations describing a remarkable property of the nonlinear chains to sustain NST.

1.3.1   Supratransmission in sine-Gordon equation

Geniet and Leon had performed a first experimental realization of NST phenomenon by considering a model for the mechanical chain of pendula coupled by harmonic torque. In this subsection, we present a short summarized of the first result published on NST. (see Refs. [42,43] for details).

Let us consider the chain of N coupled pendulums depicted in Fig. 1.2, where only pendulums numbers $n-1$, n and $n+1$ are represented. The pendulums are quasi-identical of mass m and oscillate freely around a common axis with their engeinfrequeny ω_0. Two consecutive pendulums are connected by a torsional spring given place to the frequency

ω_1.

The equation of motion for the nth pendulum which describe the dynamics of the wave in the chain therefore takes the following form:

$$\frac{d^2\theta_n}{dt^2} - \omega_1^2\left(\theta_{n+1} + \theta_{n-1} - 2\theta_n\right) + \omega_0^2 \sin\theta_n = 0. \tag{1.3}$$

The model can be further simplified by scaling time using the natural frequency, $t \to t/\omega_0$, to reach the dimensionless form,

$$\frac{d^2\theta_n}{dt^2} - c^2\left(\theta_{n+1} + \theta_{n-1} - 2\theta_n\right) + \sin\theta_n = 0, \tag{1.4}$$

on a semi-infinite line $n > 0$ with given initial-boundary value problem, namely the data of the driving boundary $\theta_0(t)$, the initial positions $\theta_n(0)$, initial velocities $\dot{\theta}_n(0)$ and boundary condition at the chain end. When one end of the chain is sinusoidally driven with weak amplitude, the linear dispersion relation $\omega(k)$ is given by

$$\omega^2 = 1 + 2c^2(1 - \cos k). \tag{1.5}$$

This dispersion relation corresponds to a typical bandpass filter with a gap defined by 1 and a cut-off frequency $\omega_{\max}^2 = 1 + 4c^2$. The chain will be submitted to an external harmonic forcing $\theta_0(t) = A\sin\Omega t$ on a medium initially at rest. For a frequency Ω in the phonon band, quasi-linear waves are generated in the medium and, for large enough amplitude A, these waves will undergo Benjamin-Feir instability hence creating localized excitations. These nonlinear modes have a very important role in the large time asymptotic properties of a nonlinear system and are suspected to be responsible for turbulent-like behavior. Restricting the study to the case of angular frequencies in the forbidden band gap, namely $\Omega < 1$, the linear theory lead to the evanescent wave while the nonlinear one give rise to a static breather with threshold amplitude given by

$$A_{thr} = 4\arctan\left[\frac{c}{\Omega}\operatorname{arccosh}\left(1 + \frac{1 - \Omega^2}{2c^2}\right)\right]. \tag{1.6}$$

Eq. 1.6 gives the supratransmission threshold amplitude in sine-Gordon chain. The supratransmission threshold had been checked numerically by the full integration of Eq. 1.4 with the following initial boundary conditions

$$\theta_0(t) = A\sin\Omega t, \quad \theta_n(0) = 0, \quad \dot{\theta}_n(0) = A\Omega e^{-\lambda n}, \tag{1.7}$$

with $\lambda = \text{arccosh}\left(1 + \frac{1-\Omega^2}{2c^2}\right)$.

The initial velocities are those of an evanescent wave such as to partly avoid the shock wave generated by vanishing initial velocities (the same results, but time consuming, are obtained for vanishing initial velocities and a driving amplitude smoothly growing from the value 0 to A).

When the driving frequency Ω lying between the forbidden gap and the driving amplitude A is slightly beyond the threshold amplitude, NST occurs, i.e, the medium starts to transmit energy by means of nonlinear mode generation. If however, Ω lies in the forbidden gap and the driving amplitude is just less than the threshold amplitude the chain exhibits an evanescent wave. Thus, no energy flows in both chains. These results have also been obtained experimentally as depicted in Fig. 1.5.
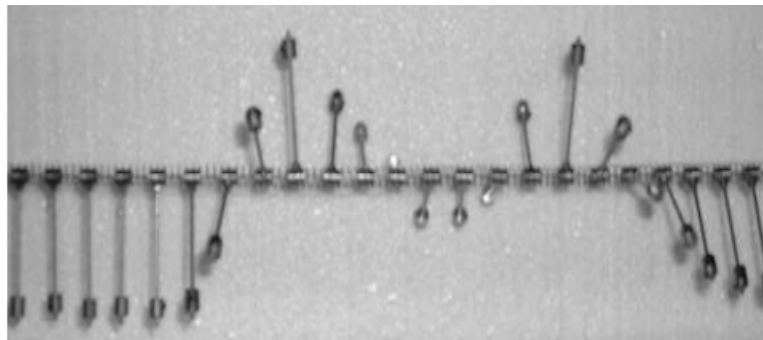
Figure 1.5: Picture of a breather generated in a mechanical pendula chain driven at one end at a frequency in the forbidden band gap [42].

The approach stems from the existence of a breather solution of the model equation,

allowing to determine the threshold amplitude. Then a fundamental question is the dependence of nonlinear supratransmission on some integrability property of the equation. To give an indication to that preoccupation, Geniet and Leon have performed numerical simulations of the nonlinear Klein-Gordon chain

1.3.2 Supratransmission in Klein-Gordon equation

The Klein-Gordon equation or sometimes Klein-Gordon-Fork equation is a relativistic wave equation, related to the Schrödinger equation. This equation was proposed in 1926 by Oskar Klein and Walter Gordon to describe the spinless relativistic electron. It was also used to describe relativistic composite particles, like pion. Geniet and Leon obtained Klein-Gordon equation by using the Taylor truncated expansion of the above sine-Gordon equation (Eq. 1.4) as follow

$$\ddot{\theta}_n - c^2 \left(\theta_{n+1} + \theta_{n-1} - 2\theta_n \right) + \theta_n - \frac{1}{3!}\theta_n^3 + \frac{1}{5!}\theta_n^5 = 0, \tag{1.8}$$

the fifth order is kept to ensure a confining potential at large θ_n. By solving this system of Klein-Gordon chain with the boundary driving of Eq. 1.7, Geniet and Leon [42] have obtained NST in the lower forbidden band gap. After these pioneer studies on NST, many authors have performed up to now the phenomenon within others equations and from different ways as in the next subsections.

1.3.3 Supratransmission in DNLS equations

DNLS equations constitute an important class of lattice models that are of great interest in their own right [91], and also find direct applications to the description of arrays of waveguides in nonlinear optics [92] where the first set of experimental realization had been done [93] using a set of parallel semiconductor waveguides made on a common

substrate [94]. It was predicted [95,96] that the DNLS equation may also serve as model of Bose-Einstein condensates (BECs) trapped in a strong optical lattice, which was confirmed by experiments [97] in photonic band gap materials [98], the mechanism of generation of gap solitons had been understood due to the result obtained on supratransmission by Geniet and Leon [42]. It was then necessary to suggest experimental setup to analyze whether or not gap transmission scenario takes place in the case of the DNLS equation and then to make predictions concerning the corresponding nonlinear process in coupled optical waveguides arrays [92].

To bring an answer to this preoccupation, Ramaz Khomeriki [60] proposed a conditions for which the optical waveguide array becomes transparent with respect to the beam injected into the single boundary waveguide if the beams intensity exceeds a certain threshold.

Also, Togueu et al [99] considered a system of waveguide arrays described by the following DNLS equation with Kerr nonlinearity

$$i\frac{db_n}{d\tau} + C\left(b_{n+1} + b_{n-1}\right) + \gamma|b_n|^2 b_n = 0 \qquad (1.9)$$

where b_n is the electromagnetic wave amplitude in the nth waveguide, C is the coupling constant, γ the nonlinear coefficient and τ is the propagation variable. To observe the nonlinear band-gap transmission, one edge of the waveguide is driven with the following boundary condition:

$$b_0 = Be^{i\Delta\tau}, \qquad (1.10)$$

where B is the amplitude of the injected beam and Δ is the angular frequency. They have shown for the first time that, supratransmission threshold can be induced by the homoclinic orbit in the DNLS equation. The obtained homoclinic thresholds was in agreement with the numerical ones even for small values of the coupling constant inducing a strongly

discrete aspect of the waveguide. This result help them to predict that, the homoclinic gap threshold can be generalized for other more complicated discrete systems which exhibit NST.

1.3.4   Supratransmission Induced by noise effect

The stochastic resonance features may undoubtedly be of great importance for information transmission in telecommunications. In order to investigate model supporting NST, Yamgoué et al. [50] were the first to generate gap transmission by using noise effect. The authors considered the electrical nonlinear lattice of Fig. 1.6, in which L_s and L_p are linear inductors while C_b is a nonlinear capacitor.
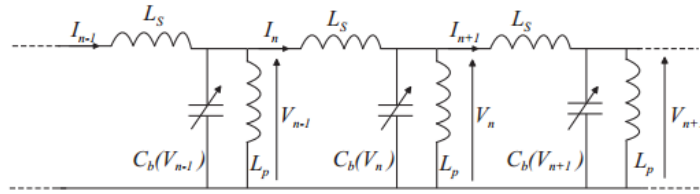
Figure 1.6: Schematic representation of the electrical line [50].

Applying Kirchhoff's laws to the array's elements at sites $n-1$, n and $n+1$; and assuming that the capacitor-voltage characteristic of the nonlinear capacitor C_b is $C_b(V_n) = C_0(1 - \alpha V_n + 3\beta V_n^2)$, one can establish that the voltage V_n is governed by the Eq. 1.11 which models a nonlinear dispersive transmission line

$$\frac{d^2V_n}{dt^2} + \omega_0^2 V_n - u_0^2(V_{n+1} + V_{n-1} - 2V_n) = \frac{d^2}{dt^2}(\alpha V_n^2 - \beta V_n^3), \qquad (1.11)$$

where $\omega_0 = (L_s C_0)^{-1/2}$, $u_0 = (L_p C_0)^{-1/2}$.

The array is driven at its left-end by

$$V_0(t) = A\cos\omega t + \eta_0(t), \qquad (1.12)$$

which corresponds to a sinusoidal signal of amplitude A and pulsation ω corrupted by an additive white noise $\eta_0(t)$. By assuming the noise as a gaussian distribution which is characterized by its root mean square amplitude, they have numerically investigated the influence of noise on the propagation in a discrete nonlinear electrical transmission line. They show that an additive noise to a periodic signal of frequency higher than the natural cutoff frequency of this system can trigger soliton generation in the medium hence NST.

Additionally, the same effect was obtained by Bodo et al. [100] in a sine-Gordon chain driven sinusoidally at one end. They show that, noise induces breather generation with a given probability depending on the noise intensity.

1.3.5   Supratransmission Induced by waves collisions

The generation of NST phenomenon has been performed for the first time in 2013 by Togueu et al. [101] by the boundary driven bi-inductance dispersive nonlinear transmission line. They numerically performed a way to produce a supratransmission phenomenon in the Salerno equation describing the dynamics of modulated waves in a discrete nonlinear transmission lattice by showing that gap transmission is possible with driven amplitude below the threshold due to the collision of different plane waves coming from both edges of the line. They considered that, one of the two plane waves has a frequency in the forbidden gap, and another has a frequency in the allowed phonon band. During collision, the wave in the allowed band was considered as a perturbation of the ones in the forbidden gap.

1.3.6   Supratransmission in Multicomponent Systems

NST has been studied from different points of view. Most of the studies on the phenomenon was focused on single-component systems. Even when studied on multicomponent systems, it was rarely a discrete one. For example, Anghel et al. generated NST in a multicomponent

nonintegrable nonlinear system models by a birefringent medium in permanent regime, namely, assuming perfect frequency matching. In this case, degenerated spatial three-wave model reduces to [102, 103]

$$i\partial_z\psi + \tfrac{\alpha}{2}\partial_x^2\psi - \delta\psi + \phi^2 = 0,$$
$$i\partial_z\phi + \tfrac{\alpha}{2}\partial_x^2\phi + \psi\phi^* = 0,$$

(1.13)

where $\phi(x,z)$ [respectively $\psi(x,z)e^{\delta z}$] is the scaled static envelope of the signal wave with frequency ω and wave number k (respectively second harmonic at frequency $\omega' = 2\omega$ and wave number k') and δ is the mismatch wave number in the propagation direction z defined by $k' = 2k - \delta$. Last, x is the transverse direction and $\alpha = 1 + \delta/k'$ by definition. The system of equation 1.13 is subject to the boundary condition

$$\psi(0,z) = Ae^{2iz}, \quad \phi(0,z) = Be^{iz},$$

(1.14)

where A and B are the driving amplitudes.

In order to generate NST, The authors develop a method based on an asymptotic solution obtained by asymptotic series expansion, which provides an accurate NST threshold prediction. As NST requires driving in the forbidden band, the linear evanescent wave is the natural keystone upon which to build the series.

Throughout, all these studies on NST have been performed on a single discrete models and continuous multicomponent systems. Up to now, no attention was paid on discrete multicomponent systems. The first question that motivated this study is: Can NST occur in a discrete multicomponent systems?

Another purpose of this thesis is to perform a way to create supratransmission in discrete multicomponent systems. that is for example in 2D sine-Gordon lattices.

1.4 Overview on MI

MI is a universal process that is inherent to most nonlinear wave systems in nature. Because of MI, small amplitude perturbations that originate from noise on top of a homogeneous wave front grow rapidly under the combined effect of non-linearity and dispersion [104,105]. In the fields of nonlinear optics and fluid dynamics, modulational instability or sideband instability is a phenomenon whereby deviations from a periodic waveform are reinforced by non-linearity, leading to the generation of spectral sidebands and the eventual breakup of the waveform into a train of pulses [104, 106, 107]. The phenomenon was first discovered and modelled for periodic surface gravity waves (Stokes waves) on deep water by T. Brooke Benjamin and Jim E. Feir, in 1967 [108]. Therefore, it is also known as the Benjamin-Feir instability. It is a possible mechanism for the generation of rogue waves [109,110]. MI only happens under certain circumstances. The most important condition is anomalous group velocity dispersion, whereby pulses with shorter wavelengths travel with higher group velocity than pulses with longer wavelength [106, 111]. There is also a threshold power, below where no instability will be seen [106]. The instability is strongly dependent on the frequency of the perturbation. At certain frequencies, a perturbation will have little effect, while at other frequencies, a perturbation will grow exponentially. Random perturbations will generally contain a broad range of frequency content, and so will cause the generation of spectral sidebands which reflect the underlying gain spectrum. The tendency of a perturbing signal to grow makes MI a form of amplification. Recent theoretical and experimental works have proven that MI can also occur with partially spatially incoherent light [112–114]. The implication of this result is that MI can appear in almost any weakly correlated nonlinear wave system. Fig. 1.7 illustrates the modulational instability phenomenon in incoherent waves.

Figure 1.7: Photograph of progressive wave trains illustrating the incoherent wave breaking into incoherent signals due to instability [79].

Moreover, it should be borne in mind that, there has been great interest in the application of MI in single coupled pendulum chains. For example, the examination of the development of MI has been found in a horizontally shaken pendulum chain [69]. Also, the destructive interference of MI has been studied in [70]. It is important to point out that, discrete MI attracted attention in diverse branches of physical and biological science due to its numerous applications [71–73]. In the domain of MI on discrete systems, the majority of research has been devoted to single-component systems. To the best of our knowledge, no attention was paid to discrete MI analysis in the transversely connected nonlinear pendulum pairs.

The last purpose of this thesis is to perform MI in a novel discrete multi-component system.

1.5   Conclusion

In this chapter, we provide in the first section the background on pendulum chains and their applications. In the second section, we point out some generalities about NST in

many models among which the coupled pendulum chains, the electrical transmission line...
And finally, we dedicate the last section to literature review of MI phenomenon. All the
concepts and dynamical systems studied in this chapter help us to define our goals which
are to perform a way to create supratransmission in 2D sine-Gordon lattices, to inves-
tigate MI phenomenon in the same model and to investigate the direction in which the
wave envelope will evolve in the lattice. In the next section, we shall present the differ-
ent analytical and numerical simulation approaches used to tackle the different purposes
stated in this chapter.

MATHEMATICAL DESCRIPTION OF THE MODEL - METHODS AND MATERIALS

2.1 Introduction

This chapter presents a brief overview on the techniques used to solve the open problems stated in chapter 1. In this chapter, we present graphically the model and the mathematical modelling. Also, the theoretical and numerical methods which can be used to achieve our goals are depicted. The chapter is closed by a conclusion.

2.2 Mathematical description of the model

We consider a chain of coupled pendulum displayed in Fig.2.1, where each pendulum is connected to the nearest neighbours in the longitudinal and transverse directions. The positive parameters C and D describe couplings between the nearest pendula in the longitudinal and transverse directions, respectively.

The Lagrangian in absence of damping for a chain of N pendula can be written as follows:

$$L = \sum_{n=1}^{N} \frac{1}{2} \left(\dot{x}_n^2 + \dot{y}_n^2 \right) + \cos(x_n) + \cos(y_n) - \frac{1}{2} C(x_{n+1} - x_n)^2 - \frac{1}{2} C(y_{n+1} - y_n)^2 - \frac{1}{2} D(x_n - y_n)^2,$$

(2.1)

where (x_n, y_n) correspond to the angles in each pair of the two pendula, dots denote
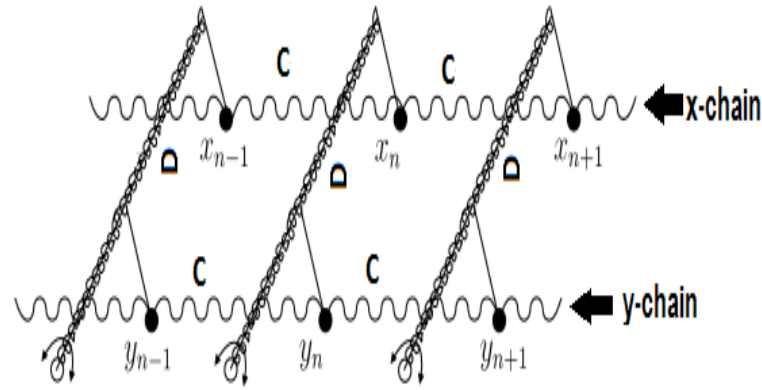
Figure 2.1: (Courtesy of Prof D. E. Pelinovsky) A graphical illustration for the chain of coupled pendula [39] where each pendulum is connected to the nearest neighbours in the longitudinal and transverse directions.

derivatives with respect to time t, $n \in \mathbb{Z}$ and $t \in \mathbb{R}$.

Using the Euler-Lagrange's equations, the equations of motion for the nth pendulum in both directions take the following form:

$$
\begin{cases}
\ddot{x}_n - C\left(x_{n+1} - 2x_n + x_{n-1}\right) - D\left(y_n - x_n\right) + \sin(x_n) = 0, \\
\\
\ddot{y}_n - C\left(y_{n+1} - 2y_n + y_{n-1}\right) - D\left(x_n - y_n\right) + \sin(y_n) = 0.
\end{cases}
\tag{2.2}
$$

Equation (2.2) is related to the energy function

$$
H\left(x_n, y_n\right) = \sum_{n=1}^{N} \tfrac{1}{2}\left(\dot{x}_n^2 + \dot{y}_n^2\right) - \cos(x_n) - \cos(y_n) + \tfrac{1}{2}C(x_{n+1} - x_n)^2 + \tfrac{1}{2}C(y_{n+1} - y_n)^2
$$
$$
+ \tfrac{1}{2}D(x_n - y_n)^2.
\tag{2.3}
$$

In order to derive the linear dispersion relation of the model which serves as a reference and provides basic information on the propagation of the plane waves, we can readily define the nth site of the lattice as a two-component vector (x_n, y_n) and seek a solution
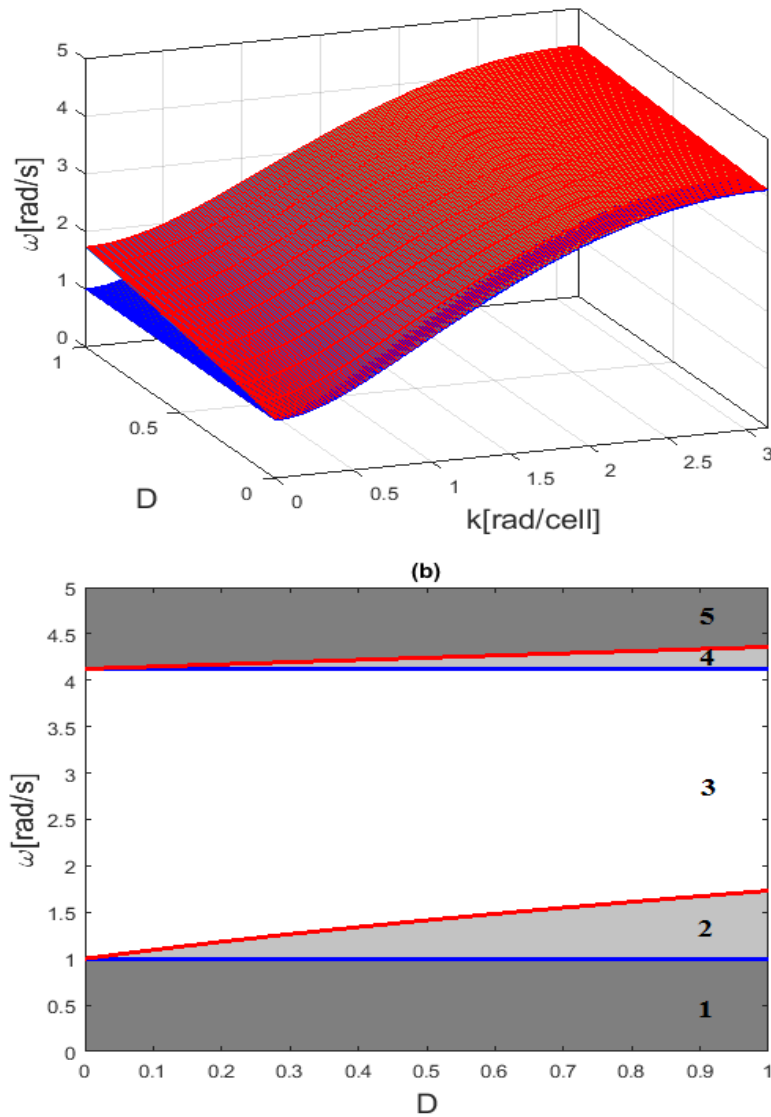
Figure 2.2: Graphs of linear dispersion relation for $C = 4$. **(a)** the red (top) curve represents the fast mode branch while the curve generated by the slow mode branch is in blue (bottom). **(b)** 2D Representation of linear dispersion relation, where we have five zones namely; (1): lower forbidden band, (2): lower "pseudo-gap", (3): allowed band, (4): upper "pseudo-gap", (5): true upper forbidden band.

in the form of plane waves:

$$(x_n, y_n) = (\gamma, \delta)\, e^{i(kn - \omega t)}, \tag{2.4}$$

with $|\gamma| \ll 1$, $|\delta| \ll 1$. ω and k are respectively the angular frequency and wave number.

Substituting Eq. (2.24) into the linearized form of Eq. (2.2), we get a linear dispersion relation of the following form:

$$\omega^4 - \left[8C\sin^2\left(\tfrac{k}{2}\right) + 2(D+1)\right]\omega^2 + \left[8C(D+1)\right]\sin^2\left(\tfrac{k}{2}\right) + 16C^2\sin^4\left(\tfrac{k}{2}\right) + (2D+1) = 0. \tag{2.5}$$

Since Eq. (2.5) is biquadratic with respect to ω, there may exist two possible modes $\omega_1(k)$ and $\omega_2(k)$ given in the following:

$$\omega_p^2 = 4C\sin^2\left(\frac{k}{2}\right) + (D+1) + (-1)^p D, \quad (p = 1, 2); \tag{2.6}$$

Fig.2.2 (a) depicts the modes $\omega_1(k)$ and $\omega_2(k)$ given by Eq. (2.6) as a function of wave number k and the transverse coupling coefficient D. One can identify the lower and upper cutoff frequencies given respectively at $k = 0$, $\omega_{0p} = \sqrt{(D+1) + (-1)^p D}$ and at $k = \pi$, $\omega_{maxp} = \sqrt{4C + (D+1) + (-1)^p D}$. Due to the linear cross-coupling, an analogy can be found with the two electrical transmission lines coupled by a linear capacitor [115–119].

Fig. 2.2 (b) depicts the variation of $\omega_{01,2}$ and $\omega_{max1,2}$ as a function of coupling in the transverse direction. In the same spirit with refs. [115, 116], we can allow our model to exhibit slow and fast mode obtained by setting $p = 1$ and $p = 2$ respectively at the cut-off frequencies. The angular frequency ω of the slow-mode is within the interval $[\omega_{01}, \omega_{max1}]$, and that of the fast-mode within the range $[\omega_{02}, \omega_{max2}]$. Both branches are separated by an upper "pseudo-gap"(zone 4) of thickness $\Delta\omega_1 = \omega_{max2} - \omega_{max1} > 0$. The slow mode branch starts at ω_{01} and that of the fast mode at ω_{02} when $k = 0$. Both branches are separated by a lower "pseudo-gap" (zone 2) of thickness $\Delta\omega_2 = \omega_{02} - \omega_{01} > 0$. Indeed,

$\Delta\omega_1$ and $\Delta\omega_2$ are not the true forbidden bands. The true forbidden bands correspond to zone 1 (true lower forbidden band) and zone 5 (true upper forbidden band) of Fig. 2.2 (b). Observing Fig. 2.2 (b), one can observe in zones 2 and 4 that, when D increases (decreases), the width of the "pseudo-gaps" increases (decreases); the width of the allowed band (zone 3) decreases (increases) as the coupling between the nearest pendula in the transverse direction D increases (decreases).
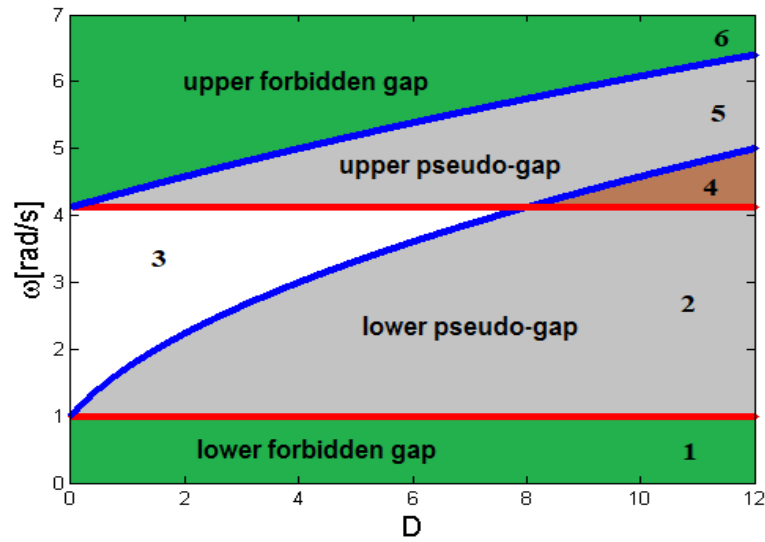
Figure 2.3: Linear dispersion law curve for $C = 4$. Blue lines represent the cut-off frequencies of the fast-mode and the red ones represent the cut-off frequencies of the slow-mode.

Also, For values of k taken in the first Brillouin zone, Fig. 2.3 represents the evolution of the angular frequency for the two directions and for different values of transverse coupling. At $D = 2C$, the intersection between the upper pseudo-gap and the lower pseudo-gap or the intersection between the lower forbidden gap of the fast-mode and the upper forbidden gap of the slow-mode starts (zone 4). In Fig. 2.3, it is seen that, the bandwidth of the allowed angular frequencies (zone 3) decreases as the coupling D between the nearest pendula in the transverse direction increases. This means that, the

linear coupling parameter D contributes to increase the network effects on the wave during its motion.

2.3 The discrete nonlinear Schrödinger model and solutions

To the best of our knowledge, no analytical solution of Eq. (2.2) has been reported, due to its discrete aspect. To overcome this situation, we will firstly expand $\sin(x_n)$ and $\sin(y_n)$ in Taylor series up to the third order, and assuming $y_n = \lambda x_n$ for some real number λ. Then, Eq. (2.2) turn to

$$
\begin{cases}
\ddot{x}_n - C\left(x_{n+1} - 2x_n + x_{n-1}\right) - D\left(\lambda - 1\right)x_n + x_n - \frac{1}{6}x_n^3 = 0, \\
\\
\lambda\ddot{x}_n - \lambda C\left(x_{n+1} - 2x_n + x_{n-1}\right) - D\left(1 - \lambda\right)x_n + \lambda x_n - \lambda^3\frac{1}{6}x_n^3 = 0.
\end{cases}
\tag{2.7}
$$

The above two equalities are equivalent if and only if λ fulfill $\lambda\left(\lambda - 1\right) = \left(1 - \lambda\right)$ and $\lambda^2 = 1$, which has solutions $\lambda = \pm 1$. When $\lambda = 1$, the two lines are in phase i.e the system reduces to an uncoupled one or to a single chain as the Klein-Gordon chain found in [42]: this correspond to the slow-mode. In the case where $\lambda = -1$, the two lines becomes coupled : This correspond to the fast-mode. In the following, we are going to be focused on the case where $\lambda = -1$ such as to take into account the transverse coupling parameter. Thus, Eq. (2.7) lead to a single discrete equation given by

$$
\ddot{x}_n - C\left(x_{n+1} - 2x_n + x_{n-1}\right) + \omega_g^2 x_n - \beta x_n^3 = 0,
\tag{2.8}
$$

where $\omega_g^2 = 2D + 1$ and $\beta = \frac{1}{6}$.

In order to derive the linear dispersion relation of Eq. (2.8), we can seek for a solution

in the form of plane waves

$$x_n = A_0 e^{i(kn - \omega t)} + c.c., \tag{2.9}$$

where c.c. stands for complex conjugate, ω and k are respectively the angular frequency and wave number. Substituting Eq. (2.9) into linearized form of Eq. (2.8), we get a linear dispersion relation of the following form

$$\omega^2 = \omega_g^2 + 4C \sin^2\left(\frac{k}{2}\right). \tag{2.10}$$

The obtained dispersion relation of Eq. (2.10) corresponds to the fast mode of the one of Eq. (2.6) which admits the same lower cutoff frequency at $k = 0$ ($\omega_{\min} = \omega_g$) and the same upper cutoff frequency at $k = \pi$ ($\omega_{\max} = \sqrt{\omega_g^2 + 4C}$). Hence, Eq. (2.8) will be used to investigate wave propagation.
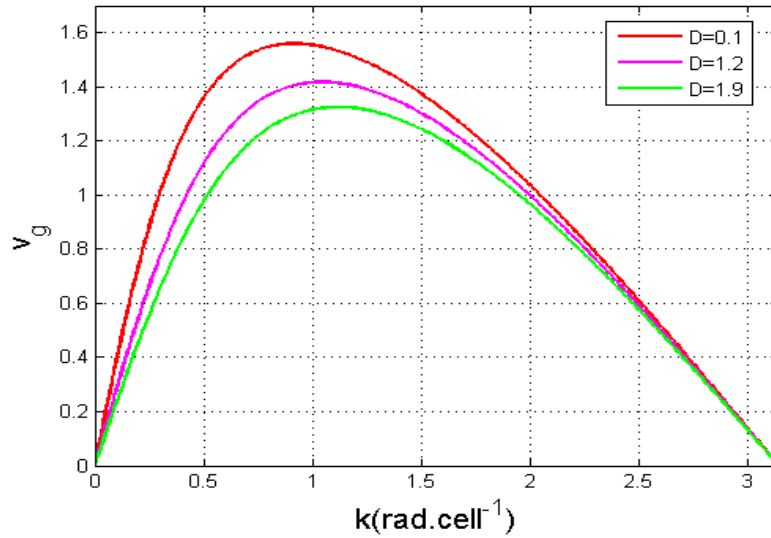
Figure 2.4: Curve of group velocity relation

The group velocity relation associated with the wave packet is defined by

$$V_g = \frac{d\omega}{dk} = \frac{C}{\omega} \sin(k) \tag{2.11}$$

The graphical representation of Eq. (2.10) shows the increase in the frequency when the wave number increases. This involves the positive values of the group velocity given by

Eq. (2.11) in the first Brillouin zone [see Fig. 2.4] which shows the variation of group velocity in terms of wave number for some fixed values of transverse coupling parameters. The group velocity decreases when the transverse coupling parameter D increases. So, this transverse coupling parameter can be used to control the magnitude of generated waves.

The mathematical model of Eq. 2.8 is less straightforward to tackle directly. For this reason, we are going to use the rotating wave approximation to derive the nonlinear Schrödinger equation describing the motion of modulated waves in the network of Fig. 2.1. This approximation allows us to consider the solution of Eq. 2.8 in the form

$$x_n = \varepsilon \left[\psi \left(X, \tau \right) \exp \left(-i\theta_n \right) + \psi^* \left(X, \tau \right) \exp \left(i\theta_n \right) \right], \tag{2.12}$$

in which the asterisk denotes complex conjugation, $\theta_n = \omega t - kn$ is the rapidly varying phase, ε is a positive small parameter $(0 < \varepsilon \leq 1)$, ψ is an unknown (continuous) slowly varying envelope function depending on the slow scale $X = \varepsilon \left(n - v_g t \right)$, and $\tau = \varepsilon^2 t$. In the following, we are going to use this expansion

$$x_{n \pm 1} = \varepsilon \left(\psi \pm \varepsilon \frac{\partial \psi}{\partial X} + \varepsilon^2 \frac{\partial^2 \psi}{\partial X^2} \right) \exp \left(\pm ik \right) \exp \left(-i\theta_n \right) + c.c, \tag{2.13}$$

where c.c. stands for the complex conjugate.

Inserting Eqs. (2.12) and (2.13) into Eq. (2.8) yield to different equations as power series of ε. Firstly, by keeping the terms proportional to $\varepsilon \exp \left(-i\theta_n \right)$ and $\varepsilon^2 \exp \left(-i\theta_n \right)$, we obtain respectively, the dispersion relation and group velocity related to the fast-mode studied above. Finally, by keeping the terms proportional to $\varepsilon^3 \exp(-i\theta_n)$, we obtain the following one-dimensional nonlinear Schrodinger evolution equation for $\psi \left(X, \tau \right)$

$$i \frac{\partial \psi}{\partial \tau} + P \frac{\partial^2 \psi}{\partial X^2} + Q|\psi|^2 \psi = 0, \tag{2.14}$$

with the dispersion coefficient (P) and nonlinear coefficient (Q) defined by

$$P = \frac{C \cos k - V_g^2}{2\omega}, \tag{2.15}$$

$$Q = \frac{1}{4\omega}. \tag{2.16}$$

Actually, we focus our attention on the analytical computation of the exact representation
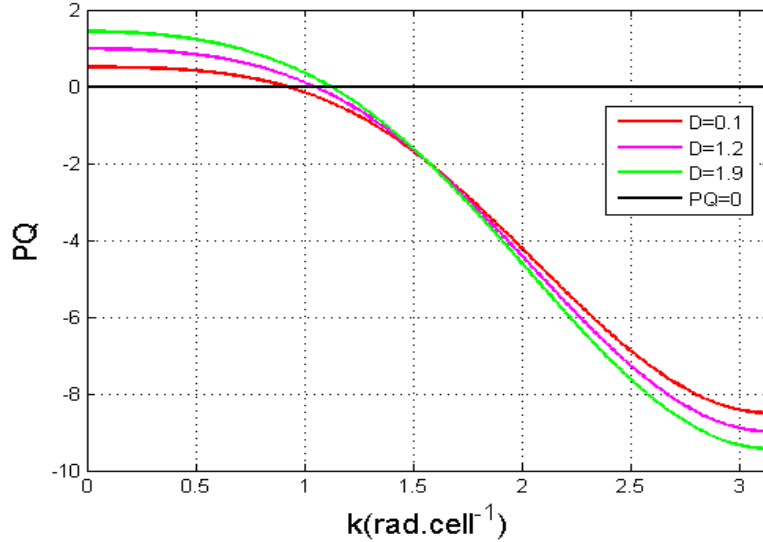
Figure 2.5: Dependence of the product PQ in term of the wave number and for $D = 0.1$, $D = 1.2$, and $D = 1.9$

of the solution of Eq. (2.14). In fact, it is well known in [120] that NLS equation supports different types of solution depending on the sign of the product of the nonlinear coefficient Q and the the linear dispersion coefficient P. That is, if $PQ > 0$, the NLS equation admits a bright soliton solutions, whereas for $PQ < 0$, it supports a dark or hole soliton solutions. Fig. 2.5 depicts the dependence of the product of dispersive and nonlinear coefficients in term of the wave number for some fixed values of transverse coupling parameter D. It appears that, in the first Brillouin zone, the increase of D leads to the expansion of the width of wave numbers for which bright soliton prevails and to the reduction of the one for which dark solitons occur. Merely, the increase of the transverse coupling parameter

extend the domain of existence of bright solitons. In the following, we will be focused on the case where $PQ > 0$ i.e on the bright soliton solutions of Eq. (2.14). This solution is given as in $[3, 10, 120]$ by

$$\psi\left(X, \tau\right) = \gamma sech\left[\rho\left(X - V\tau\right)\right] \exp i\left(KX - \Omega\tau\right). \tag{2.17}$$

Based on the above equation, the expression of the solution of Eq. (2.8) can be easily written as

$$x_n \simeq x_0 sech\left[\varepsilon\rho\left(n - v_g t\right)\right] \cos\left(kn - \Omega_0 t\right), \tag{2.18}$$

in which $\rho = \gamma\sqrt{\left|\frac{Q}{2P}\right|}$, $\Omega = \frac{K^2 - \rho^2}{2}$, $x_0 = 2\varepsilon\rho\sqrt{\left|\frac{2P}{Q}\right|}$, and $\Omega_0 = \omega + 2\varepsilon^2\Omega P$. Equation (2.18) is a modulated bright pulse signal solution of the network Eq. (2.8) whose characteristic parameters, namely the amplitude, the velocity, the inverse width and the frequency are x_0, V, ρ and Ω_0.

The bright soliton solution of Eq. (2.8) will be used in the next chapter in section 3.4 as initial condition for the full numerical integration of Eq. (2.2) to investigate the behavior of the solitary wave during its propagation while moving from one line to another.

2.4   Two dimensional map (A map approach)

Due to the high discrete aspect of Eq. (2.2), it will be difficult to obtain an analytical threshold of the model. It is why we are going to use Eq. (2.8) which is identical to a one-dimensional lattice modelling a simple mass and spring chain where the time periodic solution can be obtained by assuming the harmonic solution $x_n = u_n cos(\omega t)$ (see Refs. $[121, 122]$). Inserting the latest harmonic solution into Eq. 2.8, and by keeping the terms proportional to $\cos\left(\omega t\right)$, we obtain a steady state equation in the form :

$$\alpha u_n + C\left(u_{n+1} - 2u_n + u_{n-1}\right) + \beta u_n^3 = 0, \tag{2.19}$$

with $\alpha = \omega^2 - 2D - 1$ and $\beta = \frac{1}{8}$.

Following the way developed in Refs. [99, 121–130] the two dimensional map corresponding to the previous steady state equation can be written as

$$u_{n+1} = \left(2 - \frac{\alpha}{C}\right) u_n - \frac{\beta}{C} u_n^3 - v_n, \qquad v_{n+1} = u_n. \tag{2.20}$$

In order to confirm whether the driving frequency will be taken in the lower forbidden band as aforementioned at the beginning of this section, we are going to study the fixed points of the 2D map (Eq. (2.20)). To do so, we consider that, $u_{n+1} = u_{n-1} = u_n = v_{n+1} = v_n = u$. Then, Eq. (2.20) leads to

$$u_0 = 0 \quad \text{and} \quad u_\pm = \pm\sqrt{8\left(2D + 1 - \omega^2\right)}. \tag{2.21}$$

$u_\pm$ exists if and only if $2D + 1 - \omega^2 > 0$ that is, for $\omega < \sqrt{2D + 1}$. This confirms the fact that, the lower forbidden band of Fig.2.3 is the zone where gap transmission takes place. Thus, we are going to be focused on the true lower forbidden band (zone 1 Fig. 2.3 (b)).

2.5   The coupled discrete nonlinear Schrödinger model

In order to study the possibility of MI in coupled pendulum chains, we use the multiple scales method on Eq. (2.2) to derive the coupled discrete nonlinear Schrödinger (dNLS) equation using the algorithm in [31]. For that purpose, we make the following assumption, where $\omega_0 \approx 1$ and ε is a small fixed parameter:

$$\omega \approx \omega_0 \left(1 - \frac{\varepsilon^2}{2}\right), \omega^2 \approx \omega_0^2 \left(1 - \varepsilon^2\right), C \approx \varepsilon^2 c, \text{ and } D \approx \varepsilon^2 d.$$

By expanding $\sin(x_n)$ and $\sin(y_n)$ in Taylor series up to the third order, Eq. (2.2) can be written as:

$$\begin{cases} \ddot{x}_n - C(x_{n+1} - 2x_n + x_{n-1}) - D(y_n - x_n) + x_n - \frac{1}{6}x_n^3 = 0 \\ \\ \ddot{y}_n - C(y_{n+1} - 2y_n + y_{n-1}) - D(x_n - y_n) + y_n - \frac{1}{6}y_n^3 = 0. \end{cases} \qquad (2.22)$$

The angular displacements of the nth resonator in the two directions can be expressed as:

$$x_n(T) = 2\varepsilon \left[\psi_n(T)e^{-i\omega t} + \bar{\psi}_n(T)e^{i\omega t} \right], \qquad (2.23)$$

$$y_n(T) = 2\varepsilon \left[\phi_n(T)e^{-i\omega t} + \bar{\phi}_n(T)e^{i\omega t} \right], \qquad (2.24)$$

where $T = \frac{\varepsilon^2}{2}t$ and, ψ_n and ϕ_n are unknown complex functions. Therefore, substituting Eqs. (2.23) and (2.24) into Eq. (2.22), keeping the terms proportional to $e^{-i\omega t}$ and ε^3, and by choosing $\tau = \omega_0 T$, Eq. (2.22) becomes:

$$\begin{cases} i\frac{\partial \psi_n}{\partial \tau} - \psi_n + c(\psi_{n+1} - 2\psi_n + \psi_{n-1}) + d(\phi_n - \psi_n) + 2|\psi_n|^2\psi_n = 0 \\ \\ i\frac{\partial \phi_n}{\partial \tau} - \phi_n + c(\phi_{n+1} - 2\phi_n + \phi_{n-1}) + d(\psi_n - \phi_n) + 2|\phi_n|^2\phi_n = 0. \end{cases} \qquad (2.25)$$

For $d = 0$, Eq. (2.25) reduces to a single discrete nonlinear Schrodinger equation obtained in [31] with neither excitations ($f = 0$ and $h = 0$) nor damping($\gamma = 0$). Therefore, the system of Eq. (2.25) becomes equivalent to an uncoupled system of dNLS equations, which have many applications in physics, including nonlinear optics. For $d \neq 0$, Eq. (2.25) can be considered as the coupled discrete nonlinear Schrödinger equation with neither excitations nor damping. In the optics context, the system describes two arrays of optical waveguides with Kerr nonlinearity and nearest-neighbor interactions [131]. The d term realizes a cross-phase linear coupling between the two arrays of optical waveguides. Here,

we have shown that, the coupled pendulum pairs can be described by a coupled discrete nonlinear Schrödinger equation from which we will study the possibility of modulational instability in the next section.

2.6 Discrete MI analysis

The MI phenomenon is considered as one of the first steps leading to the localization of energy in a nonlinear network [132]. It is a means of producing intrinsic localized modes in the system through the modulation of a plane wave. This phenomenon is based on the linearization of a disturbing wave of very low amplitude compared to the initial plane wave and it is revealed in a system when certain specific conditions are reached or respected. The process of creating these localized structures will be detailed in this section. In order to determine the conditions of the instability or stability of the plane wave, we will investigate the evolution of a small perturbation that could affect the plane wave.

2.6.1 Linear instability

To proceed further, let the following exact plane-wave solution of Eqs. (2.26) and (2.27) be the solutions of Eq. (2.25). That is

$$\psi_n = \lambda_0 e^{i(qn-\omega\tau)}, \tag{2.26}$$

$$\phi_n = \mu_0 e^{i(qn-\omega\tau)}, \tag{2.27}$$

where q is the wave number, ω the angular frequency, λ_0 and μ_0 are respectively the constant amplitudes of the vibrational angular displacements ψ_n and ϕ_n. Substituting Eqs. (2.26) and (2.27) into Eq. (2.25), we arrive to this relation

$$\begin{cases} \omega - 1 + c(2\cos(q) - 2) + d(\frac{\mu_0}{\lambda_0} - 1) + 2|\lambda_0|^2 = 0 \\ \omega - 1 + c(2\cos(q) - 2) + d(\frac{\lambda_0}{\mu_0} - 1) + 2|\mu_0|^2 = 0. \end{cases} \tag{2.28}$$

The two equations of Eq. (2.28) are compatible if $d(\frac{\mu_0}{\lambda_0} - 1) + 2|\lambda_0|^2 = d(\frac{\lambda_0}{\mu_0} - 1) + 2|\mu_0|^2$.

By considering both λ_0 and μ_0 to be reals, one get a relation between the two amplitudes λ_0 and μ_0 as follows:

$$\mu_0 = \frac{d}{2\lambda_0}. \tag{2.29}$$

Thus, the nonlinear dispersion relation of the mode corresponding to the coupled chains is given as :

$$\omega = 1 + d - c(2\cos(q) - 2) - 2(\lambda_0{}^2 + \mu_0{}^2). \tag{2.30}$$

2.6.2 Modulational instablity gain

MI is a mechanism from where soliton can form during confrontation between nonlinear and dispersions term. We employed the plane waves with small perturbations as follows:

$$\psi_n = (\lambda_0 + \lambda_n(\tau))e^{i(qn - \omega\tau)}, \tag{2.31}$$

$$\phi_n = (\mu_0 + \mu_n(\tau))e^{i(qn - \omega\tau)}. \tag{2.32}$$

Substituting Eqs. (2.31) and (2.32) into Eq. (2.25), making use of the dispersion relations of Eq. (2.30), and after some mathematical computations, we obtain the following linearized set of coupled discrete differential equations for the perturbations λ_n and μ_n:

$$\begin{cases} i\frac{\partial \lambda_n}{\partial \tau} + ce^{iq}\lambda_{n+1} + ce^{-iq}\lambda_{n-1} + 2\lambda_0^2(\lambda_n + \lambda_n^*) + d\mu_n - (2c\cos(q) + 2\mu_0^2)\lambda_n = 0 \\ i\frac{\partial \mu_n}{\partial \tau} + ce^{iq}\mu_{n+1} + ce^{-iq}\mu_{n-1} + 2\mu_0^2(\mu_n + \mu_n^*) + d\lambda_n - (2c\cos(q) + 2\lambda_0^2)\mu_n = 0 \end{cases}, \tag{2.33}$$

where * denotes complex conjugate. Furthermore, the above simultaneous equation admits solutions of the form

$$\lambda_n = \alpha_1 \cos(Qn - \Omega\tau) + i\alpha_2 \sin(Qn - \Omega\tau), \tag{2.34}$$

$$\mu_n = \beta_1 \cos(Qn - \Omega\tau) + i\beta_2 \sin(Qn - \Omega\tau), \tag{2.35}$$

where Q and Ω are respectively the wave number of the perturbation and the corresponding propagation frequency of the modulation. Substituting Eqs. (2.34) and (2.35), into the coupled set, Eq. (2.33) yields a pair of coupled equations that can be written in matrix form as follows:

$$\begin{pmatrix} 4\lambda_0^2 + D_1 & \Omega - D_2 & d & 0 \\ \Omega - D_2 & D_1 & 0 & d \\ d & 0 & 4\mu_0^2 + D_3 & \Omega - D_2 \\ 0 & d & \Omega - D_2 & D_3 \end{pmatrix} \begin{pmatrix} \alpha_1 \\ \alpha_2 \\ \beta_1 \\ \beta_2 \end{pmatrix} = \begin{pmatrix} 0 \\ 0 \\ 0 \\ 0 \end{pmatrix}, \tag{2.36}$$

where,

$$D_1 = 2c\cos(Q)\cos(q) - \rho,$$
$$D_2 = 2c\sin(Q)\sin(q),$$
$$D_3 = 2c\cos(Q)\cos(q) - \sigma, \tag{2.37}$$
$$\sigma = 2c\cos(q) + 2\lambda_0^2,$$
$$\rho = 2c\cos(q) + 2\mu_0^2.$$

The solutions of the system of Eq. (2.36) are non-trivial. Given that the determinant of 4×4 matrix is zero, then, we obtain the dispersion relations given by :

$$\Omega_\pm^+ = D_2 \pm \tfrac{1}{2}\sqrt{\chi_1 + 2\sqrt{16\chi_2 + 8\chi_3 + \chi_4}},$$
$$\Omega_\pm^- = D_2 \pm \tfrac{1}{2}\sqrt{\chi_1 - 2\sqrt{16\chi_2 + 8\chi_3 + \chi_4}}, \tag{2.38}$$

with

$$\chi_1 = 8\,D_1\lambda_0{}^2 + 8\,D_3\mu_0{}^2 + 4\,d^2 + 2\,D_1{}^2 + 2\,D_3{}^2,$$

$$\chi_2 = 4\,d^2\mu_0{}^2\lambda_0{}^2 + D_1{}^2\lambda_0{}^4 - 2\,D_1 D_3\mu_0{}^2\lambda_0{}^2 + D_3{}^2\mu_0{}^4 + d^2 D_1\mu_0{}^2 + d^2 D_1\lambda_0{}^2,$$

$$\chi_3 = 2\,d^2 D_3\mu_0{}^2 + 2\,d^2 D_3\lambda_0{}^2 + D_1{}^3\lambda_0{}^2 - D_1{}^2 D_3\mu_0{}^2 - D_1 D_3{}^2\lambda_0{}^2 + D_3{}^3\mu_0{}^2,$$

$$\chi_4 = 4\,d^2 D_1{}^2 + 8\,d^2 D_1 D_3 + 4\,d^2 D_3{}^2 + D_1{}^4 - 2\,D_1{}^2 D_3{}^2 + D_3{}^4. \tag{2.39}$$

The dispersion relation of Eq. (2.38) determines the condition for stability of the plane waves with the wave number q in the network. However, our interest is the complex solutions of Ω. To have such result, $\chi_1 + 2\sqrt{16\chi_2 + 8\chi_3 + \chi_4}$ or $\chi_1 - 2\sqrt{16\chi_2 + 8\chi_3 + \chi_4}$ should be less than zero. MI occurs when wave number possesses a non zero imaginary part leading to an exponential growth of the perturbed amplitudes $\lambda_n(\tau)$ and $\mu_n(\tau)$ which set off the generation of localized modes in the transversly coupled chains. Therefore, the MI gain is the imaginary part of the propagation frequency of the modulation. It is calculated using the formula

$$G(Q) = |\text{Im}(\Omega)|. \tag{2.40}$$

2.7   Numerical methods

Numerical solution of ordinary differential equations is the most important technique in continuous time dynamics. Since most ordinary differential equations are not soluble analytically, numerical integration is the only way to obtain information about the trajectory. Many different methods have been proposed and used in an attempt to solve accurately various types of ordinary differential equations. However there are a handful of methods known and used universally namely; Runge-Kutta, Adams-Bashforth and Backward Differentiation Formula methods. All these methods discretize the differential system to produce a discrete system of equation or map. The methods obtain different maps from

the same differential equation, but they have the same aim; that the dynamics of the map should correspond closely to the dynamics of the differential equation. In this work, we use the Runge-Kutta algorithm.

The fourth order Runge-Kutta is a much more locally accurate method. Let us suppose that we have an equation of the form

$$\frac{dU}{dt} = f(t, U), \tag{2.41}$$

with initial condition with initial condition $U(t_0) = U_0$. Then if we know U^n and set $t = (n-1)h$, the value of U^{n+1} is given by the sequence of operations

$$U^{n+1} = U^n + \frac{1}{6}(L_1 + 2L_2 + 2L_3 + L_4), \tag{2.42}$$

where L_1, L_2, L_3 and L_4 are the coefficients of the fourth order Runge-Kutta given by the system below

$$\begin{cases} L_1 = h\,f(t, U^n) \\ L_2 = h\,f(t + \frac{h}{2}, U^n + \frac{L_1}{2}) \\ L_3 = h\,f(t + \frac{h}{2}, U^n + \frac{L_2}{2}) \\ L_4 = h\,f(t + h, U^n + L_3), \end{cases} \tag{2.43}$$

where h is the normalized integration time step. This method is very widely favored as:

- It is easy to use and no equations need to be solved at each stage;

- It is highly accurate for moderate h values;

- It is a one step method i.e. U^{n+1} only depends on U^n;

- It is easy to start and easy to code.

In the special case when $f(t, U) = f(t)$, we have

$$U(t) = \int_{t_0}^{t} f(t)dt + U_0, \tag{2.44}$$

and the task of evaluating this integral accurately is called quadrature. To solve any differential equation with the fourth order Runge-Kutta algorithm, we need to put it into the standard form given by Eq. 2.41.

Today, this method is not a secrecy for anybody such that certain software as Matlab implemented it as solver. In order to approximate solutions of the time dependent 2D discrete equation 2.2 describing the dynamics of our model, we can also use directly ODE45 solver of MATLAB which is the combination of 4th and 5th Runge-Kutta method.

2.8 Hardware and software

As machine support during this thesis work, we used a Laptop computer running Windows 10 Pro operating system and two major softwares: Matlab for data analysis and Maple for integral calculus.

2.9 Conclusion

This chapter is devoted to the presentation of analytical and numerical methods used to model the chain of coupled pendulum pairs, where each pendulum is connected to the nearest neighbours in the longitudinal and transverse directions. Using all these methods and materials, we are now able to follow this study and obtain different results that will help us to achieve our goals. The results are presented in chapter 3.

3.1 Introduction

This chapter presents the main results obtained in this thesis using both analytical and numerical methods presented in chapter II. It is subdivided into three parts, dealing with the nonlinear gap transmission in transversely connected nonlinear pendulum pairs, the wave propagation in transversely connected nonlinear pendulum pairs, and the MI in transversely connected nonlinear pendulum pairs.

3.2 Nonlinear gap transmission in transversely connected nonlinear pendulum pairs

Nonlinear gap transmission also known as nonlinear supratransmisssion is a phenomenon whereby a nonlinear system possessing a natural forbidden bandgap can transmit the energy of a signal with a frequency belonging in that band. The process occurs at a well defined predictable threshold amplitude. Therefore, its finding is fundamental. Here, we are going to use the 2D map approach to determine the aforementioned threshold amplitude before generating a nonlinear supratransmission phenomenon.

Generally, on the chain of longitudinally coupled pendula, the nonlinear supratransmission phenomenon appears in the lower forbidden band [42]. In the similar way, the

zones under consideration will be zones 1 of Fig. 2.3 (b) which has been confirmed in section 2.4. When the angular frequency is lying in zone 2, it is within the forbidden band of the fast mode and the allowed phonon band of the slow one while in zone 1, it is the forbidden band of both modes. Can the angular frequency with a value taken in the forbidden bands produce nonlinear bandgap transmission in our model? The answer to this question will be found in sections 3.2.1 and 3.2.2. Before, it is worth noting that the transverse and longitudinal coupled chains studied do not have two wave vectors as the two dimensional lattice [133].

3.2.1   Supratransmission threshold

The homoclinic tangle progression of the 2D map (Eq. (2.20)) while varying the dispersion coefficient C and transverse coupling D is displayed in Fig. 3.1 for $\omega = 0.8$ belonging to the true lower forbidden band. The details of the construction can be found in Ref. [127]. The dispersion coefficient increases from left to right in the first line of the Fig 3.1 while the transverse coupling D is constant: The homoclinic intersections start with the much richer structure to one homoclinic solution which can be associated with the continuous solution.

The transverse coupling D increases from left to right in the second line of the Fig 3.1 while the dispersion coefficient C is constant: we can observe the inverse effect of the first line. The richer structure of homoclinic connection increases with a constant transverse coupling. It had been demonstrated in ref. [99] that the case of the rich homoclinic connection corresponds to the case where the frequency is far from the cutoff frequency while one homoclinic solution corresponds to the frequency close to the cutoff frequency. However, in the supratransmission phenomenon, good transmission is ensured when the frequency is close to the cutoff frequency. To be in agreement with this fact, we consider
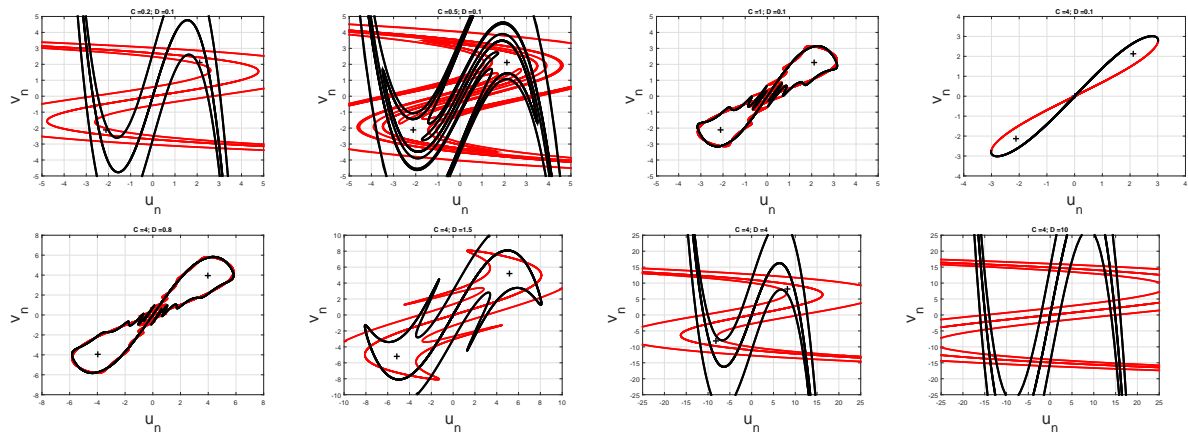
Figure 3.1: (First line) Homoclinic tangle progression of the 2D map Eq. (2.20) as a function of dispersion coefficient C for D=0.1 and $\omega = 0.8$: the dispersion coefficient increases from left to right; (Second line) Homoclinic tangle progression of the 2D map Eq. (2.20) as a function of transverse coupling D for C=4 and $\omega = 0.8$: the transverse coupling increases from left to right.
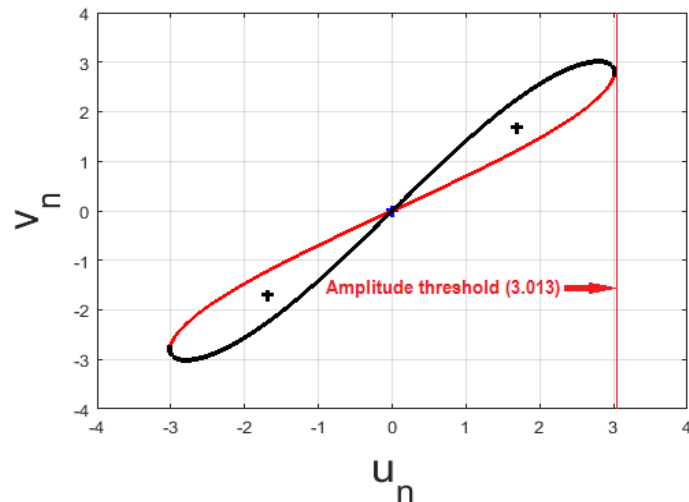
Figure 3.2: Homoclinic connection of the 2D map Eq. (2.20) for $D = 0.1$, $C = 4$, and $\omega = 0.8$. Red line corresponds to the supratransmission threshold amplitude.

the main homoclinic connection of the 2D map (2.20) for $D = 0.1$, and $C = 4$ as depicted in Fig. 3.2. In a similar way as in Ref. [99], we obtain the homoclinic supratransmission threshold amplitude equal to 3.013 (red line of Fig. 3.2).

In the next section 3.2.2, the obtained threshold will be verified by numerical simulations.

3.2.2 Numerical experiments

In this section, numerical studies are carried out on the discrete coupled pendulum pairs of Fig. 2.1 by integrating Eq. (2.2) with a small transverse coupling parameter $D = 0.1$ and longitudinal coupling parameter $C = 4$. The chains will be submitted to the following boundary driving conditions:

$$x_0(t) = A\cos(\omega_1 t) \qquad \text{and} \qquad y_0(t) = B\cos(\omega_2 t), \tag{3.1}$$

where $A(B)$ and $\omega_1(\omega_2)$ are respectively the driving amplitude of the $x-chain(y-chain)$ and the driving frequency of the chains. The external driving amplitudes A and B are gradually given from zero to their maximum values so as to avoid initial shock. In the followings, we will be considered three cases :

- Only one chain is driven. The driving conditions (3.1) become :

$$x_0(t) = A\cos(\omega_1 t) \qquad \text{and} \qquad y_0(t) = 0. \tag{3.2}$$

When the driving frequency belongs to the allowed band, a small driving amplitude ($A = 0.0001$) will produce an energy flow in both chains as illustrated in Fig. 3.3. One can see in the same figure the transfer of intensity from $x-chain$ to $y-chain$.
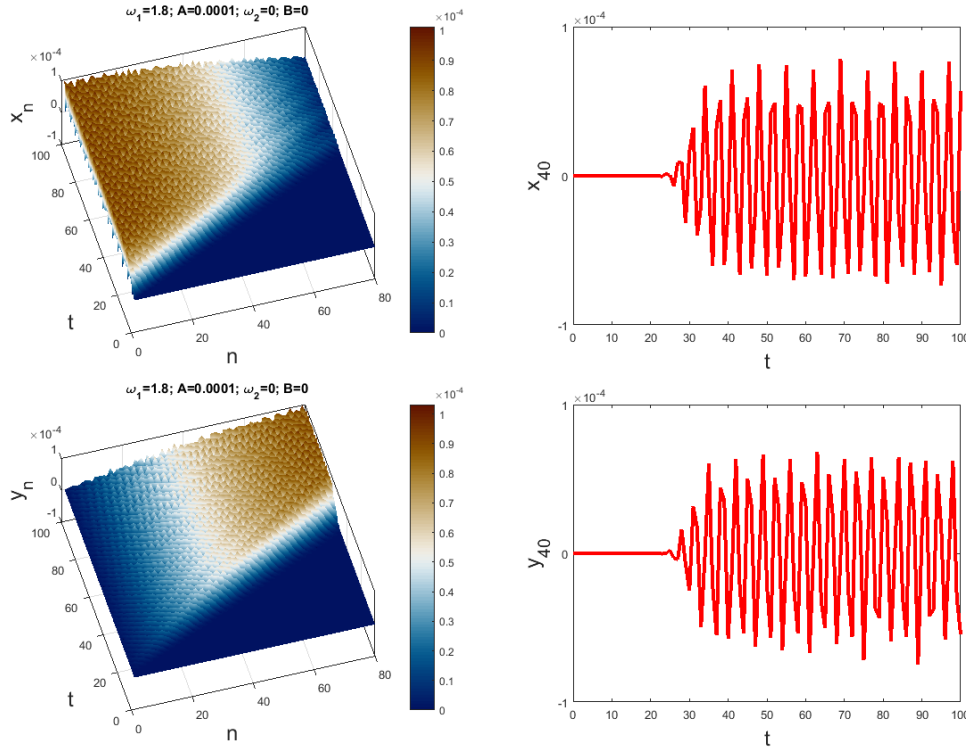
Figure 3.3: Graphs showing the evolution of the coupled chain with respect to time for the driving angular frequencies of the two chains $\omega = 1.8$ and the driving amplitude $A = 0.0001$. The first line corresponds to the behavior of $x - chain$ and the second line corresponds to the behavior of $y - chain$. One can see the intensity transmits to remote sites in the both chains

The threshold amplitude obtained from the homoclinic connection of the two-dimensional (2D) map (2.20) (see Fig. 3.2) is $A_{th} = 3.013$ for the driven frequency $\omega = 0.8$ lying in the true lower forbidden band. In order to validate this homoclinic supratransmission threshold, we consider two values of A around the value of A_{th} that is one slightly below and another slightly above and we get the following observations namely; When the amplitude is just less than 3.013 that is $A = 3.012$ each chain exhibits an evanescent wave as represented in Fig. 3.4. Thus, no energy flows in both chains. When the amplitude is slightly beyond the homoclinic threshold amplitude

of $x - chain$ that is $A = 3.014$, an energy suddenly flows in $x - chain$ and energy

even if it is small is transmitted in the form of a wave in $y - chain$ (see the bottom

panel of Fig. 3.5). Then, both chains generate soliton solutions as displayed in Figs.

3.5.
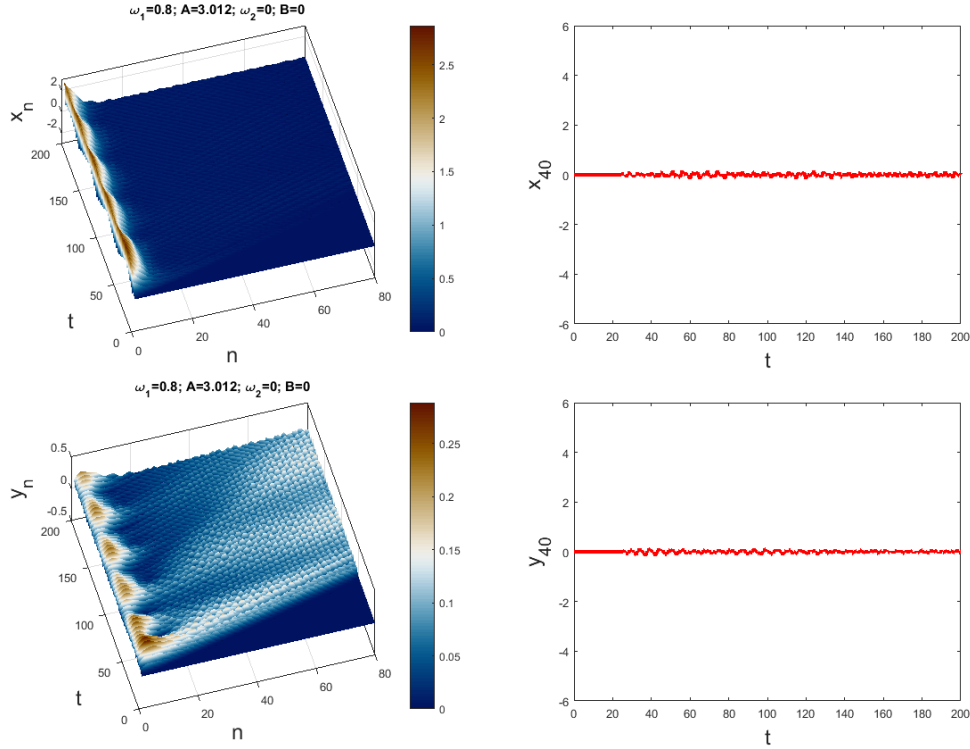
Figure 3.4: Graphs showing the evolution of the coupled chain with respect to time for

the driving angular frequencies of the two chains $\omega = 0.8$ and the driving amplitude

slightly below the threshold $A = 3.012 < A_{th}$. The up panel corresponds to the behavior

of $x - chain$ and the down panel corresponds to the behavior of $y - chain$.

- The two chains are driven at the origin. The driven boundary conditions are given

  by Eq. (3.1) with A and B different to zero. For this case, the numerical threshold

  amplitude for each chain becomes smaller than the above homoclinic threshold am-

  plitude. Due to the difficulty to obtain a common analytical threshold amplitude

  for each chain, we find it numerically and get it for both chains and for the same
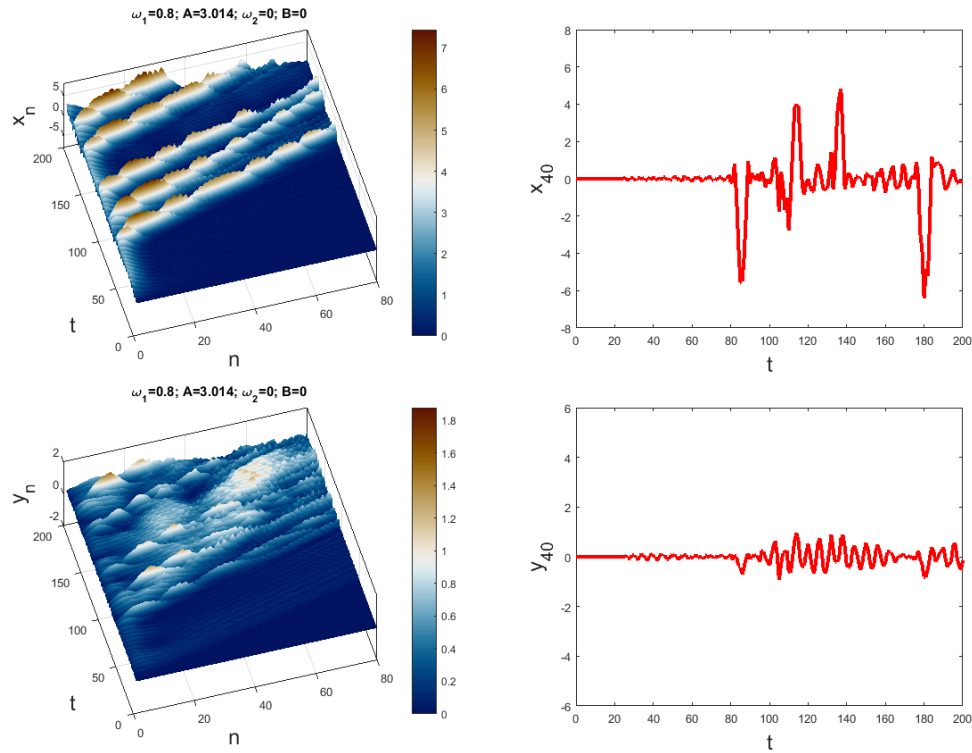
Figure 3.5: Graphs showing the evolution of the coupled chain with respect to time for the driving angular frequencies of the two chains $\omega = 0.8$ and the driving amplitude slightly above the threshold $A = 3.014 > A_{th}$. The up panel corresponds to the behavior of $x - chain$ and the down panel corresponds to the behavior of $y - chain$.

values of driving frequency in the lower forbidden band ($\omega = 0.8$), $A_{th} = 2.563$ and $B_{th} = 2.563$. We observe that when the amplitudes are less than 2.563 each chain exhibits an evanescent wave as represented in Fig. 3.6. When the amplitudes are slightly beyond the threshold amplitudes, the supratransmission phenomenon occurs as displayed in Fig. 3.7.
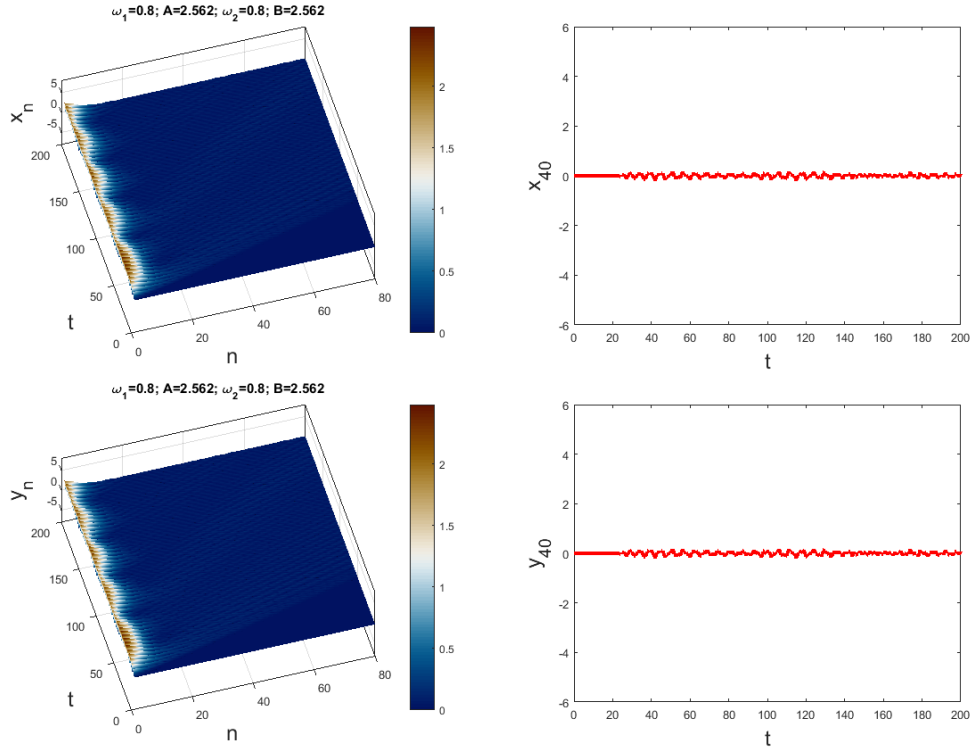
Figure 3.6: Graphs showing the evolution of the coupled chain with respect to time for the driving angular frequencies of the two chains $\omega = 0.8$ and the driving amplitudes slightly below the threshold $A = 2.562 < A_{th}$ and $B = 2.562 < B_{th}$. The up panel corresponds to the behavior of $x - chain$ and the down panel corresponds to the behavior of $y - chain$.

- The two chains are driven at the origin with different frequencies. Here, $x - chain$ is driven with $\omega_1 = 1.2$ taken in the allowed band and the driving amplitude A=0.9 while $y - chain$ is driven with $\omega_2 = 0.9$ and amplitude B=3.0 below the homoclinic threshold. One would normally observe an evanescent wave in the $y - chain$ but

Figure 3.7: Graphs showing the evolution of the coupled chain with respect to time for the driving angular frequencies of the two chains $\omega = 0.8$ and the driving amplitudes slightly above the threshold $A = 2.564 > A_{th}$ and $B = 2.564 > B_{th}$. The up panel corresponds to the behavior of $x - chain$ and the down panel corresponds to the behavior of $y - chain$.

curiously, the intensity transmits to remote sites as seen in Fig. 3.8. That is due to the collision between the travelling wave from the phonon band $(x-chain)$ and the evanescent wave from the bandgap $(y-chain)$ because of the transverse coupling of the chains.
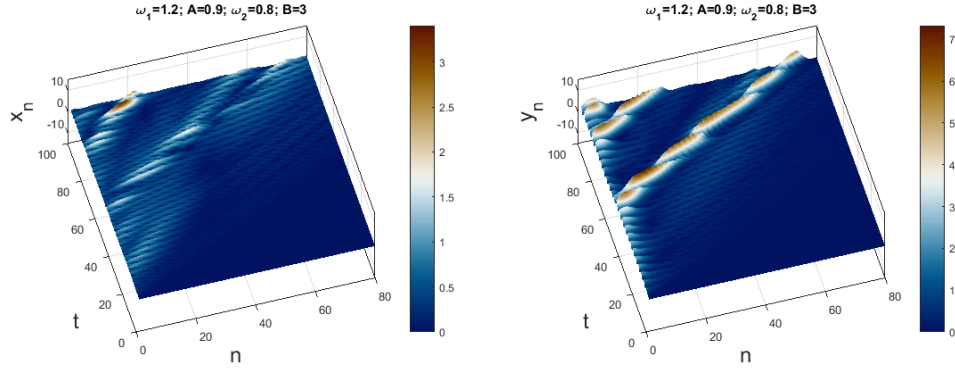
Figure 3.8: Graphs showing the evolution of the coupled chain with respect to time for the driving angular frequency of the $x-chain$ $\omega_1 = 1.2$ and the driving amplitudes A=0.9. $y-chain$ is driven with $\omega_2 = 0.9$ and the driving amplitude B=3.0 (below amplitude threshold). The up panel corresponds to the behavior of $x-chain$ and the down panel corresponds to the behavior of $y-chain$.

The same phenomenon has been observed in discrete electrical lattice [101] but with both left and right edges excited. The phenomenon is also qualitatively identical to the amplification of phonons by phonons on the basis of a nonlinear band-gap transmission process as in Refs. [134] and the amplification of magnetic pulses by an electric field with a frequency close to the band edge of the magnetic branch [135].

Besides the transmission of binary information and the detection of the weak signal, which are part of the applications of the supratransmission phenomenon, the results of this work enriched the applications in the case where the signal amplifier in lattice could be avoided by using an input signal in another lattice transversally coupled by the original

lattice.

3.3 MI in transversely connected nonlinear pendulum pairs

As we have seen in section 2.6 of chapter 2, modulational instability (MI) qualitatively refers to the ability for an excitation that propagates to be able to split into packets of energy (isolated pulses) and is of great interest in several areas of physics. In this section, we check by means of numerical methods the theoretical analysis made in section 2.6 concerning discrete MI. However, the appearance of this phenomenon of MI only occurs when certain conditions (linking the wave vectors of the initial plane wave q to the disturbance Q) are respected.

Now, we investigate the behavior of the MI gains G^+ and G^- or MI zones by playing on the values of the transverse coupling parameter d. The MI gains exhibit two bands namely, the stable band and the unstable band. It is worth noting that, the unstable zone of the MI corresponds to the generation of modulated plane wave solutions. That is, in unstable regions, the plane waves are supposed to be broken up into trains of solitary waveforms or pulses, or it is considered as stable when the wave numbers q and Q belong to the stability bands. In Figs. 3.9, 3.10 and 3.12, we have fixed $c = 4$, $\lambda_0 = 0.6$, and varied the transverse coupling parameter respectively as $d = 0.1$, $d = 0.5$, and $d = 1.5$. The transverse coupling parameter appears to dramatically impact the instability features. That is, it influences the stability and instability zones as well observed in the left panel of those figures. There, the regions surrounded by bright greenish areas represents the unstable band while the dark bluish areas indicate the regions of stability. Thus, it is observed that, for the instability growth rate G^+, when one increases the transverse coupling parameter, the amplitude of
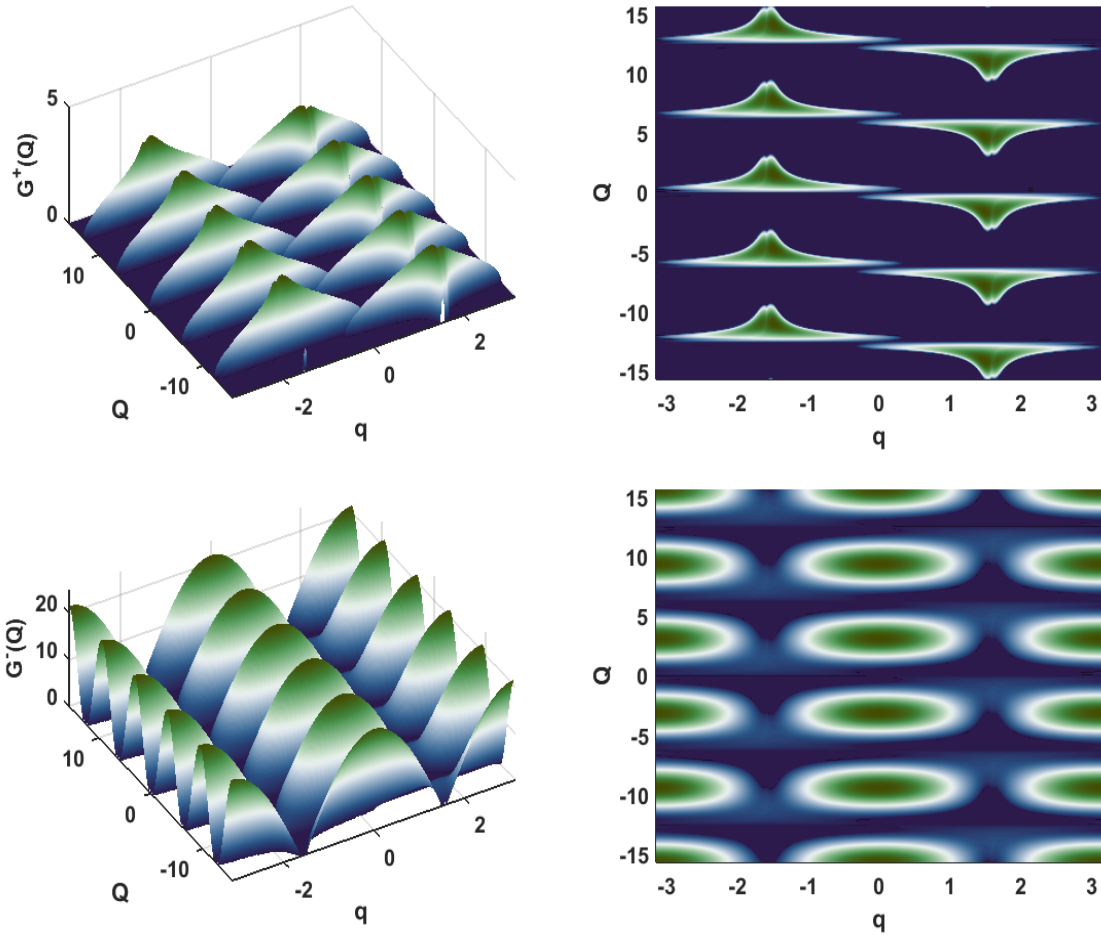
Figure 3.9: (left panel): Growth rate of MI gain associated with solutions G^+ and G^- of equation 2.40 versus the wave numbers Q and q for the parameters $d = 0.1$, $c = 4$, and $\lambda_0 = 0.6$. (Right panel): Regions of stability in the (q, Q) plane are indicated by the dark bluish area(s) and the regions of modulational instability in the (q, Q) plane are indicated by the area(s) surrounded by bright greenish color.

the gain increases as we can clearly observe on the left panel of Fig. 3.11 while the stable bands decrease and the MI regions increase as clearly shown in Fig. 3.12. Hence, the chances of observing MI in the lattice reduce with a decrease in the transverse coupling parameter. On the other hand, for the instability growth rate G^-, when one increases the transverse coupling parameter, the amplitude of the gain increases slightly as we can clearly observe on the right panel of fig. 3.11 while the stable bands and the MI regions slightly change. Also, it can be clearly observed that the MI gains are symmetric with respect to $q = 0$. Therefore, it has been shown that, the instability growth rate and MI band are dramatically affected by the transverse coupling parameter.
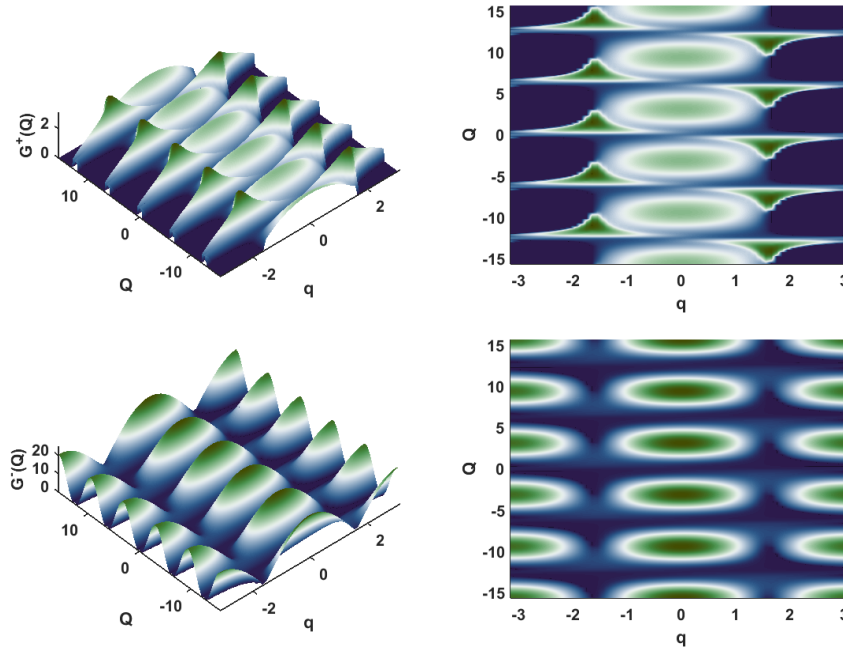
Figure 3.10: (left panel): Growth rate of MI gain associated with solutions G^+ and G^- of Eq. (2.40) versus the wave numbers Q and q for the parameters $d = 0.5$, $c = 4$, and $\lambda_0 = 0.6$. (Right panel): Regions of stability in the (q, Q) plane are indicated by the dark bluish area(s) and the regions of modulational instability in the (q, Q) plane are indicated by the area(s) surrounded by bright greenish color.
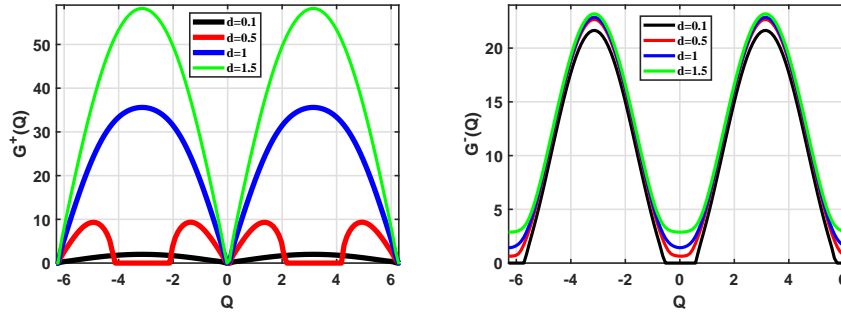
Figure 3.11: Growth rate of MI gain for different values of the transverse coupling parameter d versus the wave number of the perturbation Q for $q = \frac{\pi}{100}$. Where the other parameters are: $c = 4$, $\lambda_0 = 0.6$. We observe that, the MI gain spectrum is symmetric with respect to $Q = 0$.

In Fig. 3.11, the behavior of the amplitude of MI growth rate for carrier waves versus the wave number of perturbation Q for the wave number $q = \frac{\pi}{100}$ with four values of transverse coupling parameter d has been displayed. It is observed in Fig. 3.11 that, the instability growth rate G^+ is significantly sensitive to the transverse coupling term. For $d = 0.1$, the dynamics of the network displays a very weak growth rate amplitude. Whereas, the instability growth rate G^- does not change considerably with the transverse coupling term. Also, it is important to point out that, for $Q = \pi$, the amplitude of MI gain is maximum.

In the left panel of Figs 3.9, 3.10 and 3.12, the unstable regions of MI are clearly depicted; consequently, the plane wave solutions of the transversely coupled pendulum chains model become unstable. Hence, the dynamics of the generated unstable plane wave solutions will be studied numerically in the next paragraph.

In order to check the validity of the linear stability analysis which does not tell us anything about the behavior of the propagation of the slowly modulated waves when the instability grows, we perform some numerical investigations of the equation of motion
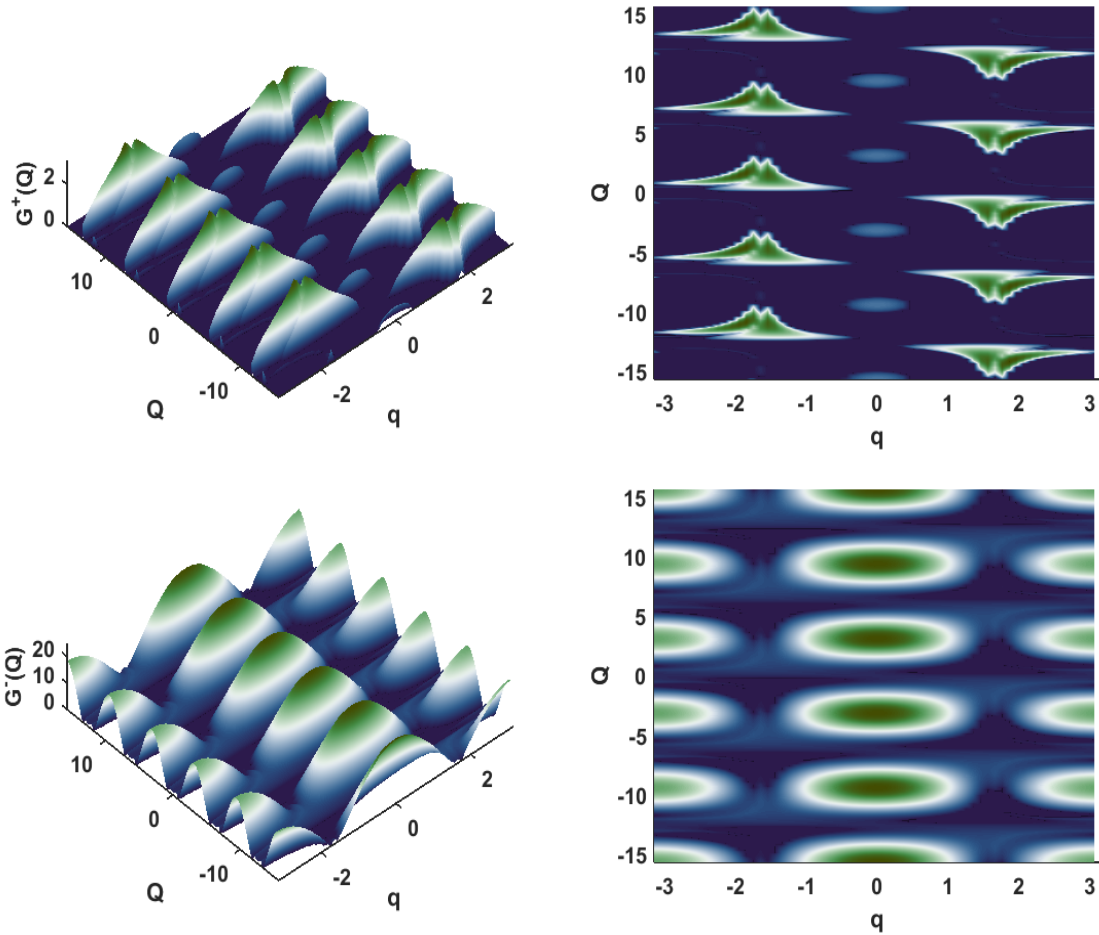
Figure 3.12: (left panel): Growth rate of MI gain associated with solutions G^+ and G^- of Eq. (2.40) versus the wave numbers Q and q for the parameters $d = 1.5$, $c = 4$, and $\lambda_0 = 0.6$. (Right panel): Regions of stability in the (q, Q) plane are indicated by the dark bluish area(s) and the regions of modulational instability in the (q, Q) plane is indicated by the area(s) surrounded by bright greenish color.

Eq. (2.2). This numerical simulation is done in order to understand the dynamics of the transversely connected nonlinear pendulum chains under MI in the nonlinear regime.

To this end, it is carried out by integrating the full Eq. (2.2) using a fourth order Runge Kutta scheme with normalized time step $\Delta t = 10^{-8}$. We consider the number of sites N in the n direction to be equal to 200 with periodic boundary conditions such as to avoid the wave reflection at the end of the line. In accordance with Eqs. 2.31 and 2.32, the initial modulated plane waves with slightly modulated amplitudes introduced are in this form

$$
\begin{aligned}
x_n(t=0) &= \lambda_0\left[1 + 0.01\cos(Qn)\right]\cos(qn); &\quad \dot{x}_n(t=0) &= \lambda_0\omega\left[1 + 0.01\cos(Qn)\right]\sin(qn) \\
y_n(t=0) &= \mu_0\left[1 + 0.01\cos(Qn)\right]\cos(qn); &\quad \dot{y}_n(t=0) &= \mu_0\omega\left[1 + 0.01\cos(Qn)\right]\sin(qn)
\end{aligned},
$$

$$(3.3)$$

with the set of wave numbers q and Q taken in a given unstable zones of Figs. 3.9, 3.10, and 3.12 obtained from the linear stability analysis and the wave frequency ω calculated from the dispersion relation of Eq. (2.30).

We introduce in the network the initial conditions of Eq. (3.3) by considering different values of the transverse coupling term. Firstly, for $d = 0.1$, we choose a wave with $q = \frac{\pi}{100}rad$ perturbed at wave number $Q = 0.911\pi rad$ belonging to the unstable region of Fig. 3.9. Using these parameters, we obtained Fig. 3.13 which illustrates the generation of localized pulses in the cause of the MI. We can clearly see that the initial solution tends to disintegrate during propagation, which leads to the break up of the wave into a periodic localized pulses or envelope soliton train. It is important to point out that, the wave displayed an oscillating and breathing behaviour and each component of the train has the shape of a soliton-like object; this is due to the existence of MI in the network.

We display in Fig. 3.14, the spatiotemporal evolution of amplitudes for $d = 1.0$ by choosing a wave with $q = \frac{\pi}{100}rad$ perturbed at wave number $Q = 0.911\pi rad$ belonging to
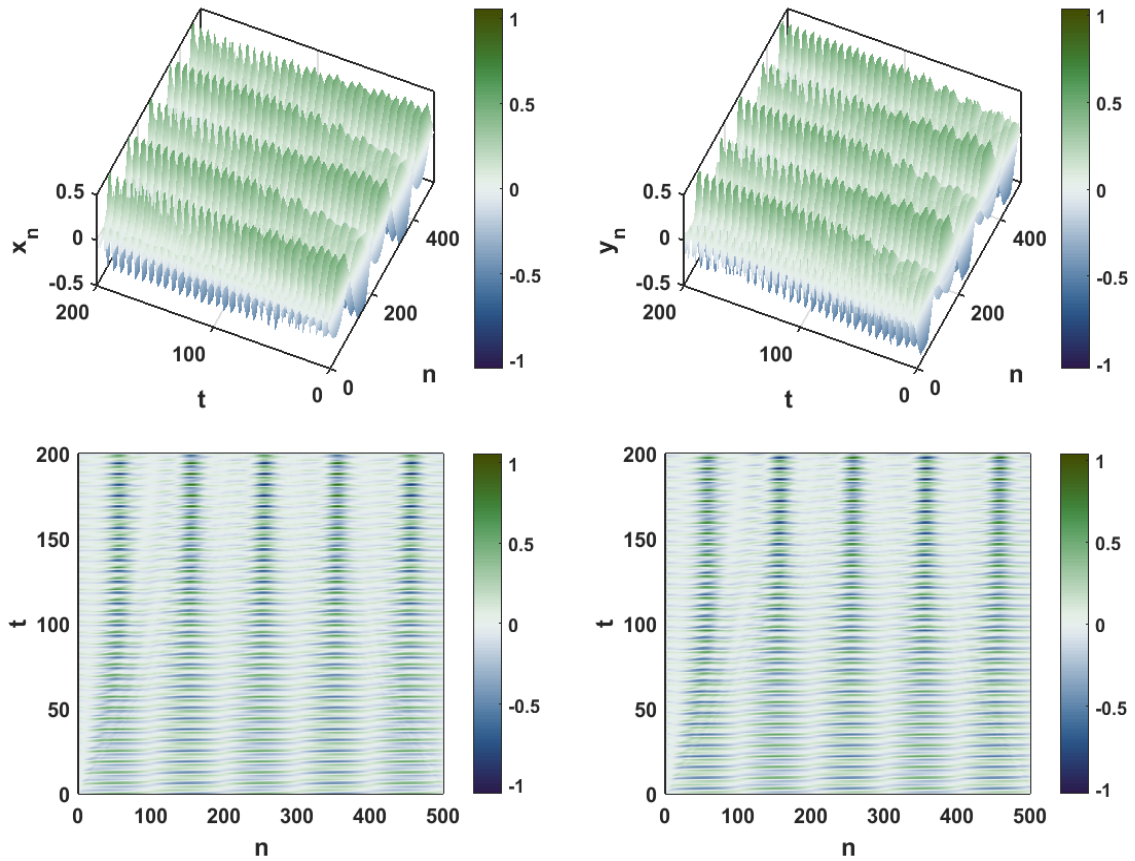
Figure 3.13: Spatiotemporal evolution of the amplitudes of the initial plane waves which break into a wave train having the shape of a soliton due to the MI manifestation in a transversely connected nonlinear pendulum chains as predicted analytically, for $d = 0.1$, $c = 4$, $\lambda_0 = 0.6$, $q = \frac{\pi}{100} rad$ and $Q = 0.911\pi rad$. (top panel): 3D representation, (down panel): 2D representation.

the unstable region (not shown here) where the envelope pulses also emerge due to the existence of MI. Thus, the localization in time is observed. For d=1.5 the number of localization solution in time increases as illustrated in Fig. 3.15. Hence, Transversely connected nonlinear pendulum pairs can be convenient tools for the study of wave propagation in nonlinear dispersive media.
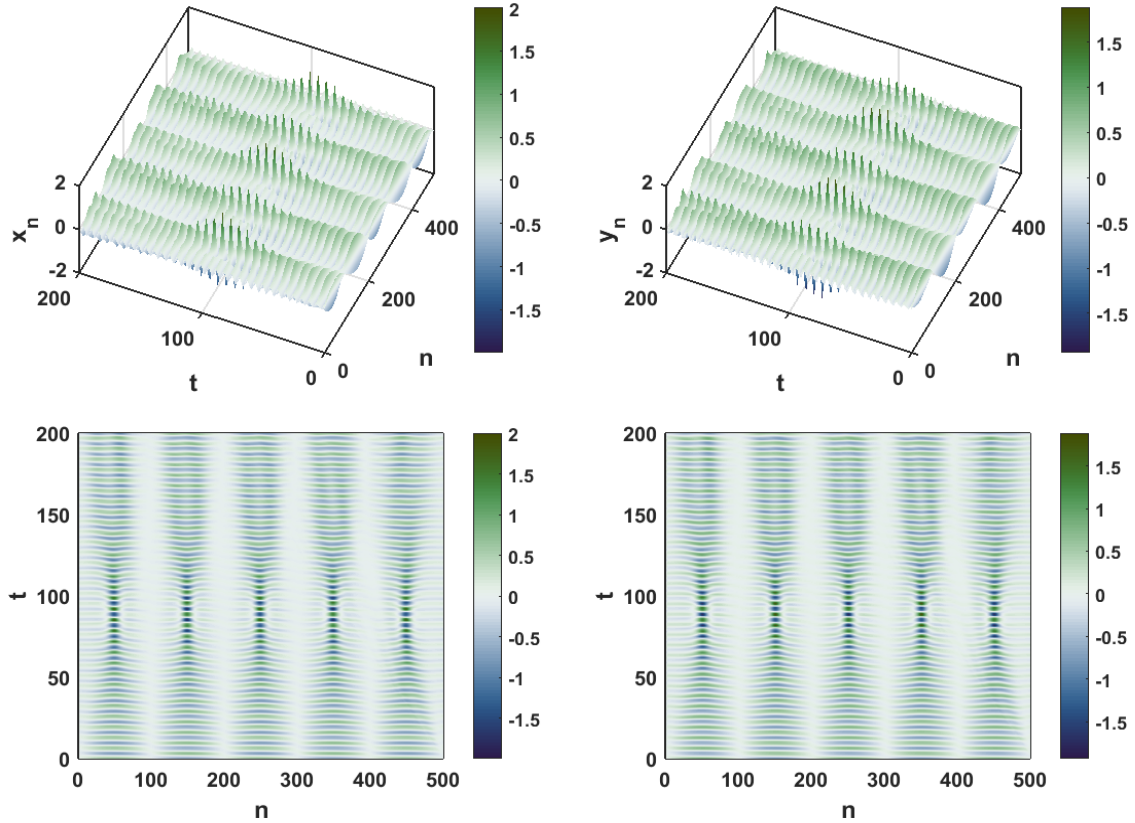
Figure 3.14: Spatiotemporal evolution of the amplitudes of the initial plane waves which break into a wave train having the shape of a soliton due to the MI manifestation in a transversely connected nonlinear pendulum chains as predicted analytically, for $d = 1.0$, $c = 4$, $\lambda_0 = 0.6$, $q = \frac{\pi}{100} rad$ and $Q = 0.911\pi rad$. (top panel): 3D representation, (down panel): 2D representation.
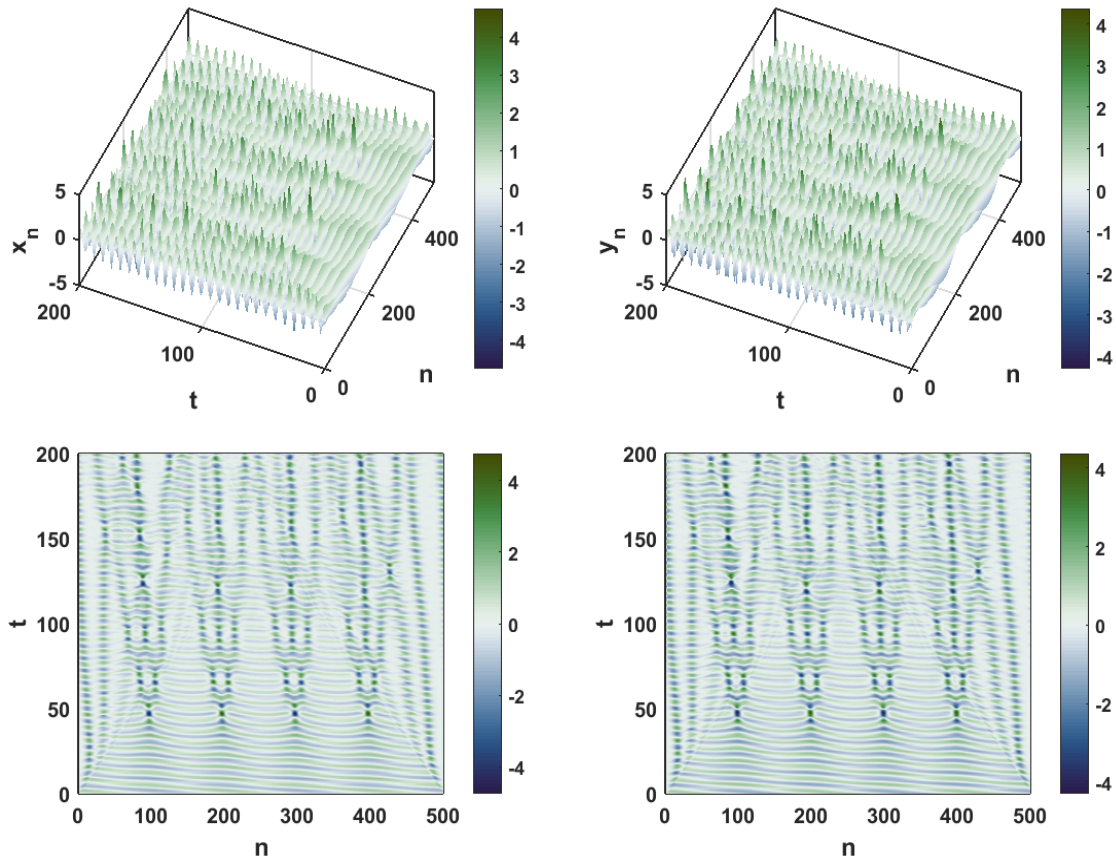
Figure 3.15: Spatiotemporal evolution of the amplitudes of the initial plane waves which break into a wave train having the shape of a soliton due to the MI manifestation in a transversely connected nonlinear pendulum chains as predicted analytically, for $d = 1.5$, $c = 4$, $\lambda_0 = 0.6$, $q = \frac{\pi}{100} rad$ and $Q = 0.911\pi rad$. (top panel): 3D representation, (down panel): 2D representation.

3.4 Wave propagation in transversely connected non-linear pendulum pairs

Now, to consolidate the validity of analytical results, let us proceed to study numerically the evolution of the previous bright soliton in the network of Fig. 2.1. In this section, we report the results of the numerical experiments performed on the exact discrete equation (2.2) of the network. We use the Ode45 solver of Matlab with periodic boundary conditions using the following parameters $\gamma = 1$, $\varepsilon = 0.02$, and $C = 4$.

For a given value of wave number k depending of the domain of each soliton (see Fig. 2.5), we evaluate the angular frequency ω using the dispersion relation of Eq. (2.10), the nonlinear coefficient Q, the dispersion coefficient P and other soliton's parameters given just after Eq. (2.18). Similarly, the number of cells for both lines is chosen to be equal to 1001.

For the effectiveness of the investigations, we consider different values of the transverse coupling parameter so as to examine its effect on the progression of the solitary wave from one line to another. for this purpose, let us consider two cases depending on the input signal or initial conditions applying on each line.

- Firstly, as initial condition, we take as the input signal the profile of the bright soliton for the $x - line$ such

$$x_n(0) \simeq x_0 sech\left(\varepsilon\rho n\right)\cos\left(kn\right),\tag{3.4}$$

and consider that at $t = 0$, $y - line$ is at rest, that is

$$y_n(0) \simeq 0.\tag{3.5}$$

With zero velocity (k=0 $rad/cell$), we obtain Fig. 3.16. The no transverse coupling case (D=0) is depicted in the first line: Ones can observe the localization of the

wave in the $x-line$ while no wave is propagating in the $y-line$. For the transverse coupling parameter different to zero (second and third line of Fig. 3.16), we observe the localization in both $x-$ and $y-lines$. The remarkable phenomenon here is the fact that, for a given time, the wave exists in the x-line while simultaneously, there is no wave in the $y-line$. This is similar to the gain and loss phenomenon observed in the optical waveguide arrays [136]. Despite the fact that only one chain is excited, there is an alternative transfer of energy between both lines. What is the behavior of the lattice for the nonzero group velocity? Fig. 3.17 displays the spatiotemporal evolution of the wave for $k = 0.5\ rad/cell$. It is well seen in this figure in the first line (D=0) that, no wave is propagating in the $y-line$ as expected. For $D = 0.01$ (second line) the energy transfer from the $x-line$ to the $y-line$ is observed and the gain and loss phenomenon is observed. The same phenomenon is obtained for $D = 0.1$. This is in agreement with the first idea of the construction of the lattice in Fig. 2.1 by Destyl et al. [39]. For a large value of the transverse coupling constant as it can be seen in Fig. 3.18, we observe that, the wave introduced at the origin at $t = 0$ exhibits some nonlinear distortions of the envelope when time grows. Then, the fission of the initial wave occurs with time as shown in that figure.

- Secondly, considering the fact that $y_n = -x_n$ (as shown in section 2.3 i.e the two lines are out of phase) as initial condition, we take as the input signal the profile of the bright soliton for the $x-line$ such

$$x_n(0) \simeq x_0 sech\left(\varepsilon\rho n\right)\cos\left(kn\right),\qquad(3.6)$$

and consider that at $t = 0$, $y-line$ is the opposite of $x-line$, that is

$$y_n(0) \simeq -x_0 sech\left(\varepsilon\rho n\right)\cos\left(kn\right).\qquad(3.7)$$

Following the initial conditions of Eqs. (3.6) and (3.7), we obtain Fig. 3.19. We
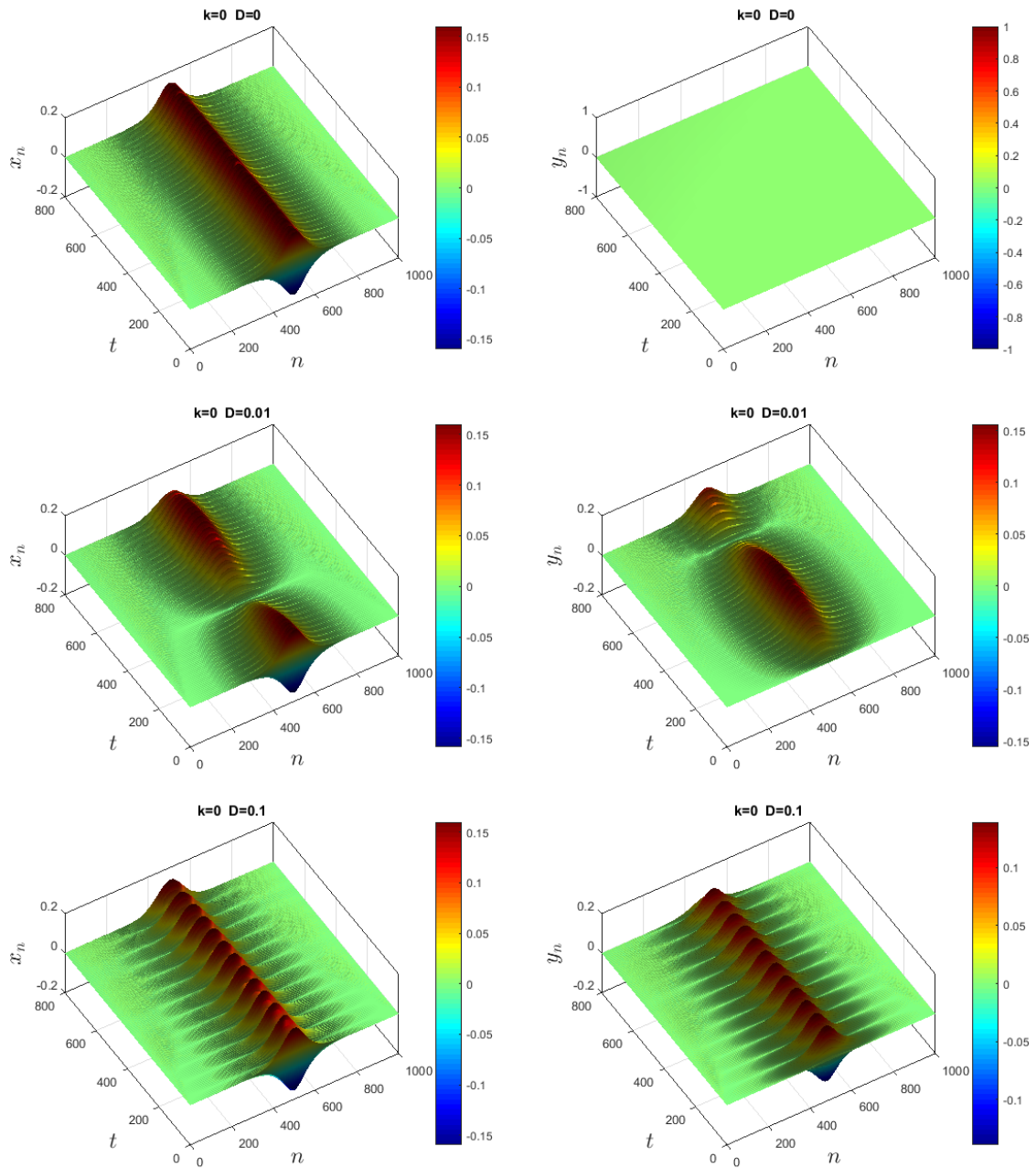
Figure 3.16: Space time evolution plot of angles x_n (left panel) and y_n (right panel) showing the behavior of the bright soliton with zero velocity (k=0) in the network.
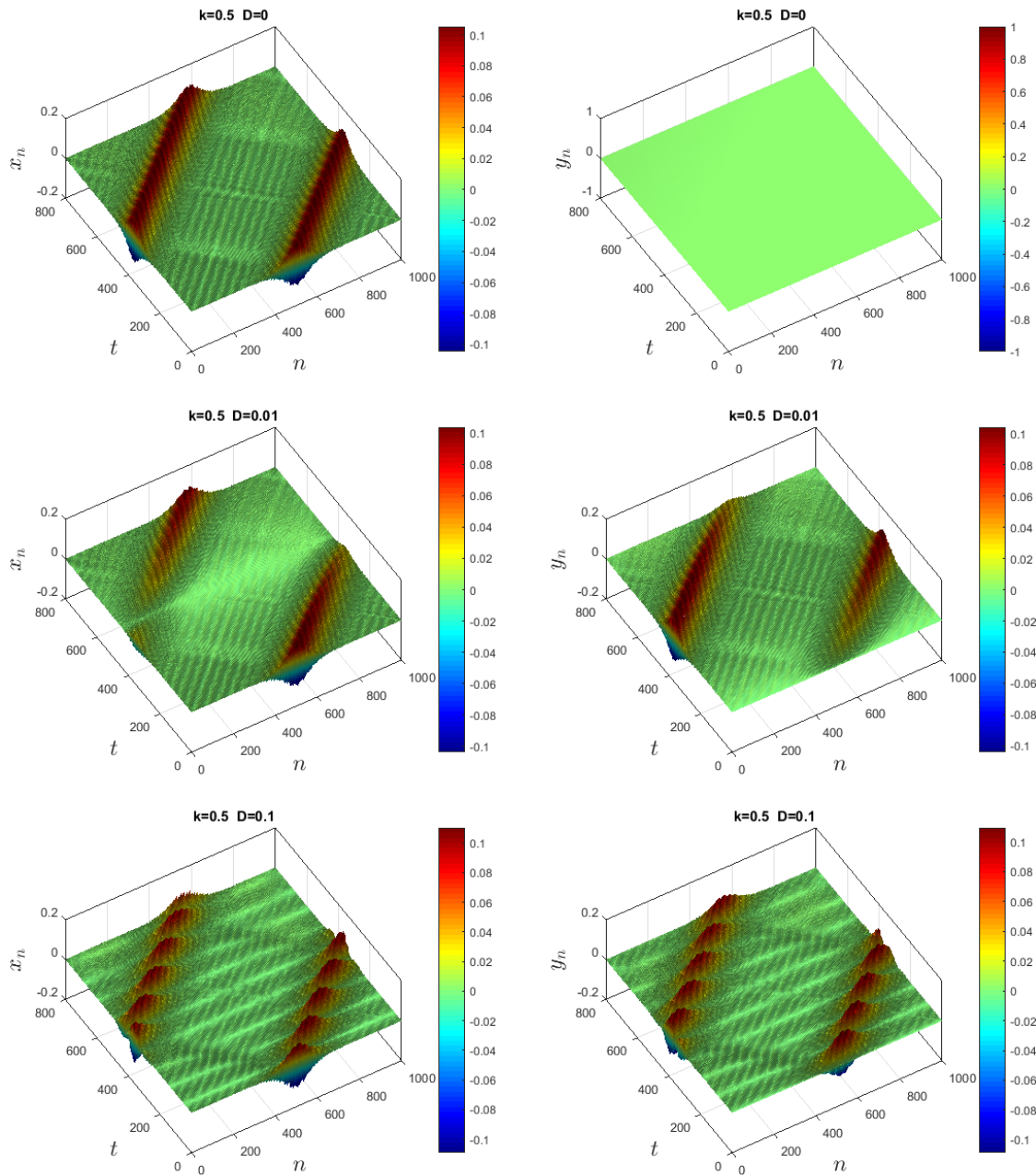
Figure 3.17: Space time evolution plot of angles x_n (left panel) and y_n (right panel) showing the propagation of the bright soliton for $k = 0.5$ in the network.
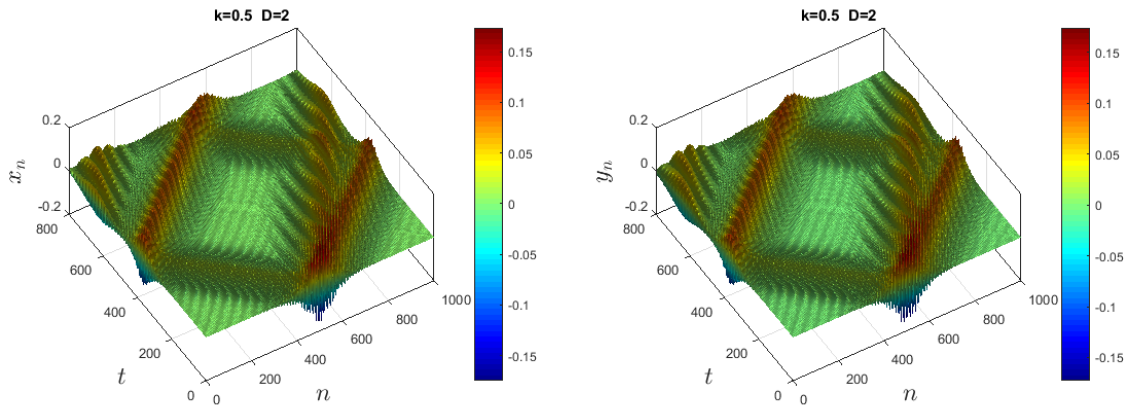
Figure 3.18: Space time evolution plot of angles x_n (left panel) and y_n (right panel) showing the propagation of the bright soliton in the network with large transverse coupling parameter.
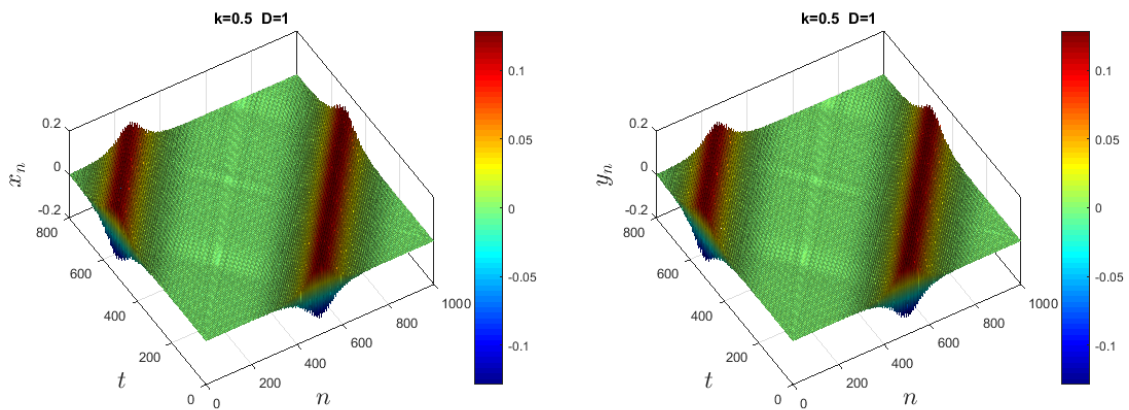
Figure 3.19: Space time evolution plot of angles x_n (left panel) and y_n (right panel) showing the propagation of the bright soliton in the network with the initial conditions given by Eqs. (3.6) and (3.7).

observe the propagation of the wave on the right-hand side. As both chains are excited, the loss on the $x - line$ is compensated by the gain of the $y - line$ and vice versa. The compensation of the loss by the gain in both chains induces the coherency of the waves during the propagation.

3.5   Conclusion

In this chapter, we have created a way to generate NST in a 2D sine-Gordon equation that is in the equation governing a transversely connected nonlinear pendulum pairs. Secondly, we have shown that the model can exhibit the gain and loss phenomenon and can also be used to investigate wave propagation in nonlinear dispersive media. The condition for which the network can exhibit modulational instability is also determined. We have observed a good agreement between analytical calculations and numerical simulations. The main results will be summarized in the next section.

General conclusion

In this thesis, we have considered nonlinear discrete coupled pairs of pendulum chains connected to the nearest neighbours in the longitudinal and transverse directions.

This novel model has been used to investigate the nonlinear supratransmission phenomenon in the common lower forbidden bandgap of the two pendulum chains. We used Euler-Lagrange's equations to derive the equation governing the motion for the nth pendulum in both directions. We used the obtained equation to look into the supratransmission threshold amplitude. To do so, we have employed the two-dimensional map approach to determine the amplitude and the numerical result to confirm the validity of the obtained homoclinic supratransmission threshold amplitude for the case where only one chain was driven. We also numerically performed the supratransmission threshold amplitude in the case where the two chains were driven.

Besides, in order to study the existence of MI in the model, the multiple scale method was used to derive the coupled discrete nonlinear Schrödinger equation. By carrying out the linear stability analysis we have calculated and plotted the growth rate of the MI. It has been revealed that both the gain and the MI bands are sensitive to the transverse coupling term. Therefore, with the results obtained from MI analysis, we predicted the formation of the periodic localized solitons in the network. Thus, numerical simulations of MI have been carried out and let to the generation of periodic localized pulses in the system. We have observed that the transverse coupling term has an influence on the

localization of envelope pulses.

Finally, we obtained the corresponding linear dispersion law describing the small amplitude waves of the network. We allowed our model to exhibit two modes of propagation of waves namely, the fast- and the slow-mode. The slow-mode was equivalent to the case of a single chain where as the fast one was not. This let our attention to be focused only on the fast-mode. Moreover, by considering the fact that the two chains of the model are proportional, we obtained a single equation which obeyed the linear dispersion relation of the fast mode. Afterwards, applying the rotating wave approximation method on the obtained single equation, we have shown that the generalized coordinate of the system is governed by a nonlinear Schrödinger equation. We deduced that, the obtained NLS equation supports bright and dark or hole solitons as solutions. Due to the fact that, the transverse coupling parameter had the same effects on each soliton, we focused our attention only on bright soliton. We used the obtained bright soliton as initial conditions for numerical investigation to follow the progression of the generated waves in the network from one line to the other when varying the transverse coupling parameter. From the interesting results obtained in this work, we saw clearly that, the transverse coupling plays a significant role in the model of the nonlinear coupled pendulum lines and could be used to generate the gain and loss phenomenon.

From the interesting results obtained in this work, we can say that transversely connected nonlinear pendulum chains can be convenient tools for studying wave propagation in dispersive nonlinear media. It opens up the possibility of additional mathematical analysis on discrete simultaneous equation describing the dynamics of discrete multicomponent systems and opens the way to understanding supratransmission phenomenon in multicomponent discrete systems.

Another interest in the future will be to see the effect of transverse direction with

common string [137] on the nonlinear bandgap phenomenon and to characterize breathers (periodic or quasi-periodic solutions) of the model and to see how existence and stability of such solutions is related to the nonlinear stability of the zero equilibrium.

Bibliography

Bibliography

[1] N. J. Zabusky and M. D. Kruskal, interaction of "solitons" in a collisionless plasma and the recurrence of initial states, Phys. Rev. Lett. **15**, (1965) 240.

[2] E. Fermi, J. Pasta, and S. Ulam, Nonlinear wave motion, Lectures in Applied Mathematics **15**, (1974).

[3] A. B. Togueu Motcheyo, T. Kanaa, S. Ndjakomo Essiane, Backward energy Propagation in Nonlinear Magnetic Metamaterials, Journal of Superconductivity and Novel Magnetism **34**, (2021) 2619.

[4] S. Abdoulkary, L.Q. English, A. Mohamadou, Envelope solitons in a left-handed nonlinear transmission line with Josephson junction, Chaos, Solitons and Fractals **85**, (2016) 44.

[5] G. P. Veldes, J. Cuevas, P. G. Kevrekidis, and D. J. Frantzeskakis, Coupled backward-and forward-propagating solitons in a composite right and left-handed transmission line, Phys. Rev. E **88**, (2013) 013203.

[6] A. B. Togueu Motcheyo, J. D. Tchinang Tchameu, S. I. Fewo, C. Tchawoua, T. C. Kofane, Chameleon's behavior of modulable nonlinear electrical transmission line, Communications in Nonlinear Science and Numerical Simulation **53**, (2017) 22.

[7] G. R. Deffo, S. B. Yamgoué, and F. B. Pelap, Existence and dynamics of solitary waves in a two-dimensional Noguchi nonlinear electrical network, Phys. Rev. E **98**, (2018) 062201.

[8] A. S. Tchakoutio Nguetcho, G. M. Nkeumaleu, J. M. Bilbault, Anharmonic effects .on the dynamic behavior's of Klein Gordon model's Author links open overlay panel, Applied Mathematics and Computation **403**, (2021) 126136.

[9] A. V. Porubov, Wave modulation in a nonlinear acoustic metamaterial, International Journal of Non-Linear Mechanics **137**, (2021) 103788.

[10] A. B. Togueu Motcheyo, E. Nkendji Kenkeu, J. Djako, C. Tchawoua, Backward-wave propagation with vertical dust grain oscillations in dusty plasma crystals, Physics of Plasmas **25**, (2018) 123701.

[11] E. Nkendji Kenkeu, A. B. Togueu Motcheyo, Thomas Kanaa, and C. Tchawoua, Wave propagation with longitudinal dust grain oscillations in dusty plasma crystals, Phys. Plasmas **29**, (2022) 043702.

[12] B. Sadjo, C. B. Tabi, H. Edongue, and M. Alidou, Coupled energy patterns in zigzag molecular chains, Wave Motion **72**, (2017) 342.

[13] C. J. McKinstrie and R. Bingham, the modulational istability of coupled waves, Phys. Fluids B: Plasma Phys. **1**, (1989) 230.

[14] C. L. Gninzanlong, F. T. Ndjomatchoua, and C. Tchawoua, Forward and backward propagating breathers in a DNA model with dipole-dipole long-range interactions Phys. Rev. E **102**, (2020) 052212 .

[15] J. D. Tchinang Tchameu, C. Tchawoua, A. B. Togueu Motcheyo, Nonlinear supra-
transmission of multibreathers in discrete nonlinear Schrödinger equation with sat-
urable nonlinearities, Wave Motion **65**, (2016) 112.

[16] A. B. Aceves, G. Fibich, and B. Ilan, Gap-soliton bullets in waveguide gratings,
Physica D: Nonlinear Phenomena **189**, (2004) 277.

[17] M. Alidou, A. Kenfack-Jiotsa, and T. C. Kofane, Modulatioal instability and spa-
tiotemporal transition to chaos, Chaos, Solitons Fractals **27**, (2006) 914.

[18] R. Nath, P. Pedri, and L. Santos, Stability of dark solitons in three dimensional
dipolar Bose-Einstein condensates, Phys. Rev. Lett. **101**, (2008) 210402.

[19] H. N. Chan, K. W. Chow, Periodic and localized wave patterns for coupled Ablowltz-
Ladik systems with negative cross phase modulation, Communications in Nonlinear
Science and Numerical Simulation **65**, (2018) 185.

[20] E. Lorin, M. Lytova, A. Memarian, and A. D. Bandrauk, Development of nonper-
turbative nonlinear optics models including effects of high order nonlinearities and
of free electron plasma, J. Phys. A: Math. Theor. **48**, (2015) 105201.

J. F. R. Archilla , S. M. M. Coelho, F. D. Auret, V.I. Dubinkoc, V. Hizhnyakov,
Long range annealing of defects in germanium by low energy plasma ions, Physica D
297, (2015) 56.

[21] F. Maucher, D. Buccoliero, S. Skupin, M. Grech, A. S. Desyatnikov, and W. Kro-
likowski, Tracking azimuthons in nonlocal nonlinear media, Opt. Quantum Electron.
41, (2009) 337.

[22] E. Kenig, B. A. Malomed, M. Cross, R ifshitz, Intrinsic localized modes in paramet-
rically driven arrays of nonlinear resonators, Phys. Rev. E **80**, (2009) 046202.

[23] F. Palmero, J. Han, L. Q. English, T. J. Alexander, P. G. Kevrekidis, Multifrequency and edge breathers in the discrete sine-Gordon system via subharmonic driving: Theory, computation and experiment, Phys. Lett. A **380**, (2016) 402.

[24] L. M. Floria, J. J. Mazo, Dissipative dynamics of the Frenkel-Kontorova model, Advances in Physics **45**, (1996) 505.

[25] J. Wu, R. Keolian,I. Rudnick, Observation of a nonpropagating hydrodynamic soliton, Phys. rev. lett. **52**, (1984) 1421.

[26] B. Denardo, W. Wright, S. Putterman, A. Larraza, Observation of a kink soliton on the surface of a liquid, Phys. Rev. Lett. **64**, (1990) 1518.

[27] X. Wang, R. Wei, Dynamics of Multisoliton Interactions in Parametrically Resonant Systems, Phys. Rev. Lett. **78**, (1997) 2744.

[28] O. M. Braun, Y. Kivshar,The Frenkel-Kontorova Model: Concepts, Methods, and Applications, Springer-Verlag, Berlin, Heidelberg, 2004.

[29] C. Vasanthi, M. Latha, Heisenberg ferromagnetic spin chain with the bilinear and biquadratic interactions in $(2 + 1)$ dimensions, Comm. in Non. Sci. and Num. Sim. **28**, (2015) 109.

[30] I. Barashenkov, M. Bogdan,V. Korobov, Stability diagram of the phase-locked solitons in the parametrically driven, damped nonlinear Schrodinger equation, E. phy. Lett. **15**, (1991) 113.

[31] A. Jallouli , N. Kacem, N. Bouhaddi,Stabilization of solitons in coupled nonlinear pendulums with simultaneous external and parametric excitations, Comm. in Non. Sci. and Num. Sim **42**, (2015) 1.

[32] N. V. Alexeeva, I. V. Barashenkov, Impurity-induced stabilization of solitons in arrays of parametrically driven nonlinear oscillators, Phys. Rev. Lett. **14**, (2017) 48.

[33] H. Susanto, Q. E. Hoq, P. G. Kevrekidis, Stability of discrete solitons in the presence of parametric driving, Phys. Rev. E **74**, (2006) 067601.

[34] M. Syafwan, H. Susanto, S. M. Cox, Discrete solitons in electromechanical resonators, Phys. Rev. E **81**, (2010) 026207.

[35] J. Cuevas, L. Q. English, P. G. Kevrekidis, M. Anderson, Discrete Breathers in a Forced-Damped Array of Coupled Pendula: Modeling, Computation, and Experiment, Phys. Rev. Lett. **102**, (2009) 224101.

[36] N. V. Alexeeva, I. V. Barashenkov, A. A. Sukhorukov, and Y. S. Kivshar, Optical solitons in $PT-symmetric$ nonlinear couplers with gain and loss, Phys. Rev. A **85**, (2012) 063837.

[37] I. V. Barashenkov, S. V. Suchkov, A. A. Sukhorukov, S. V. Dmitriev, and Y. S. Kivshar, Breathers in $PT-symmetric$ optical couplers, Phys. Rev. A **86**, (2012) 053809.

[38] N. V. Alexeeva, I. V. Barashenkov, and Y. S. Kivshar, Solitons in $PT-symmetric$ ladders of optical waveguides, New J. Phys. **19**, (2017) 113032.

[39] E. Destyl, S. P. Nuiro, D. E. Pelinovsky and P. Poullet, Coupled pendula chains under parametric PT-symmetric driving force, Phys. Lett. A **381**, (2017) 3884.

[40] A. Chernyavsky and D. E. Pelinovsky, Breathers in Hamiltonian PT-Symmetric Chains of Coupled Pendula under a Resonant Periodic Force, Symmetry **8**, (2016) 59.

[41] A. Chernyavsky and D.E. Pelinovsky, Long-time stability of breathers in Hamiltonian PT-symmetric lattices, Journal of Physics A: Mathematical Theoretical **49**, (2016) 475201.

[42] F. Geniet and J. Leon, Energy transmission in the forbidden band gap of a nonlinear chain, Phys. Rev. Lett. **89**, (2002) 134102.

[43] F. Geniet and J. Leon, Nonlinear supratransmission, J. Phys.: Condens. Matter **15**, (2003) 2933.

[44] J. E. Macías-Díaz, Numerical study of the transmission of energy in discrete arrays of sine-Gordon equations in two space dimensions, Phys. Rev. E. **77**, (2008) 016602.

[45] J. E. Macías-Díaz, Numerical study of the process of nonlinear supratransmission in Riesz space-fractional sine-Gordon equations, Commun Nonlinear Sci Numer Simulat **46**, (2017) 89.

[46] J.E. Macías-Díaz and A.B. Togueu Motcheyo, Energy transmission in nonlinear chains of harmonic oscillators with long-range interactions, Results in Physics **18**, (2020) 103210.

[47] D. Chevriaux, R. Khomeriki and J. Leon, Theory of a Josephson junction parallel array detector sensitive to very weak signals, Phys. Rev. B **73**, (2006) 214516.

[48] J. E. Macías-Díaz, Persistence of nonlinear hysteresis in fractional models of Josephson transmission lines, Commun Nonlinear Sci Numer Simulat **53**, (2018) 31.

[49] J. Leon and A. Spire, Gap soliton formation by nonlinear supratransmission in Bragg media, Phys. Lett. A **327**, (2004) 474.

[50] S. B. Yamgoué, S. Morfu and P. Marquié, Noise effects on gap wave propagation in a nonlinear discrete LC transmission line, Phys. Rev. E **75**, (2007) 036211.

[51] K. Tse Ve Koon, J. Leon, P. Marquié, P. Tchofo-Dinda, Cutoff solitons and bistability of the discrete inductance-capacitance electrical line: Theory and experiments, Phys. Rev. E **75**, (2007) 066604;

K. Tse Ve Koon, P. Marquié, P. Tchofo Dinda, Experimental observation of the generation of cutoff solitons in a discrete LC nonlinear electrical line, Phys. Rev. E **90**, (2014) 052901.

[52] A. B. Togueu Motcheyo, C. Tchawoua, M. Siewe Siewe and J. D. Tchinang Tchameu, Supratransmission phenomenon in a discrete electrical lattice with nonlinear dispersion, Commun. Nonlinear. Sci. Numer. Simulat. **18**, (2013) 946.

[53] F. Kenmogne , G. B. Ndombou, D. Yemélé and A. Fomethe, Nonlinear supratransmission in a discrete nonlinear electrical transmission line: Modulated gap peak solitons, Chaos, Solitons and Fractals **75**, (2015) 263.

[54] A. B. Togueu Motcheyo and J. E. Macías-Díaz, On the wave transmission in a discrete nonlinear left-handed electrical lattice, Waves in Random and Complex Media **32**, (2022) 2718.

[55] R. Khomeriki, S. Lepri and S. Ruffo, Nonlinear supratransmission and bistability in the Fermi-Pasta-Ulam model, Phys. Rev. E **70**, (2004) 066626.

[56] T. Dauxois, R. Khomeriki, S. Ruffo, Modulational instability in isolated and driven Fermi-Pasta-Ulam lattices, Eur. Phys. J. Special Topics **147**, (2007) 3.

[57] J. E. Macías-Díaz, Numerical simulation of the nonlinear dynamics of harmonically driven Riesz-fractional extensions of the Fermi-Pasta-Ulam chains, Commun. Nonlinear Sci. Numer. Simulat. **55**, (2018) 248.

[58] J. E. Macías-Díaz, A. Bountis, Supratransmission in β-Fermi-Pasta-Ulam chains with different ranges of interactions, Commun. Nonlinear Sci. Numer. Simulat. **63**, (2018) 307.

[59] A. B. Togueu Motcheyo and J. E. Macías-Díaz, Energy transmission in the forbidden band-gap of a nonlinear chain with global interactions, J. Phys. A: Math. Theor. **53**, (2020) 505701.

[60] R. Khomeriki, Nonlinear band gap transmission in optical waveguide arrays, Phys. Rev. Lett. **92**, (2004) 063905.

[61] J. Lydon, G. Theocharis, C. Daraio, Nonlinear resonances and energy transfer in finite granular chains, Phys. Rev. E **91**, (2015) 023208.

[62] R. Alima, S. Morfu, P. Marquié, B. Bodo and B. Essimbi, Influence of a nonlinear coupling on the supratransmission effect in modified sine-gordon and klein-gordon lattices, Chaos, Solitons and Fractals **100**, (2017) 91.

[63] Q. Zhang, H. Fang, and J. Xu, Programmable stopbands and supratransmission effects in a stacked Miura-Origami metastructure, Phys. Rev. E **101**, (2020) 042206.

[64] M. J. Frazier, D. M. Kochmann, Band gap transmission in periodic bistable mechanical systems, Journal of Sound and Vibration **388**, (2017) 315;

J. E. Pechac , M . J. Frazier, Non-Reciprocal Supratransmission in Mechanical Lattices with Non-Local Feedback Control Interactions, Crystals **11**, (2021) 94.

[65] J. E. Macías-Díaz, A. Bountis, Nonlinear Supratransmission in Quartic Hamiltonian Lattices With Globally Interacting Particles and On-Site Potentials, J. Comput. Nonlinear Dynam. **16**, (2021) 021001.

[66] F. Tao, W. Chen, J, Pan, Wen Xu, Sidan Du, Experimental observation on asymmetric energy flux within the forbidden frequency band in the LC transmission line, Chaos, Solitons and Fractals **45** (2012) 810;

J.D. Tchinang Tchameu, C. Tchawoua, A.B. Togueu Motcheyo, Nonlinear supratransmission of multibreathers in discrete nonlinear Schrodinger equation with saturable nonlinearities, Wave Motion **65** (2016) 112;

Y. Watanabe, T. Nishida, Y. Doi, N. Sugimoto, Experimental demonstration of excitation and propagation of intrinsic localized modes in a mass-spring chain, Phys. Lett. A **382** (2018) 1957;

Y. Watanabe, M. Nishimoto, C. Shiogama, Experimental excitation and propagation of nonlinear localized oscillations in an air-levitation-type coupled oscillator array, Nonlinear Theory and Its Applications, IEICE **8**, (2017) 146.

J.E. Macías-Dáz, Nonlinear wave transmission in harmonically driven hamiltonian sine-Gordon regimes with memory effects, Chaos, Solitons and Fractals **42**, (2021) 110362.

[67] I. S. Lutsenko, P. V. Zakharov, M. D. Starostenkov, S. V. Dmitriev and E. A. Korznikova, Stability of supratransmission waves in a crystal of A3B stoichiometry upon interaction with single dislocations, J. Phys.: Conf. Ser. **2103**, (2021) 012079.

[68] P. Anghel-Vasilescu, J. Dorignac, F. Geniet, J. Leon and M. Taki, Nonlinear supratransmission in multicomponent systems, Phys. Rev. Lett. **105**, (2010) 074101 .

[69] Y. Xu, T. J. Alexander, H. Sidhu, P. G. Kevrekidis, Instability dynamics and breather formation in a horizontally shaken pendulum chain, Phys. Rev. E **90**, (2014) 042921.

[70] V. M. Burlakov, Interference of mode instabilities and pattern formation in anharmonic lattices, Phys. Rev. Lett. **80**, (1998) 3988.

[71] J. Leon, M. Manna, Discrete instability in nonlinear lattices, Phys. Rev. Lett. **83**, (1999) 2324.

[72] A. V. Gorbach, M. Johanson, Gap and out-gap breathers in a binary modulated discrete nonlinear Schrodinger model, EPJ D **29**, (2004) 77.

[73] J. Meier, G. I. Stegeman, D. N. Christodoulides, Y. Silberberg, R. Morandotti, H. Yang, G. Salamo, M. Sorel, J. S. Aitchison, Experimental observation of discrete modulational instability, Phys. Rev. Lett. **92**, (2004) 163902.

[74] http://www.google.com/pe.soliton.free.fr/montage-pendule.html, (Page consulted on 16th august 2018).

[75] M. Peyrard, T. Dauxois, Physique des solitons, CNRS Editions-EDP Science (2004).

[76] http://motherboard.vice.com/read/bizarre-disappearing-matter-waves-aretheghosts-of-physics (Page consulted on 2nd september 2018).

[77] D. Chevriaux, supratransmission et bistabilité nonlinéaire dans les milieux à bandes interdites photoniques et électroniques, Thèse de Doctorat Université de Montpellier II (2007).

[78] F. Qi, Z. Hou, H. Xin, Ordering chaos by random shortcuts, Phys. rev. lett. **91**, (2003) 064102.

[79] W. Chen, Y. Zhu, L. Lu, Observations of impurity-soliton interactions in driven Frenkel-Kontorova chains, Phys. Rev. B **67**, (2003) 184301.

[80] I. V. Barashenkov, M. Gianfreda, An exactly solvable PT-symmetric dimer from a Hamiltonian system of nonlinear oscillators with gain and loss, J. Phys. A, Math. Theor. **47**, (2014) 282001.

[81] I. V. Barashenkov, D. E. Pelinovsky, P. Dubard, Dimer with gain and loss: integrability and P T-symmetry restoration, J. Phys. A, Math. Theor. **48**, (2015) 325201.

[82] C. M. Bender, Making sense of non-Hermitian Hamiltonians, Rep. Prog. Phys. **70**, (2007) 947.

[83] C. M. Bender, B. Berntson, D. Parker, E. Samuel, Observation of PT phase transition in a simple mechanical system, Am. J. Phys. **81**, (2013) 173.

[84] J. Schindler, A. Li, M.C. Zheng, F.M. Ellis, T. Kottos, Experimental study of active LRC circuits with PT symmetries, Phys. Rev. A **84**, (2011) 040101.

[85] L. Brillouin, Wave propagation in periodic structures: electric filters and crystal lattices, McGraw-Hill, New York, (1946).

[86] W. Chen and D. Mills, Gap solitons and the nonlinear optical response of superlattices, Phys. rev. lett. **58**, (1987) 160.

[87] S. John and J. Wang, Quantum electrodynamics near a photonic band gap: Photon bound states and dressed atoms, Phys. rev. lett. **64**, (1990) 2418.

M. Scalora, J. P. Dowling, C. M. Bowden, and M. J. Bloemer, Optical limiting and switching of ultrashort pulses in nonlinear photonic band gap materials, Phys. rev. lett. **73**, (1994) 1368.

E. A. Ostrovskaya and Y. S. Kivshar, Matter-wave gap solitons in atomic band-gap structures, Phys. rev. lett. **90**, (2003) 160407.

A. S. Desyatnikov, E. A. Ostrovskaya, Y. S. Kivshar, and C. Denz, Composite band-gap solitons in nonlinear optically induced lattices, Phys. rev. lett. **91**, (2003) 153902.

P. J. Louis, E. A. Ostrovskaya, C. M. Savage, and Y. S. Kivshar, Bose-einstein condensates in optical lattices: Band-gap structure and solitons, Phys. Rev. A **67**, (2003) 013602.

B. Essimbi and D. Jäger, Observation of localized solitary waves along a bi-modal transmission line, Journal of Physics D: Applied Physics **39**, (2006) 390.

[88] D. Taverner, N. Broderick, D. Richardson, R. Laming, and M. Ibsen, Nonlinear self-switching and multiple gap-soliton formation in a fiber bragg grating, Optics letters **23**, (1998) 328.

[89] J. Leon, Nonlinear supratransmission as a fundamental instability, Phys. Lett. A **319**, (2003) 130.

J. Leon, Nonlinear tunneling in a fiber guide array resonator, Phys. Rev. E **70**, (2004) 056604.

[90] B. Bodo, S. Morfu, P. Marquié, and M. Rosse, Klein-gordon electronic network exhibiting supratransmission effect, Electronics lett. **46**, (2010) 123.

[91] P. G. Kevrekidis, K. Ø. Rasmussen, and A. R. Bishop, The discrete nonlinear Schrödinger equation: a survey of recent results, Internat.l J. of Modern Phys. B **15**, (2001) 2833.

[92] D. N. Christodoulides and R. I. Joseph, Discrete self-focusing in nonlinear arrays of coupled waveguides, Opt. lett. **13**, (1988) 794.

[93] H. S. Eisenberg, et al., Discrete spatial optical solitons in waveguide arrays, Phys. Rev. Lett. **81**, (1998) 3383.

[94] D. N. Christodoulides, F. Lederer, and Y. Silberberg, Discretizing light behaviour in linear and nonlinear waveguide lattices, Nature **424**, (2003) 817.

[95] A. Trombettoni, and A. Smerzi, Discrete solitons and breathers with dilute Bose-Einstein condensates, Phys. Rev. Lett. **86**, (2001) 2353.

[96] G. L. Alfimov, P. G. Kevrekidis, V. V. Konotop, and M. Salerno, Wannier functions analysis of the nonlinear Schrödinger equation with a periodic potential, Phy. Rev. E **66**, (2002) 046608.

[97] F. S. Cataliotti, S. Burger, C. Fort, P. Maddaloni, F. Minardi, A.Trombettoni, and M. Inguscio, Josephson junction arrays with Bose-Einstein condensates, Science **293**, (2001) 843;

M. Greiner, O. Mandel, T. Esslinger, T. W. Hänsch and I. Bloch, Quantum phase transition from a superfluid to a Mott insulator in a gas of ultracold atoms, nature **415**, (2002) 39.

[98] W. Chen, and D. L. Mills, Gap solitons and the nonlinear optical response of super-lattices, Phys. Rev. Lett. **58**, (1987) 160.

D. L. Mills, and S. E. Trullinger, Gap solitons in nonlinear periodic structures, Phys. Rev. B **36**, (1987) 947.

[99] A. B. Togueu Motcheyo, J. D. Tchinang Tchameu, M. Siewe Siewe and C. Tchawoua, Homoclinic nonlinear band gap transmission threshold in discrete optical waveguide arrays, Commun. Nonlinear Sci. Numer. Simulat. **50**, (2017) 29.

[100] B. Bodo, S. Morfu, P. Marquié and B. Z. Essimbi, Noise induced breather generation in a sine-Gordon chain, Journal of Statistical Mechanics: Theory and Experiment **1**, (2009) 01026.

[101] A. B. Togueu Motcheyo, C. Tchawoua, and J. D. Tchinang Tchameu, Supratransmission induced by waves collisions in a discrete electrical lattice, Phys. Rev. E **88**, (2013) 040901.

[102] A. V. Buryak, P. Di Trapani, D. V. Skryabin, and S. Trillo, Optical solitons due to quadratic nonlinearities: from basic physics to futuristic applicatons, Phys. Rep. **370**, (2002) 63.

[103] V. A. Brazhnyi, V. V. Konotop, S. Coulibaly, and M. Taki, Field patterns in periodically modulated optical parametric amplifiers and oscillators, Chaos **17**, (2007) 037111.

[104] T. B. Benjamin, and K. Hasselmann, Instability of periodic wavetrains in nonlinear dispersive systems [and discussion], Proceedings of the Royal Society of London A: Mathematical, Physical and Engineering Sciences **299**, (1967) 1456.

[105] M. I. Carvalho, S. R. Singh and D. N. Christodoulides, Phys. Rev. Lett. **82**, (1999) 394.

[106] J. E. Feir, The disintegration of wave trains on deep water. Part 1. Theory, J. Fluid Mech. **27**, (1967) 417.

[107] G. P. Agrawal, Nonlinear fiber optics, Nonlinear Science at the Dawn of the 21st Century **542**, (2000) 195.

[108] H. C. Yuen and M. L. Bruce, Instabilities of waves on deep water, Annu. Rev. Fluid Mech. **12**, (1980) 303.

[109] P. Janssen, Wave-induced stress and the drag of air flow over sea waves, Journal of Physical Oceanography **19**, (1989) 745.

[110] K. Dysthe, H. E. Krogstad, and P. Müller, Oceanic rogue waves, Annu. Rev. Fluid Mech. **40**, (2008) 287.

[111] V. I. Bespalov and V. I. Talanov, Filamentary structure of light beams in nonlinear liquids, ZhETF Pisma Redaktsiiu **3**, (1966) 471.

[112] M. Soljacic, et al., Modulation instability of incoherent beams in non-instantaneous nonlinear media, Phys. Rev. Lett. **84**, (2000) 467.

[113] K. Detlef, et al., Modulation instability and pattern formation in spatially incoherent light beams, Science **290**, (2000) 495.

[114] J. Klinger, H. Martin, and Z. Chen, Experiments on induced modulational instability of an incoherent optical beam, Optics letters **26**, (2001) 271.

[115] B. Z. Essimbi, L. Ambassa and T. C. Kofane, Gap solitons on a coupled nonlinear transmission line, Physica D **106**, (1997) 207.

[116] B. Z. Essimbi, T. C. Kofane and J. M. Ngundam, Asymmetric gap solitons on a coupled nonlinear transmission line, Phys. Scr. **67**, (2003) 157.

[117] A. Kenfack-Jiotsa and E. Tala-Tebue, Effect of Second-Neighbor Inductive Coupling on the Modulational Instability in a Coupled Line of Transmission, J. Phys. Soc. Jpn **80**, (2011) 034003.

[118] K. Narahara, Head-on collision of solitary waves in coupled Korteweg de Vries systems modeling nonlinear transmission lines, Wave Motion **51**, (2015) 935.

[119] K. Narahara, Asymmetrical solitary waves in coupled nonlinear transmission lines, Wave Motion **58**, (2015) 13.

[120] G. P. Veldes, J. Cuevas, P. G. Kevrekidis, and D. J. Frantzeskakis, Quasidiscrete microwave solitons in a split-ring-resonator-based left-handed coplanar waveguide, Phys. Rev. E **83** (2011) 046608.

[121] P. Panagopoulos, T. Bountis and C. Skokos, Existence and Stability of Localized Oscillations in 1-Dimensional Lattices With Soft-Spring and Hard-Spring Potentials, J. Vib. Acoust. **126**, (2004) 520.

[122] F. Romeo and G. Rega, Periodic and localized solutions in chains of oscillators with softening or hardening cubic nonlinearity, Meccanica **50** (2015) 721.

[123] F. Palmero, R. Carretero-Gonzàlez, J. Cuevas, P. G. Kevrekidis and W. Królikowski, Solitons in one-dimensional nonlinear Schrödinger lattices with a local inhomogeneity, Phys. Rev. E **77**, (2008) 036614.

[124] T. Bountis, H. W. Capel, M. Kollmann, J.C. Ross, J. M. Bergamin, J. P. Van der Weele, Multibreathers and homoclinic orbits in 1-dimensional nonlinear lattices, Phys. Lett. A **268**, (2000) 50.

[125] R. Carretero-Gonzàlez, J. D. Talley, C. Chong and B. A. Malomed, Multistable solitons in the cubic-quintic discrete nonlinear Schrödinger equation, Physica D **216**, (2006) 77.

[126] R. Carretero-Gonzàlez, A Map Approach to Stationary Solutions of the DNLS Equation In: The Discrete Nonlinear Schrödinger Equation, Springer Tracts in Modern Physics **232**, (2009) 221.

[127] A. B. Togueu Motcheyo, C. Tchawoua, M. Siewe Siewe and J. D. Tchinang Tchameu, Multisolitons and stability of two hump solitons of upper cutoff mode in discrete electrical transmission line, Phys. Lett. A **375**, (2011) 1104.

[128] J. D. Tchinang Tchameu, A. B. Togueu Motcheyo and C. Tchawoua, Mobility of discrete multibreathers in the exciton dynamics of the Davydov model with saturable nonlinearities, Phys. Rev. E **90**, (2014) 043203.

[129] S. Anastassiou, T. Bountis and A. Bäcker, Homoclinic points of 2D and 4D maps via the parametrization method, Nonlinearity **30**, (2017) 3799.

[130] A. B. Togueu Motcheyo, M. Kimura, Y. Doi and C. Tchawoua, Supratransmission in discrete one-dimensional lattices with the cubic-quintic nonlinearity, Nonlinear Dyn **95**, (2019) 2461.

[131] P. G. Kevrekidis, The Discrete Nonlinear Schrödinger Equation, Springer-Verlag: Berlin/Heidelberg, Germany, (2009).

[132] I. Daumont, T. Dauxois, M. Peyrard, Modulational instability : first step towards energy localization in nonlinear lattices, Nonlinearity **10**, (1997) 617.

[133] J. E. Macías-Díaz, Numerical study of the transmission of energy in discrete arrays of sine-Gordon equations in two space dimensions, Phys. Rev. E **77**, (2008) 016602;

[134] M. Malishava and R. Khomeriki, All-phononic digital transistor on the basis of gap-soliton dynamics in an anharmonic oscillator ladder, Phys. Rev. Lett. **115**, (2015) 104301.

[135] R. Khomeriki, L. Chotorlishvili, B. A. Malomed, J. Berakdar, Creation and amplification of electromagnon solitons by electric field in nanostructured multiferroics, Phys. Rev. B **91** (2015) 041408.

[136] R. El-Ganainy, K. G. Makris, M. Khajavikhan, Z. H. Musslimani, S. Rotter and D. N. Christodoulides, Non-Hermitian physics and PT symmetry, Nature Phys. **14**, (2018) 11.

[137] A. Chernyavsky and D. E. Pelinovsky, Breathers in Hamiltonian PT -Symmetric Chains of Coupled Pendula under a Resonant Periodic Force, Symmetry **8**, (2016) 59.

List of publications

1- **A. Kamdoum Kuitche**, A. B. Togueu Motcheyo, Thomas Kanaa, C. Tchawoua, ***Supra-transmission in transversely connected nonlinear pendulum pairs***, Chaos, Solitons and Fractals, **160**, (2022) 112196. doi.org/10.1016/ j.chaos.2022.112196 (©-Elsevier, 2022). Impact factor: 9.922.

2- **A. Kamdoum Kuitche**, A. B. Togueu Motcheyo, Thomas Kanaa, C. Tchawoua, ***Modulational instability in transversely connected nonlinear pendulum pairs***, European Physical Journal Plus, **138**, (2023) 142. doi.org/10.1140/ epjp/s13360-023-03761-4 (©- Springer, 2023). Impact factor: 3.758.

3- **A. Kamdoum Kuitche**, A. B. Togueu Motcheyo, Zakari Yaou, Thomas Kanaa, C. Tchawoua, ***Bright soliton propagation with loss and gain phenomena in transversely connected nonlinear pendulum pairs***, Modern Physics Letters B, **147**, (2024) 2450216. doi.org/ 10.1142 /S0217984924502166 (©- World Scientific Publishing Company, 2024). Impact factor: 1.948.

Oral presentations in conferences

1- **A. Kamdoum Kuitche**, A. B. Togueu Motcheyo, Thomas Kanaa, C. Tchawoua, ***Energy transmission in the forbidden band-gap of multicomponent coupled nonlinear pendulum chains***, IOP Institute of Physics, Localization in Condensed Matter, CDM 29 online series, November 17-18, 2021.

2- **A. Kamdoum Kuitche**, A. B. Togueu Motcheyo, Thomas Kanaa, C. Tchawoua, ***Nonlinear supratransmission in transversely connected nonlinear pendulum chains,*** Doctoral seminar 2022, Organized by the Research and Postgraduate Training unit for Physics and Application, April 25-26, 2023.

This is to certify that

KAMDOUM KUITCHE Alex

attended

LCM 2021

on

17/11/2021 to 18/11/2021

THE UNIVERSITY OF YAOUNDE I

P.O. Box : 337 Yaounde
Phone/Fax : +237 222 22 13 20
https://uy1.uninet.cm

This is to certify that

KAMDOUM KUITCHE Alex

participated in and completed the

Doctoral Seminar 2022

Organized by the

Research and Postgraduate Training Unit for Physics and Applications

Postgraduate School of Science Technology and Geosciences

25 - 26 April 2023

Faculty of Science, The University of Yaounde I, Yaounde, Cameroon

Research and Postgraduate Training Unit
for Physics and Applications
Luc C. OWONO OWONO, Coordinator
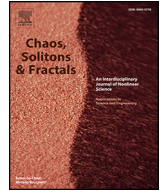
Supratransmission in transversely connected nonlinear pendulum pairs

A. Kamdoum Kuitche [a], A.B. Togueu Motcheyo [b,*], Thomas Kanaa [b], C. Tchawoua [a]

[a] Laboratory of Mechanics, Department of Physics, Faculty of Science, University of Yaounde I, P.O. Box 812, Yaounde, Cameroon
[b] Department of Mechanical Engineering, Higher Technical Teacher's Training College (ENSET) Ebolowa, University of Ebolowa, P.O. Box 886, Ebolowa, Cameroon

ARTICLE INFO

ABSTRACT

In this work, we generate a nonlinear supratransmission phenomenon in a chain of coupled pendulum pairs, where each pendulum is connected to the nearest neighbours in the longitudinal and transverse directions. By considering the angular displacement of one chain proportional to the other, we derive the homoclinic supratransmission threshold amplitude using the two-dimensional map approach which is in agreement with the numerical one; in the case where only one chain is driven. We also consider the case where both chains are driven and perform numerically the supratransmission threshold amplitude of the two chains in the case of the same driven frequency while the phonon amplification is obtained when both lattices are driven with frequencies in different bands. The actual work extends the deep understanding of supratransmission phenomenon in discrete coupled pendulum systems.

1. Introduction

At the beginning of the 21st century, it appeared in the literature an exotic phenomenon called nonlinear supratransmission. The pioneers of this phenomenon namely; Geniet and Leon discovered that a nonlinear system possessing a naturally forbidden bandgap can transmit the energy of a signal with a frequency lying in that forbidden band [1]. They named the process nonlinear supratransmission. The fact that the driving frequency was taken in the forbidden band was not sufficient, the process occurred at a well-defined predictable amplitude called a threshold amplitude.

For more than two decades, the nonlinear supratransmission phenomenon has been studied up to now from different points of view in various physical systems, such as, in sine-Gordon chains [2–5], in Josephson junction [6,7], in Bragg media [8], in discrete nonlinear electrical transmission lines [9–13], in the Fermi-Pasta-Ulam model [14–17], among many other [18–26]. The majority of research on this phenomenon was done on single chains or single-component systems. Even when studied on a multicomponent system, it was rarely a discrete Sine-Gordon one. For example, in [27], supratransmission phenomenon was studied in multicomponent nonintegrable nonlinear systems.

Moreover, knowing that the supratrasnsmission phenomenon occurs at a well-defined threshold amplitude, its prediction is fundamental importance for physical applications. Nowadays, this threshold has

been obtained in single-component systems by making use of explicit solution of the model equation, and looking for its maximum allowed amplitude at the boundary [2,11,13,28] or by using saddle-node bifurcation [29]. Other ways to investigate this amplitude threshold are the nonlinear response manifold technique [30], and the two dimensional (2D) map approach [31]. Also, when the model equation is intractable, a method based on an asymptotic solution obtained by asymptotic series expansion can be developed [27]. Nevertheless, despite all these studies, to the best of our knowledge, no attention was paid to the gap transmission in transversely connected nonlinear pendulum pairs.

In this work, we address a way to generate a gap transmission in a novel multicomponent discrete system which has only quite recently appeared in the literature [32]. The model studied here is the chain of coupled pendulum pairs, where each pendulum is connected to the nearest neighbours in the longitudinal and transverse directions. The equation governing this chain has the feature that, it is a discrete simultaneous one.

The rest of the paper is organized as follows: In Section 2, we present the mathematical model and the linear dispersion relation. In Section 3, we derive from the mathematical model the value of threshold amplitude. In Section 4, we numerically integrate the full governing equation of our model. Finally, a conclusion is given in Section 5.

2. Mathematical description of the model

Inspired by the model presented in [32], we consider a chain of coupled pendulum displayed in Fig. 1, where each pendulum is connected to the nearest neighbours in the longitudinal and transverse directions.

* Corresponding author.
E-mail addresses: kamdoumkuitchealex@yahoo.com (A. Kamdoum Kuitche), abtogueu@yahoo.fr (A.B. Togueu Motcheyo), t_kanaa@yahoo.fr (T. Kanaa), ctchawa@yahoo.fr (C. Tchawoua).
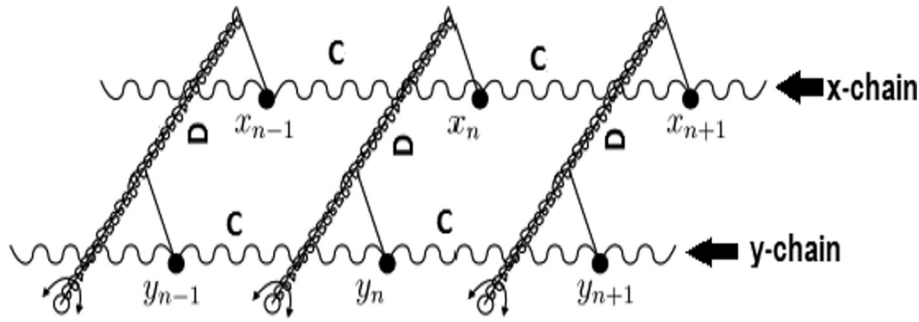
Fig. 1. (Courtesy of Prof D. E. Pelinovsky) A graphical illustration for the chain of coupled pendula [32] where each pendulum is connected to the nearest neighbours in the longitudinal and transverse directions. The positive parameters C and D describe couplings between the nearest pendula in the longitudinal and transverse directions, respectively. The positive parameters C and D describe couplings between the nearest pendula in the longitudinal and transverse directions, respectively.

The Lagrangian in absence of damping for a chain of N pendula can be written as follows:

$$L = \sum_{n=1}^{N} \frac{1}{2}\left(\dot{x}_n^2 + \dot{y}_n^2\right) + \cos(x_n) + \cos(y_n)$$
$$- \frac{1}{2}C(x_{n+1}-x_n)^2 - \frac{1}{2}C(y_{n+1}-y_n)^2$$
$$- \frac{1}{2}D(x_n-y_n)^2, \tag{1}$$

where (x_n, y_n) correspond to the angles in each pair of the two pendula, dots denote derivatives with respect to time t.

Using the Euler-Lagrange's equations, the equations of motion for the nth pendulum in both directions take the following form:

$$\begin{cases} \ddot{x}_n - C(x_{n+1} - 2x_n + x_{n-1}) - D(y_n - x_n) + \sin(x_n) = 0, \\ \ddot{y}_n - C(y_{n+1} - 2y_n + y_{n-1}) - D(x_n - y_n) + \sin(y_n) = 0. \end{cases} \tag{2}$$

In order to derive the linear dispersion relation of the model which serves as a reference and provides basic information on the propagation of the plane waves, we can readily define the nth site of the lattice as a two-component vector (x_n, y_n) and seek a solution in the form of plane waves:

$$(x_n, y_n) = (\gamma, \delta)e^{i(kn-\omega t)}, \tag{3}$$

with $|\gamma| \ll 1$, $|\delta| \ll 1$. ω and k are respectively the angular frequency and wave number.

Substituting Eq. (3) into the linearized form of Eq. (2), we get a linear dispersion relation of the following form:

$$\omega^4 - \left[8C \sin^2\left(\frac{k}{2}\right) + 2(D+1)\right]\omega^2 + [8C(D+1)] \sin^2\left(\frac{k}{2}\right)$$
$$+ 16C^2 \sin^4\left(\frac{k}{2}\right) + (2D+1) = 0. \tag{4}$$

Since Eq. (4) is biquadratic with respect to ω, there may exist two possible modes $\omega_1(k)$ and $\omega_2(k)$ given in the following:

$$\omega_p^2 = 4C \sin^2\left(\frac{k}{2}\right) + (D+1) + (-1)^p D, \quad (p = 1, 2). \tag{5}$$

Fig. 2(a) depicts the modes $\omega_1(k)$ and $\omega_2(k)$ given by Eq. (5) as a function of wave number k and the transverse coupling coefficient D. One can identify two lower cut-off mode frequencies at $k = 0$ given by

$$\omega_{01} = 1,$$
$$\omega_{02} = \sqrt{1 + 2D}, \tag{6}$$

and two upper cut-off frequencies at $k = \pi$ given by

$$\omega_{max\ 1} = \sqrt{4C + 1},$$
$$\omega_{max\ 2} = \sqrt{4C + 2D + 1}. \tag{7}$$

Fig. 2(b) depicts the variation of $\omega_{01,2}$ and $\omega_{max1,2}$ as a function of coupling in the transverse direction. An analogy with the electrical transmission line [33,34] allows identifying the slow mode branch and the fast mode ends at $k = \pi$ by ω_{max1} and ω_{max2} respectively. The angular frequency ω of the slow-mode is within the interval $[\omega_{01}, \omega_{max1}]$, and that of the fast-mode within the range $[\omega_{02}, \omega_{max2}]$. Both branches are separated by an upper "pseudo-gap"(zone 4) of thickness $\Delta\omega_1 = \omega_{max2} - \omega_{max1} > 0$. The slow mode branch starts at ω_{01} and that of the fast mode at ω_{02} when $k = 0$. Both branches are separated by a lower "pseudo-gap" (zone 2) of thickness $\Delta\omega_2 = \omega_{02} - \omega_{01} > 0$. Indeed, $\Delta\omega_1$ and $\Delta\omega_2$ are not the true forbidden bands. The true forbidden bands correspond to zone 1 (true lower forbidden band) and zone 5 (true upper forbidden band) of Fig. 2(b). Observing Fig. 2(b), one can observe in zones 2 and 4 that, when D increases (decreases), the width of the "pseudo-gaps" increases (decreases); the width of the allowed band (zone 3) decreases (increases) as the coupling between the nearest pendula in the transverse direction D increases (decreases).

Generally, on the chain of longitudinally coupled pendula, the nonlinear supratransmission phenomenon appears in the lower forbidden band [1]. In the same way, the zones under consideration will be zones 2 and 1 (to be confirmed in the next section). When the angular frequency is lying in zone 2, it is within the forbidden band of the fast mode and the allowed phonon band of the slow one while in zone 1, it is the forbidden band of both modes. Can the angular frequency with a value taken in the forbidden bands produce nonlinear bandgap transmission in our model? The answer to this question will be found in the next sections. Before, it is worth noticing that the transverse and longitudinal coupled chains studied don't have two wave vectors as the two dimensional lattice [35].

3. Supratransmission threshold

To the best of our knowledge, no analytical solution of Eq. (2) has been reported, due to its discrete aspect. Then, it will be difficult to obtain an analytical threshold of the model. To overcome this situation, we will firstly expand $\sin(x_n)$ and $\sin(y_n)$ in Taylor series up to the third order. Then, Eq. (2) turn to
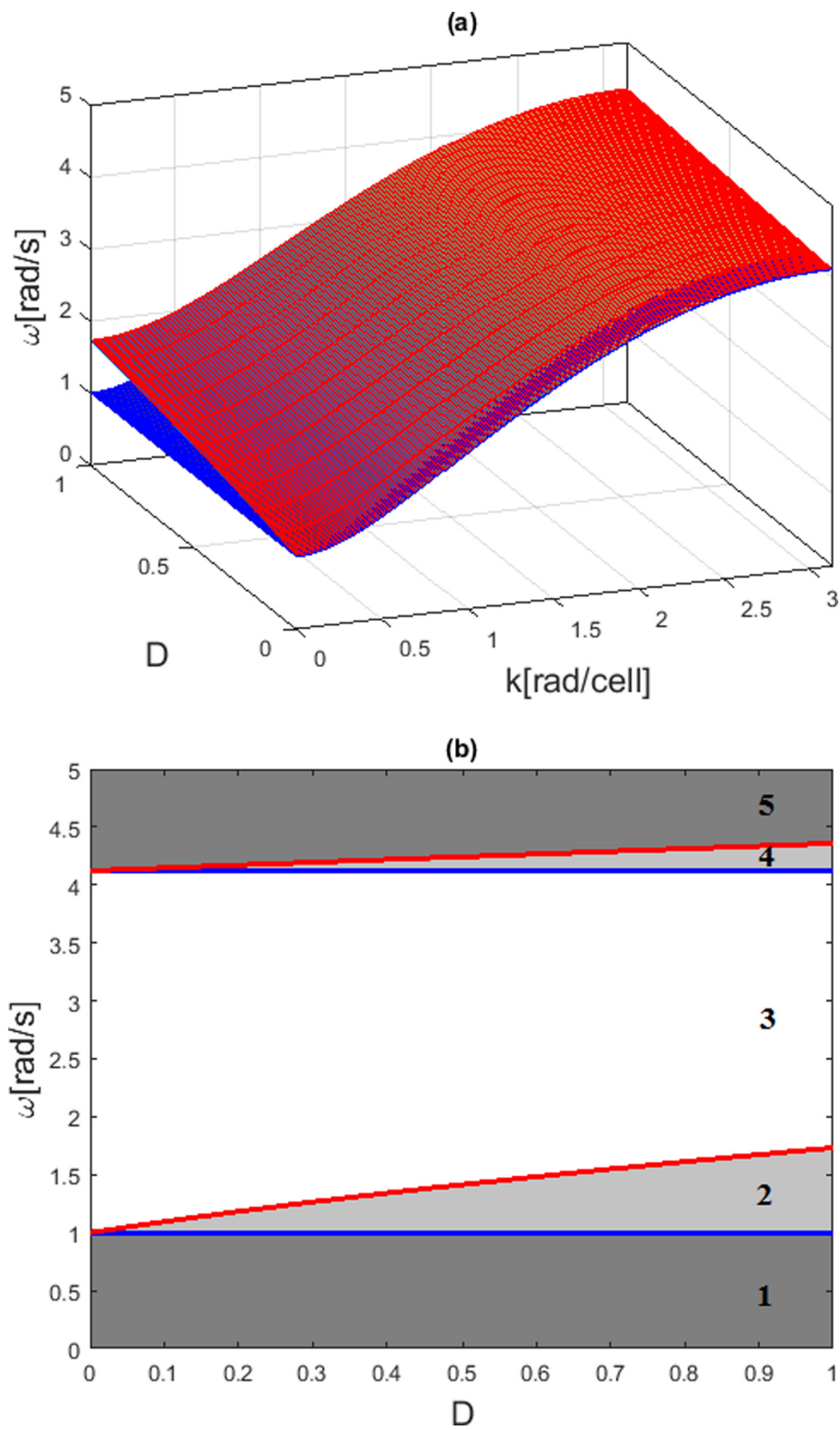
Fig. 2. Graphs of linear dispersion relation for $C = 4$. (a) the red (top) curve represents the fast mode branch while the curve generated by the slow mode branch is in blue (bottom). (b) 2D Representation of linear dispersion relation, where we have five zones namely; (1): lower forbidden band, (2): lower "pseudo-gap", (3): allowed band, (4): upper "pseudo-gap", (5): true upper forbidden band. (For interpretation of the references to colour in this figure legend, the reader is referred to the web version of this article.)

$$\begin{cases} \ddot{x}_n - C(x_{n+1} - 2x_n + x_{n-1}) - D(y_n - x_n) + \left(x_n - \frac{1}{6}x_n^3\right) = 0, \\ \ddot{y}_n - C(y_{n+1} - 2y_n + y_{n-1}) - D(x_n - y_n) + \left(y_n - \frac{1}{6}y_n^3\right) = 0. \end{cases} \quad (8)$$

Secondly, considering the angular displacement of $x - chain$ proportional to that of $y - chain$, mathematically expressed as $y_n = \lambda x_n$, where λ is the constant of proportionality, Eq. (8) becomes:

$$\begin{cases} \ddot{x}_n - C(x_{n+1} - 2x_n + x_{n-1}) - D(\lambda - 1)x_n + x_n - \frac{1}{6}x_n^3 = 0, \\ \lambda\ddot{x}_n - \lambda C(x_{n+1} - 2x_n + x_{n-1}) - D(1 - \lambda)x_n + \lambda x_n - \frac{\lambda^3}{6}x_n^3 = 0. \end{cases} \quad (9)$$

The two equations of this simultaneous equation are identical if and only if $\lambda = \pm 1$. When $\lambda = 1$, the effect of transverse coupling parameter vanishes. The equation will become the Klein-Gordon found in [1]. In the following, we are going to be focused on the case where $\lambda = -1$ such as to take into account the transverse coupling parameter. Thus, Eq. (9) lead to a single discrete equation given by

$$\ddot{x}_n - C(x_{n+1} - 2x_n + x_{n-1}) + (2D+1)x_n - \frac{1}{6}x_n^3 = 0, \quad (10)$$

which is identical to a one-dimensional lattice modelling a simple mass and spring chain where the time periodic solution can be obtained by assuming the harmonic solution $x_n = u_n \cos(\omega t)$ (see Refs. [36,37]). Inserting the latest harmonic solution into Eq. 10, and by keeping the terms proportional to $\cos(\omega t)$, we obtain a steady state equation in the form:

$$\alpha u_n + C(u_{n+1} - 2u_n + u_{n-1}) + \beta u_n^3 = 0, \quad (11)$$

with $\alpha = \omega^2 - 2D - 1$ and $\beta = \frac{1}{8}$.

Following the way developed in Refs. [31,36–45] the two dimensional map corresponding to the previous steady state equation can be written as

$$u_{n+1} = \left(2 - \frac{\alpha}{C}\right)u_n - \frac{\beta}{C}u_n^3 - v_n, \quad v_{n+1} = u_n. \quad (12)$$
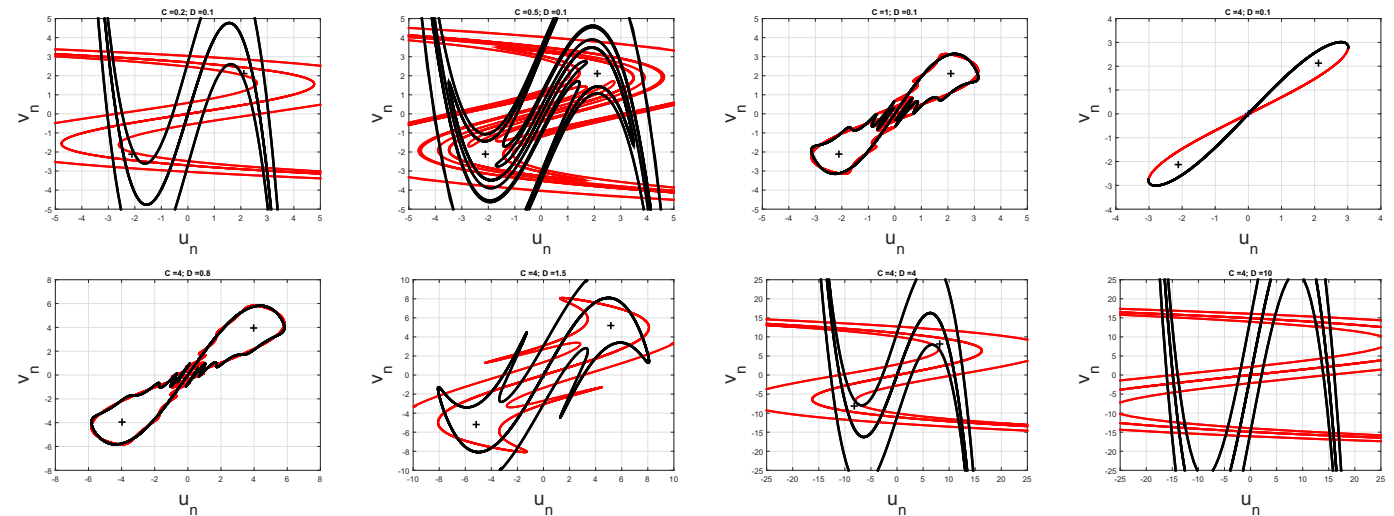
In order to confirm whether the driving frequency will be taken in the lower forbidden band as aforementioned at the end of Section 2, we are going to study the fixed points of the 2D map (Eq. (12)). To do so, we consider that, $u_{n+1} = u_{n-1} = u_n = v_{n+1} = v_n = u$. Then, Eq. (12) leads to

$$u_0 = 0 \quad \text{and} \quad u_\pm = \pm\sqrt{8(2D + 1 - \omega^2)}. \quad (13)$$

$u_\pm$ exists if and only if $2D + 1 - \omega^2 > 0$ that is, for $\omega < \sqrt{2D + 1}$. This confirms the fact that, the lower forbidden band of Fig. 2 is the zone where gap transmission takes place. Thus, we are going to be focused on the true lower forbidden band (zone 1 Fig. 2(b)). In the following, we will consider $\omega = 0.8$ belonging to the true lower forbidden band.

The homoclinic tangle progression of the 2D map (Eq. (12)) while varying the dispersion coefficient C and transverse coupling D is displayed in Fig. 3 for $\omega = 0.8$. The details of the construction can be found in Ref. [42]. The dispersion coefficient increases from left to right in the first line of the Fig. 3 while the transverse coupling D is constant: The homoclinic intersections start with the much richer structure to one homoclinic solution which can be associated with the continuous solution. The transverse coupling D increases from left to right in the second line of the Fig. 3 while the dispersion coefficient D is constant: we can observe the inverse effect of the first line. The richer structure of homoclinic connection increases with a constant transverse coupling. It had been demonstrated in ref. [31] that the case of the rich homoclinic connection corresponds to the case where the frequency is far from the cutoff frequency while one homoclinic solution corresponds to the frequency close to the cutoff frequency. However, in the supratransmission phenomenon, good transmission is ensured when the frequency is close to the cutoff frequency. To be in agreement with this fact, we consider the main homoclinic connection of the 2D map (12) for $D = 0.1$, and $C = 4$ as depicted in Fig. 4. In a similar way as in Ref. [31], we obtain the homoclinic supratransmission threshold amplitude equal to 3.013 (red line of Fig. 4). In the next section, the obtained threshold will be verified by numerical simulations.

4. Numerical experiment

In this section, numerical studies are carried out on the discrete coupled pendulum pairs of Fig. 1 by integrating Eq. (2) with a small

Fig. 3. (First line) Homoclinic tangle progression of the 2D map Eq. (12) as a function of dispersion coefficient C for D = 0.1 and $\omega = 0.8$: the dispersion coefficient increases from left to right; (Second line) Homoclinic tangle progression of the 2D map Eq. (12) as a function of transverse coupling D for C = 4 and $\omega = 0.8$: the transverse coupling increases from left to right.
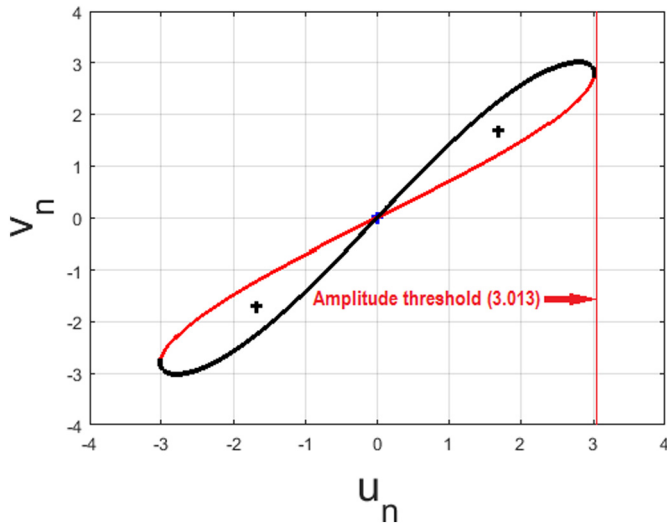
Fig. 4. Homoclinic connection of the 2D map Eq. (12) for $D = 0.1$, $C = 4$, and $\omega = 0.8$. Red line corresponds to the supratransmission threshold amplitude. (For interpretation of the references to colour in this figure legend, the reader is referred to the web version of this article.)

transverse coupling parameter $D = 0.1$ and longitudinal coupling parameter $C = 4$. The chains will be submitted to the following boundary driving conditions:

$$x_0(t) = A \cos(\omega_1 t) \quad \text{and} \quad y_0(t) = B \cos(\omega_2 t), \quad (14)$$

where $A(B)$ and $\omega_1(\omega_2)$ are respectively the driving amplitude of the $x - chain(y - chain)$ and the driving frequency of the chains. The external driving amplitudes A and B are gradually given from zero to their maximum values so as to avoid initial shock. In the followings, we will be considered three cases:

- Only one chain is driven. The driving conditions (14) become:

$$x_0(t) = A \cos(\omega_1 t) \quad \text{and} \quad y_0(t) = 0. \quad (15)$$

When the driving frequency belongs to the allowed band, a small driving amplitude ($A = 0.0001$) will produce an energy flow in both chains as illustrated in Fig. 5. One can see in the same figure the transfer of intensity from $x - chain$ to $y - chain$.

The threshold amplitude obtained from the homoclinic connection of the two-dimensional (2D) map (12) (see Fig. 4) is $A_{th} = 3.013$ for the driven frequency $\omega = 0.8$ lying in the true lower forbidden band. In order to validate this homoclinic supratranmission threshold, we consider two values of A around the value of A_{th} that is one slightly below and another slightly above and we get the following observations namely; When the amplitude is just less than 3.013 that is $A = 3.012$ each chain exhibits an evanescent wave as represented in Fig. 6. Thus, no energy flows in both chains. When the amplitude is slightly beyond the homoclinic threshold amplitude of $x - chain$ that is $A = 3.014$, an energy suddenly flows in $x - chain$ and energy even if it is small is transmitted in the form of a wave in $y - chain$ (see the bottom panel of Fig. 7). Then, both chains generate soliton solutions as displayed in Fig. 7.

- The two chains are driven at the origin. The driven boundary conditions are given by (14) with A and B different to zero. For this case, the numerical threshold amplitude for each chain becomes smaller
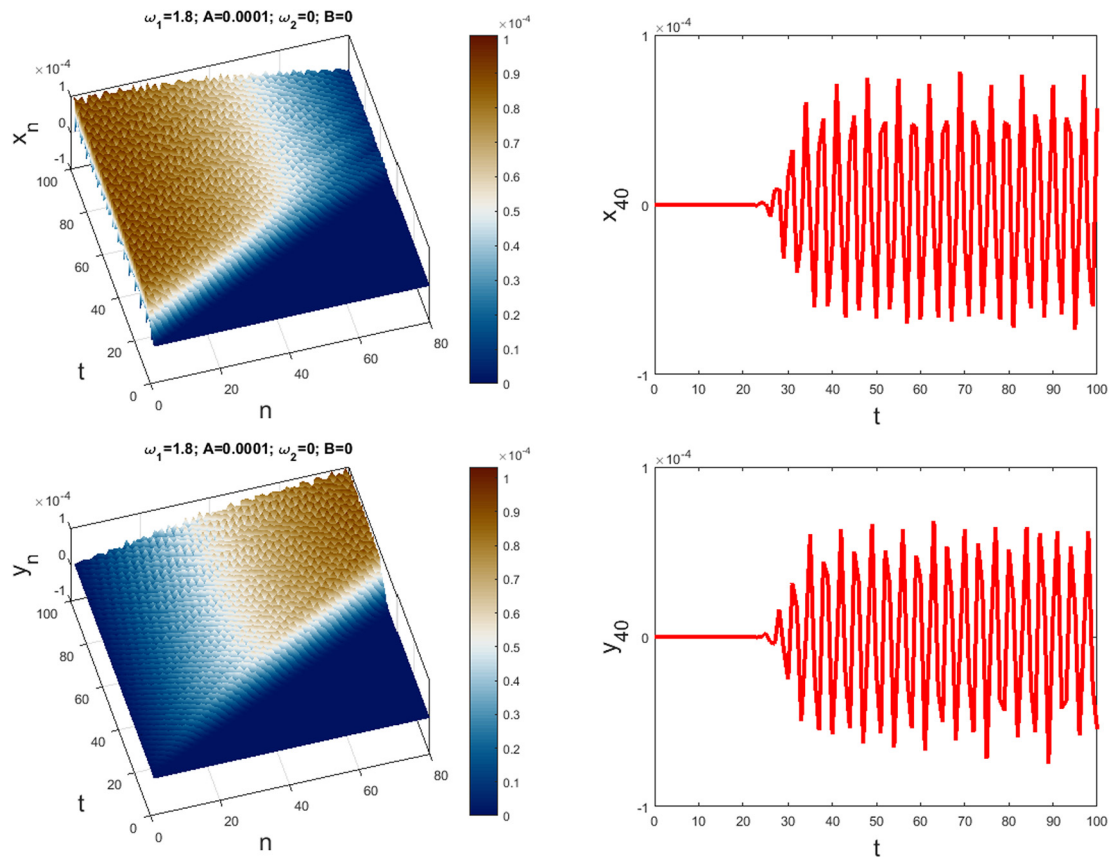
Fig. 5. Graphs showing the evolution of the coupled chain with respect to time for the driving angular frequencies of the two chains $\omega = 1.8$ and the driving amplitude $A = 0.0001$. The first line corresponds to the behavior of $x - chain$ and the second line to the behavior of $y - chain$. One can see the intensity transmits to remote sites in the both chains.
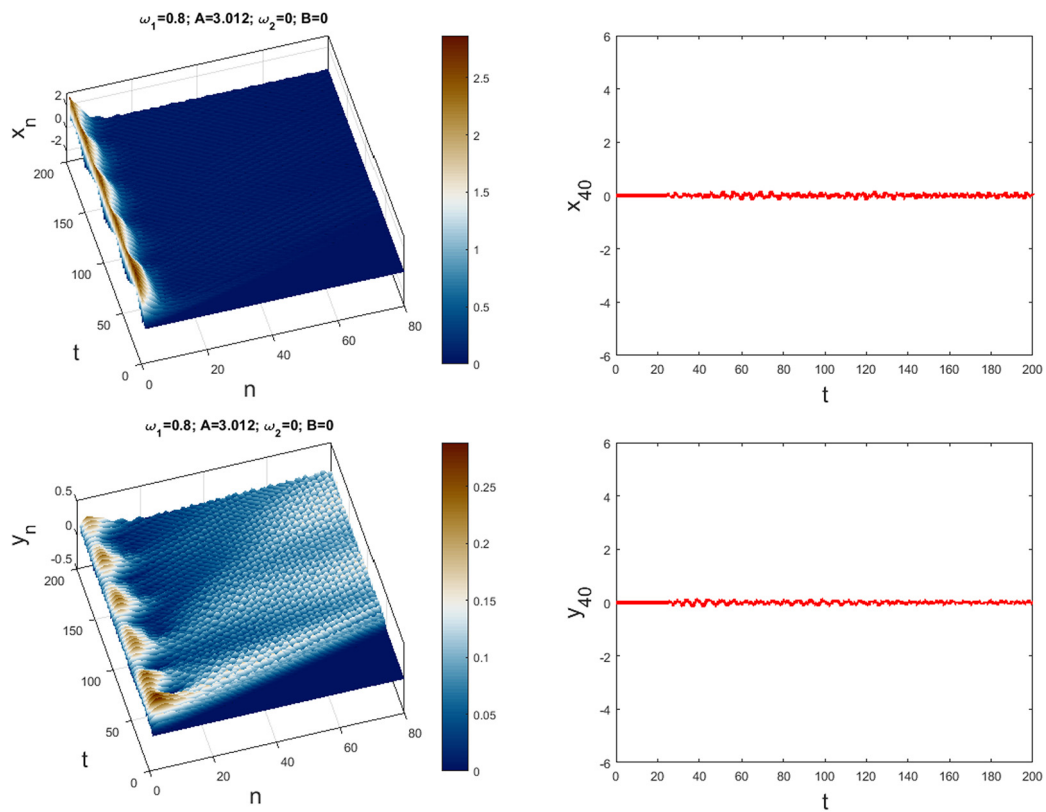
Fig. 6. Graphs showing the evolution of the coupled chain with respect to time for the driving angular frequencies of the two chains $\omega = 0.8$ and the driving amplitude slightly below the threshold $A = 3.012 < A_{th}$. The up panel correspond to the behavior of $x - chain$ and the down panel to the behavior of $y - chain$.
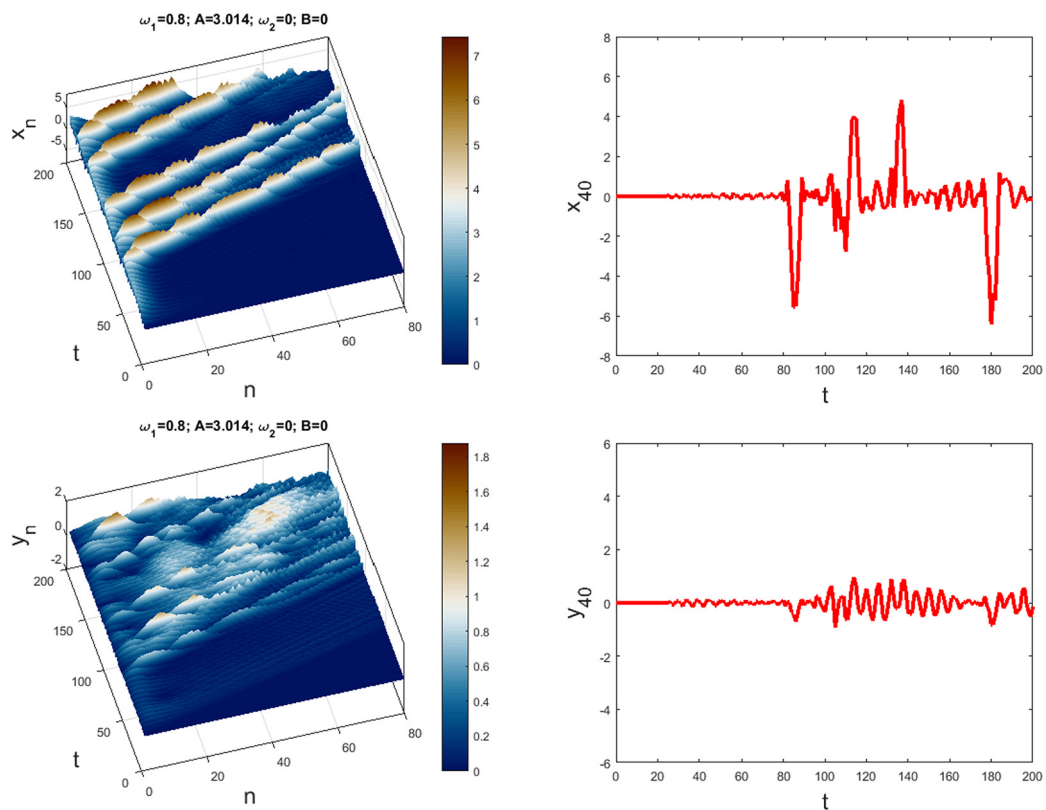
Fig. 7. Graphs showing the evolution of the coupled chain with respect to time for the driving angular frequencies of the two chains $\omega = 0.8$ and the driving amplitude slightly above the threshold $A = 3.014 > A_{th}$. The up panel correspond to the behavior of $x - chain$ and the down panel to the behavior of $y - chain$.
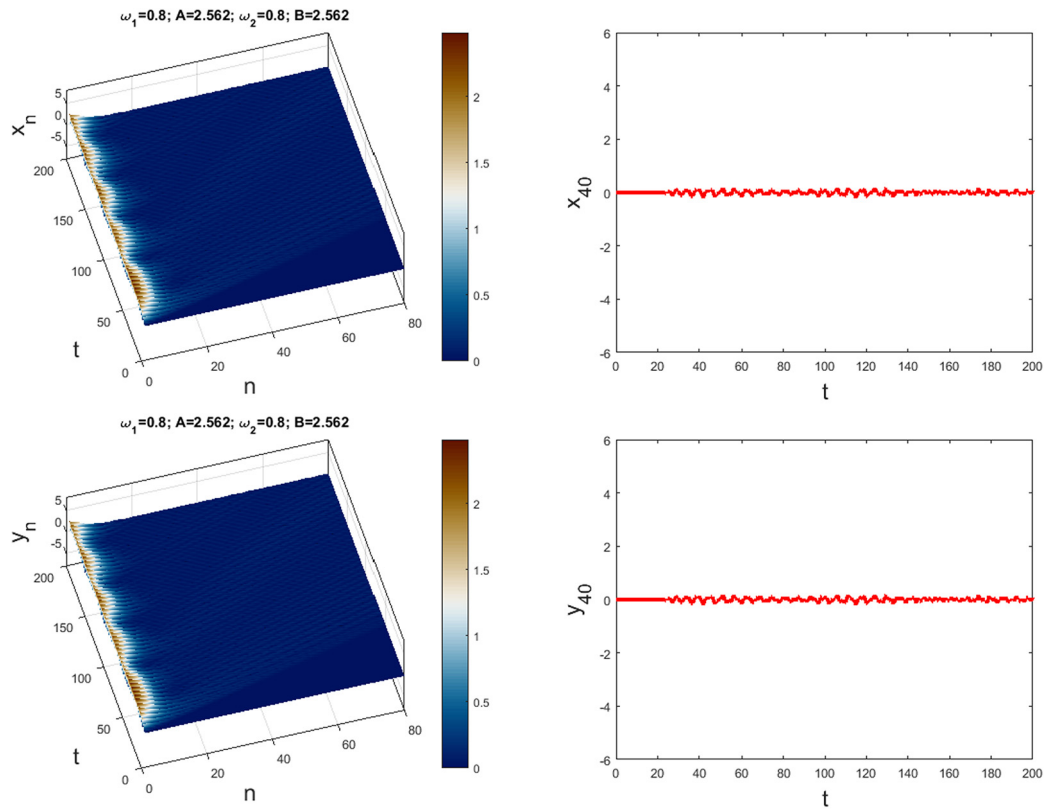
Fig. 8. Graphs showing the evolution of the coupled chain with respect to time for the driving angular frequencies of the two chains $\omega = 0.8$ and the driving amplitudes slightly below the threshold $A = 2.562 < A_{th}$ and $B = 2.562 < B_{th}$. The up panel correspond to the behavior of $x - chain$ and the down panel to the behavior of $y - chain$.


Fig. 9. Graphs showing the evolution of the coupled chain with respect to time for the driving angular frequencies of the two chains $\omega = 0.8$ and the driving amplitudes slightly above the threshold $A = 2.564 > A_{th}$ and $B = 2.564 > B_{th}$. The up panel correspond to the behavior of $x - chain$ and the down panel to the behavior of $y - chain$.

ω_1=1.2; A=0.9; ω_2=0.8; B=3

ω_1=1.2; A=0.9; ω_2=0.8; B=3
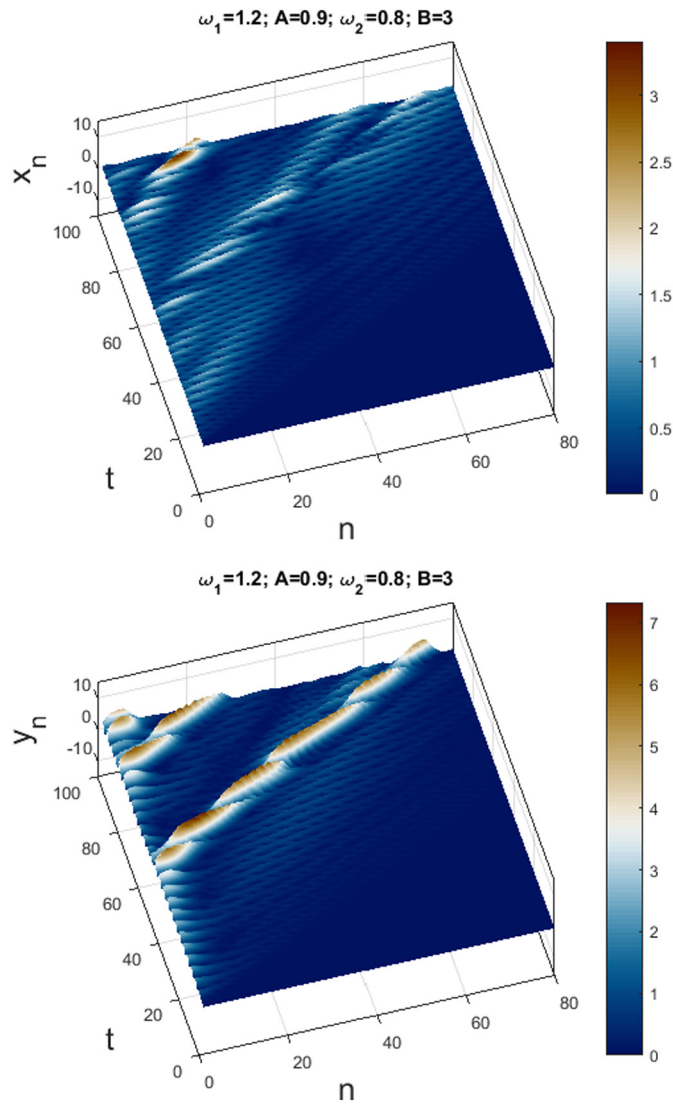
Fig. 10. Graphs showing the evolution of the coupled chain with respect to time for the driving angular frequency of the $x - chain$ $\omega_1 = 1.2$ and the driving amplitudes A = 0.9. $y - chain$ is driven with $\omega_2 = 0.9$ and the driving amplitude B = 3.0 (below amplitude threshold). The up panel correspond to the behavior of $x - chain$ and the down panel to the behavior of $y - chain$.

than the above homoclinic threshold amplitude. Due to the difficulty to obtain a common analytical threshold amplitude for each chain, we find it numerically and get it for both chains and for the same values of driving frequency in the lower forbidden band ($\omega = 0.8$), $A_{th} = 2.563$ and $B_{th} = 2.563$. We observe that when the amplitudes are less than 2.563 each chain exhibits an evanescent wave as represented in Fig. 8. When the amplitudes are slightly beyond the threshold amplitudes, the supratransmission phenomenon occurs as displayed in Fig. 9.

- The two chains are driven at the origin with different frequencies. Here, $x - chain$ is driven with $\omega_1 = 1.2$ taken in the allowed band and the driving amplitude A = 0.9 while $y - chain$ is driven with $\omega_2 = 0.9$ and amplitude B = 3.0 below the homoclinic threshold. One would normally observe an evanescent wave in the $y - chain$ but curiously, the intensity transmits to remote sites as seen in Fig. 10. That is due to the collision between the travelling wave from the phonon band ($x - chain$) and the evanescent wave from the bandgap ($y - chain$) because of the transverse coupling of the chains. The same phenomenon has been observed in discrete electrical lattice [28] but with both left and right edges excited. The

phenomenon is also qualitatively identical to the amplification of phonons by phonons on the basis of a nonlinear band-gap transmission process as in Refs. [46] and the amplification of magnetic pulses by an electric field with a frequency close to the band edge of the magnetic branch [47].

Besides the transmission of binary information and the detection of the weak signal, which are part of the applications of the supratransmission phenomenon, the results of this work enriched the applications in the case where the signal amplifier in lattice could be avoided by using an input signal in another lattice transversally coupled by the original lattice.

5. Conclusion

In this paper, we have considered nonlinear discrete coupled pairs of pendulum chains connected to the nearest neighbours in the longitudinal and transverse directions. This novel model has been used to investigate for the first time the nonlinear supratransmission phenomenon in the common lower forbidden bandgap of the two pendulum chains. We used Euler-Lagrange's equations to derive the equation governing the motion for the nth pendulum in both directions. We used the obtained equation to look into the supratransmission threshold amplitude. To do so, we have employed the two-dimensional map approach to determine the amplitude and the numerical result confirmed the validity of the obtained homoclinic supratransmission threshold amplitude for the case where only one chain was driven. We also numerically performed the supratransmission threshold amplitude in the case where the two chains were driven. This work opens the way to understanding supratransmission phenomenon in multicomponent discrete systems. Another interest in the future will be to see the effect of transverse direction with common string [48,49] on the nonlinear bandgap phenomenon.

CRediT authorship contribution statement

AKK: analytical and numerical studies, Methodology, Software, writing original draft.
ABTM: conceptualization, analytical and numerical studies, Software, writing original draft, validation, writing-review and editing.
TK: conceptualization, validation, supervision.
CT: conceptualization, validation, supervision.

Declaration of competing interest

The authors declare that they have no known competing financial interests or personal relationships that could have appeared to influence the work reported in this paper.

References

[1] Geniet F, Leon J. Energy transmission in the forbidden band gap of a nonlinear chain. Phys Rev Lett. 2002;89:134102.

[2] Geniet F, Leon J. Nonlinear supratransmission. J Phys Condens Matter. 2003;15:2933.

[3] Macías-Díaz JE. Numerical study of the transmission of energy in discrete arrays of sine-Gordon equations in two space dimensions. Phys Rev E. 2008;77:016602.

[4] Macías-Díaz JE. Numerical study of the process of nonlinear supratransmission in riesz space-fractional sine-Gordon equations. Commun Nonlinear Sci Numer Simulat. 2017;46:89.

[5] Macías-Díaz JE, Togueu Motcheyo AB. Energy transmission in nonlinear chains of harmonic oscillators with long-range interactions. Results Phys. 2020;18:103210.

[6] Chevriaux D, Khomeriki R, Leon J. Theory of a Josephson junction parallel array detector sensitive to very weak signals. Phys Rev B. 2006;73:214516.

[7] Macías-Díaz JE. Persistence of nonlinear hysteresis in fractional models of Josephson transmission lines. Commun Nonlinear Sci Numer Simulat. 2018;53:31.

[8] Leon J, Spire A. Gap soliton formation by nonlinear supratransmission in Bragg media. Phys Lett A. 2004;327:474–80.

[9] Yamgoué SB, Morfu S, Marquié P. Noise effects on gap wave propagation in a nonlinear discrete LC transmission line. Phys Rev E. 2007;75:036211.

[10] Koon KTse Ve, Leon J, Marquié P, Tchofo-Dinda P. Cutoff solitons and bistability of the discrete inductance-capacitance electrical line: theory and experiments. Phys Rev E. 2007;75:066604.
Koon KTse Ve, Marquié P, Dinda PTchofo. Experimental observation of the generation of cutoff solitons in a discrete LC nonlinear electrical line. Phys Rev E. 2007;90:052901.

[11] Togueu Motcheyo AB, Tchawoua C, Siewe Siewe M, Tchinang Tchameu JD. Supratransmission phenomenon in a discrete electrical lattice with nonlinear dispersion. Commun Nonlinear Sci Numer Simulat. 2013;18:946–52.

[12] Kenmogne F, Ndombou GB, Yémélé D, Fomethe A. Nonlinear supratransmission in a discrete nonlinear electrical transmission line: modulated gap peak solitons. Chaos Solitons Fractals. 2015;75:263.

[13] Togueu Motcheyo AB, Tchawoua C, Macías-Díaz JE. On the wave transmission in a discrete nonlinear left-handed electrical lattice. Waves Random Complex Media. 2020. https://doi.org/10.1080/17455030.2020.1859166.

[14] Khomeriki R, Lepri S, Ruffo S. Nonlinear supratransmission and bistability in the Fermi-pasta-ulam model. Phys Rev E. 2004;70:066626.

[15] Dauxois T, Khomeriki R, Ruffo S. Modulational instability in isolated and driven Fermi-Pasta-Ulam lattices. Eur Phys J Spec Top. 2007;147:3.

[16] Macías-Díaz JE. Numerical simulation of the nonlinear dynamics of harmonically driven riesz-fractional extensions of the Fermi-Pasta-Ulam chains. Commun Nonlinear Sci Numer Simulat. 2018;55:248.

[17] Macías-Díaz JE, Bountis A. Supratransmission in -Fermi-Pasta-Ulam chains with different ranges of interactions. Commun Nonlinear Sci Numer Simulat. 2018;63:307.

[18] Togueu Motcheyo AB, Macías-Díaz JE. Energy transmission in the forbidden band-gap of a nonlinear chain with global interactions. J Phys A Math Theor. 2020;53:505701.

[19] Khomeriki R. Nonlinear band gap transmission in optical waveguide arrays. Phys Rev Lett. 2004;92:063905.

[20] Lydon J, Theocharis G, Daraio C. Nonlinear resonances and energy transfer in finite granular chains. Phys Rev E. 2015;91:023208.

[21] Alima R, Morfu S, Marquié P, Bodo B, Essimbi B. Influence of a nonlinear coupling on the supratransmission effect in modified sine-Gordon and klein-Gordon lattices. Chaos Solitons Fractals. 2017;100:91.

[22] Zhang Q, Fang H, Xu J. Programmable stopbands and supratransmission effects in a stacked Miura-origami metastructure. Phys Rev E. 2020;101:042206.

[23] Frazier MJ, Kochmann DM. Band gap transmission in periodic bistable mechanical systems. J Sound Vib. 2017;388:315.
Pechac JE, Frazier MJ. Non-reciprocal supratransmission in mechanical lattices with non-local feedback control interactions. Crystals. 2017;11:94.

[24] Macías-Díaz JE, Bountis A. Nonlinear supratransmission in quartic hamiltonian lattices with globally interacting particles and on-site potentials. J Comput Nonlinear Dynam. 2021;16:021001.

[25] Tao F, Chen W, Pan J, Xu Wen, Du Sidan. Experimental observation on asymmetric energy flux within the forbidden frequency band in the LC transmission line. Chaos Solitons Fractals. 2012;45:810.
Tchinang Tchameu JD, Tchawoua C, Togueu Motcheyo AB. Nonlinear supratransmission of multibreathers in discrete nonlinear Schrodinger equation with saturable nonlinearities. Wave Motion. 2012;65:112.
Watanabe Y, Nishida T, Doi Y, Sugimoto N. Experimental demonstration of excitation and propagation of intrinsic localized modes in a mass–spring chain. Phys Lett A. 2012;382:1957.
Watanabe Y, Nishimoto M, Shiogama C. Experimental excitation and propagation of nonlinear localized oscillations in an air-levitation-type coupled oscillator array. Nonlinear Theory Appl IEICE. 2012;8:146. https://doi.org/10.1587/nolta.8.146.

Macías-Dáz JE. Nonlinear wave transmission in harmonically driven Hamiltonian sine-Gordon regimes with memory effects. Chaos Solitons Fractals. 2012;142:110362.

[26] Lutsenko IS, Zakharov PV, Starostenkov MD, Dmitriev SV, Korznikova EA. Stability of supratransmission waves in a crystal of A3B stoichiometry upon interaction with single dislocations. J Phys Conf Ser. 2021;2103:012079.

[27] Anghel-Vasilescu P, Dorignac J, Geniet F, Leon J, Taki M. Nonlinear supratransmission in multicomponent systems. Phys Rev Lett. 2010;105:074101.

[28] Togueu Motcheyo AB, Tchawoua C, Tchinang Tchameu JD. Supratransmission induced by waves collisions in a discrete electrical lattice. Phys Rev E. 2013;88:040901.

[29] Susanto H. Boundary driven waveguide arrays: supratransmission and saddle-node bifurcation. SIAM J Appl Math. 2008;69:111–25.
Susanto H, Karjanto N. Calculated threshold of supratransmission phenomena in waveguide arrays with saturable nonlinearity. J Nonlinear Opt Phys Mater. 2008;17:159.

[30] Kopidakis G, Aubry S. Discrete breathers and delocalization in nonlinear disordered systems. Phys Rev Lett. 2000;84:3236.

[31] Togueu Motcheyo AB, Tchinang Tchameu JD, Siewe Siewe M, Tchawoua C. Homoclinic nonlinear band gap transmission threshold in discrete optical waveguide arrays. Commun Nonlinear Sci Numer Simulat. 2017;50:29.

[32] Destyl E, Nuiro SP, Pelinovsky DE, Poullet P. Coupled pendula chains under parametric PT-symmetric driving force. Phys Lett A. 2017;381:3884–92.

[33] Essimbi BZ, Ambassa L, Kofane TC. Gap solitons on a coupled nonlinear transmission line. Physica D. 1997;106:207.

[34] Essimbi BZ, Kofane TC, Ngundam JM. Asymmetric gap solitons on a coupled nonlinear transmission line. Phys Scr. 2003;67:157–63.

[35] Macías-Díaz JE. Numerical study of the transmission of energy in discrete arrays of sine-Gordon equations in two space dimensions. Phys Rev E. 2008;77:016602.
Macías-Díaz JE. Bit propagation in (2+1)-dimensional systems of coupled sine-Gordon equations. Commun Nonlinear Sci Numer Simulat. 2008;14:1025–31.
Macías-Díaz JE. On the controlled propagation of wave signals in a sinusoidally forced two-dimensional continuous frenkel-kontorova model. Wave Motion. 2008;48:13.

[36] Panagopoulos P, Bountis T, Skokos C. Existence and stability of localized oscillations in 1-dimensional lattices with soft-spring and hard-spring potentials. J Vib Acoust. 2004;126(4):520.

[37] Romeo F, Rega G. Periodic and localized solutions in chains of oscillators with softening or hardening cubic nonlinearity. Meccanica. 2015;50:721.

[38] Bountis T, Capel HW, Kollmann M, Ross JC, Bergamin JM, Van der Weele JP. Multibreathers and homoclinic orbits in 1-dimensional nonlinear lattices. Phys Lett A. 2000;268:50.

[39] Carretero-Gonzàlez R, Talley JD, Chong C, Malomed BA. Multistable solitons in the cubic-quintic discrete nonlinear Schrödinger equation. Physica D. 2006;216:77.

[40] Palmero F, Carretero-Gonzàlez R, Cuevas J, Kevrekidis PG, Królikowski W. Solitons in one-dimensional nonlinear Schrödinger lattices with a local inhomogeneity. Phys Rev E. 2008;77:036614.

[41] Carretero-Gonzàlez R. A map approach to stationary solutions of the DNLS equation. The discrete nonlinear Schrödinger equation. Springer tracts in modern physics, vol 232. Berlin, Heidelberg: Springer; 2009.https://doi.org/10.1007/978-3-540-89199-4-11.

[42] Togueu Motcheyo AB, Tchawoua C, Siewe Siewe M, TchinangTchameu JD. Multisolitons and stability of two hump solitons of upper cutoff mode in discrete electrical transmission line. Phys Lett A. 2011;375:1104.

[43] Tchinang Tchameu JD, Togueu Motcheyo AB, Tchawoua C. Mobility of discrete multibreathers in the exciton dynamics of the davydov model with saturable nonlinearities. Phys Rev E. 2014;90:043203.

[44] Anastassiou S, Bountis T, Bäcker A. Homoclinic points of 2D and 4D maps via the parametrization method. Nonlinearity. 2017;30:3799.

[45] Togueu Motcheyo AB, Kimura M, Doi Y, Tchawoua C. Supratransmission in discrete one-dimensional lattices with the cubic-quintic nonlinearity. Nonlinear Dyn. 2019;95:2461.

[46] Malishava M, Khomeriki R. All-phononic digital transistor on the basis of gap-soliton dynamics in an anharmonic oscillator ladder. Phys Rev Lett. 2015;115:104301.

[47] Khomeriki R, Chotorlishvili L, Malomed BA, Berakdar J. Creation and amplification of electromagnon solitons by electric field in nanostructured multiferroics. Phys Rev B. 2015;;91 041408(R).

[48] Chernyavsky A, Pelinovsky DE. Breathers in hamiltonian PT -symmetric chains of coupled pendula under a resonant periodic force. Symmetry. 2016;8(7):59. https://doi.org/10.3390/sym8070059.

[49] Chernyavsky A, Pelinovsky DE. Long-time stability of breathers in Hamiltonian PT-symmetric lattices. J Phys A Math Theor. 2016;49:475201.

Regular Article

Modulational instability in transversely connected nonlinear pendulum pairs

A. Kamdoum Kuitche[1,a], A. B. Togueu Motcheyo[1,2,b] (iD), Thomas Kanaa[2,c], C. Tchawoua[1,d]

[1] Laboratory of Mechanics, Department of Physics, Faculty of Science, University of Yaounde I, P.O. Box 812, Yaoundé, Cameroon
[2] Department of Mechanical Engineering, Higher Technical Teacher's Training College (ENSET) Ebolowa, University of Ebolowa, P.O. Box 886, Ebolowa, Cameroon

Abstract In this work, we investigate the modulational instability (MI) phenomenon in a chain of coupled pendulum pairs, where each pendulum is connected to the nearest neighbors in the longitudinal and transverse directions. Based on the obtained equation describing the dynamics of the model, we derive the coupled discrete nonlinear Schrödinger equation using the multiple scale method. We use the obtained coupled discrete nonlinear Schrödinger equation to study the possibility of modulational instability. The linear stability analysis leads us to obtain the growth rate of the MI. It reveals that the instability growth rate and MI band are dramatically affected by the transverse coupling parameter. Finally, we use the MI analysis to study the dynamics of the generated unstable plane wave solutions numerically. This confirms that the existence of MI in the lattice leads to the breakup of wave into periodic localized pulses which have the shape of soliton-like objects.

1 Introduction

In the 1960s, it has been discovered in the literature an exotic phenomenon called modulational instability (MI). It is widely believed that the phenomenon was first discovered and modeled for periodic gravity waves in deep water by Brooke Benjamen and Jim Feir in 1967 [1]. However, spatial MI of high-power lasers in organic solvents was observed in 1965 [2] and the mathematical derivation of MI was published in 1966 [3]. Up to now, MI is a widespread and well-known type of instability that has appeared in most nonlinear wave systems in nature such as nonlinear electrical transmission lines [4–9], molecular chains [10–14], Frenkel–Kontorova [15], dark matter halos [16], model neural models [17, 18], plasma waves [19], optical fibers [20], hydrodynamics waves [21], Bose–Einstein condensates [22–24], and biological systems [25, 26]. The aforementioned phenomenon is due to the interplay between nonlinearity and dispersion or diffraction and is characterized by small amplitude and phase perturbations growing exponentially. Moreover, this interplay can help the generation of spectral sidebands and the eventual breakup of the waveform into a train of pulses [27, 28]. That is, MI can be considered a suitable precursor to the formation of soliton trains. One of the systems in nature in which the interplay between nonlinearity and dispersion can exist is the coupled pendulum model.

Coupled pendulum models and their properties are fundamental in theoretical physics and can be used to model many interesting phenomena such as the intrinsic localized modes in lattices [29, 30], solitons in Josephson junction [31] and fluid mechanics [32–34], among many others [35–37]. Moreover, there has been great interest in the application of MI in single-coupled pendulum chains. For example, the examination of the development of MI has been found in a horizontally shaken pendulum chain [38]. Also, the destructive interference of MI has been studied in [39]. It is important to point out that discrete MI attracted attention in diverse branches of physical and biological science due to its numerous applications [40–42]. In the domain of MI on discrete systems, the majority of research has been devoted to single-component systems.

Nevertheless, many interesting coupled ladders have been studied up to now from different points of view. For example, in continuous limit, spatial and temporal soliton [43] and breathers [44] were realized in the PT-symmetric coupler with gain in one waveguide and loss. Also, discrete solitons were generated in a PT-symmetric ladder-shaped optical array consisting of a chain of waveguides with gain coupled to a parallel chain of waveguides with loss in [45]. Moreover, a novel multicomponent discrete system which is PT-symmetric as the previous has only quite recently appeared in the literature [46–48]. In [46], coupled pendulum chains under parametric PT-symmetric driving force were studied. Here, the authors consider a chain of coupled pendulum pairs, where each pendulum is connected to the nearest neighbors in the longitudinal and transverse directions. The common strings in

[a] e-mail: kamdoumkuitchealex@yahoo.com

[b] e-mails: abtogueu@yahoo.fr; alain.togueu@univ-yaounde1.cm (corresponding author)

[c] e-mail: t_kanaa@yahoo.fr

[d] e-mail: ctchawa@yahoo.fr

Fig. 1 (Courtesy of Prof D. E. Pelinovsky) A schematic representation of the coupled pendulum pairs. Where each pendulum is connected to the nearest neighbors in the longitudinal and transverse directions by a common string
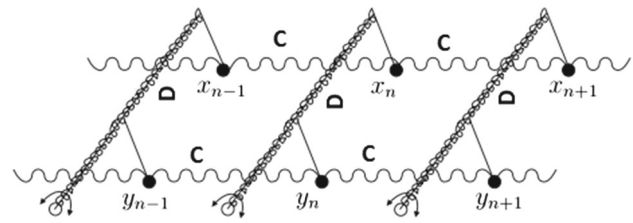
each pair are modulated periodically by an external force. In the limit of small coupling and near the parametric resonance, they derived a novel system of coupled PT-symmetric discrete nonlinear Schrödinger equations, which has Hamiltonian symmetry but no phase invariance. By using the conserved energy, they found the parameter range for the linear and nonlinear stability of the zero equilibrium. Numerical experiments illustrated how the destabilization of the zero equilibrium takes place when the stability constraints are not satisfied. Compared to the works in [43, 44], the authors considered different couplings between the two pendulums in a pair and that the model is Hamiltonian but not phase invariant. This coupling describes interactions between the two pendulums connected to each other by a common horizontal string. Inspired by the model proposed in [46], A. Kamdoum Kuitche et al. [49] generate a nonlinear supratransmission phenomenon in that chain of coupled pendulum pairs. To the best of our knowledge, no attention was paid to discrete MI analysis in the transversely connected nonlinear pendulum pairs.

In this work, we investigate analytically and numerically the discrete MI which leads to the generation of localized solitary waves in the chain of the coupled pendulum pairs, where each pendulum is connected to the nearest neighbors in the longitudinal and transverse directions.

The paper is organized as follows: In Sect. 2, we present the mathematical model and implement the multiple scale method to derive the coupled nonlinear Schrödinger equation of the model. In Sect. 3, we perform the analytical framework in which we analyze the linear stability and display the MI gain as a function of the frequency of infinitesimal modulation perturbations. Then, in Sect. 4, we numerically integrate the full governing equation of our model to check the validity of the predictions found by linear stability analysis. Finally, Sect. 5 concludes the work.

2 Hamiltonian and coupled nonlinear Schrödinger equation of the model

The model considered in this work is a chain of coupled pendulums displayed in Fig. 1 [46], where each pendulum is connected to the nearest neighbors in the longitudinal and transverse directions by a common horizontal string. The positive parameters C and D describe couplings between the nearest pendulums in the longitudinal and transverse directions, respectively.

The model of Fig. 1 comprises of two degrees of freedom $x_n(t)$ and $y_n(t)$ which represent the angular displacements in each pair of the pendulums site n with respect to their equilibrium positions. The Hamiltonian in the absence of damping for a chain of N pendulums of the model that describes the dynamics of the whole network is written as

$$H = \sum_{n=1}^{N} \frac{1}{2}\left(\dot{x}_n^2 + \dot{y}_n^2\right) - \cos(x_n) - \cos(y_n) + \frac{1}{2}C(x_{n+1} - x_n)^2 + \frac{1}{2}C(y_{n+1} - y_n)^2 + \frac{1}{2}D(x_n - y_n)^2, \tag{1}$$

where dots denote derivatives with respect to time t. From Hamilton's equations, the equation governing the motion of the nth pendulum in both directions takes the following form:

$$\begin{cases} \ddot{x}_n - C(x_{n+1} - 2x_n + x_{n-1}) - D(y_n - x_n) + \sin(x_n) = 0 \\ \ddot{y}_n - C(y_{n+1} - 2y_n + y_{n-1}) - D(x_n - y_n) + \sin(y_n) = 0. \end{cases} \tag{2}$$

In order to study the possibility of MI in coupled pendulum chains, we use the multiple scale method on Eq. (2) to derive the coupled discrete nonlinear Schrödinger (DNLS) equation using the algorithm in [50]. For that purpose, we make the following assumption, where $\omega_0 \approx 1$ and ε is a small fixed parameter:

$$\omega \approx \omega_0\left(1 - \frac{\varepsilon^2}{2}\right), \omega^2 \approx \omega_0^2\left(1 - \varepsilon^2\right), C \approx \varepsilon^2 c, \text{ and } D \approx \varepsilon^2 d.$$

By expanding $\sin(x_n)$ and $\sin(y_n)$ in Taylor series up to the third order, Eq. (2) can be written as:

$$\begin{cases} \ddot{x}_n - C(x_{n+1} - 2x_n + x_{n-1}) - D(y_n - x_n) + x_n - \frac{1}{6}x_n^3 = 0 \\ \ddot{y}_n - C(y_{n+1} - 2y_n + y_{n-1}) - D(x_n - y_n) + y_n - \frac{1}{6}y_n^3 = 0. \end{cases} \tag{3}$$

The angular displacements of the nth resonator in the two directions can be expressed as:

$$x_n(T) = 2\varepsilon\left[\psi_n(T)e^{-i\omega t} + \bar{\psi}_n(T)e^{i\omega t}\right], \tag{4}$$
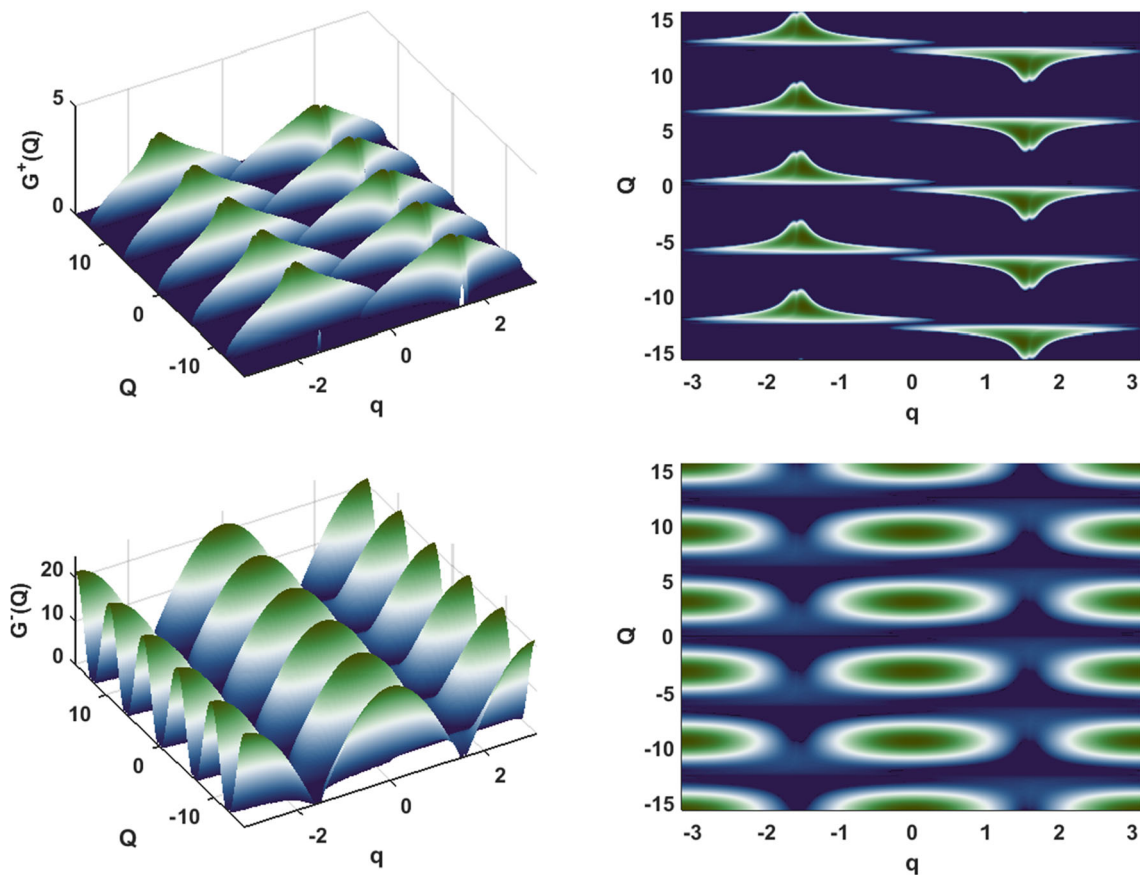
Fig. 2 (left panel): Growth rate of MI gain associated with solutions G^+ and G^- of Eq. 21 versus the wave numbers Q and q for the parameters $d = 0.1$, $c = 4$, and $\lambda_0 = 0.6$. (Right panel): Regions of stability in the (q, Q) plane are indicated by the dark bluish area(s), and the regions of modulational instability in the (q, Q) plane are indicated by the area(s) surrounded by bright greenish color

$$y_n(T) = 2\varepsilon\left[\phi_n(T)e^{-i\omega t} + \bar{\phi}_n(T)e^{i\omega t}\right], \tag{5}$$

where $T = \frac{\varepsilon^2}{2}t$ and, ψ_n and ϕ_n are unknown complex functions. Therefore, substituting Eqs. (4) and (5) into Eq. (3), keeping the terms proportional to $e^{-i\omega t}$ and ε^3, and by choosing $\tau = \omega_0 T$, Eq. (3) becomes:

$$\begin{cases} i\frac{\partial \psi_n}{\partial \tau} - \psi_n + c(\psi_{n+1} - 2\psi_n + \psi_{n-1}) + d(\phi_n - \psi_n) + 2|\psi_n|^2\psi_n = 0 \\ i\frac{\partial \phi_n}{\partial \tau} - \phi_n + c(\phi_{n+1} - 2\phi_n + \phi_{n-1}) + d(\psi_n - \phi_n) + 2|\phi_n|^2\phi_n = 0. \end{cases} \tag{6}$$

For $d = 0$, Eq. (6) reduces to a single discrete nonlinear Schrodinger equation obtained in [50] with neither excitations ($f = 0$ and $h = 0$) nor damping($\gamma = 0$). Therefore, the system of Eq. (6) becomes equivalent to an uncoupled system of DNLS equations, which have many applications in physics, including nonlinear optics. For $d \neq 0$, Eq. (6) can be considered as the coupled discrete nonlinear Schrödinger equation with neither excitations nor damping. In the optics context, the system describes two arrays of optical waveguides with Kerr nonlinearity and nearest-neighbor interactions [51]. The d term realizes a cross-phase linear coupling between the two arrays of optical waveguides. Here, we have shown that the coupled pendulum pairs can be described by a coupled discrete nonlinear Schrödinger equation from which we will study the possibility of modulational instability in the next section.

3 Modulational instability analysis

In order to determine the conditions of the instability or stability of the plane wave, we are going to investigate the evolution of a small perturbation that could affect the plane wave.
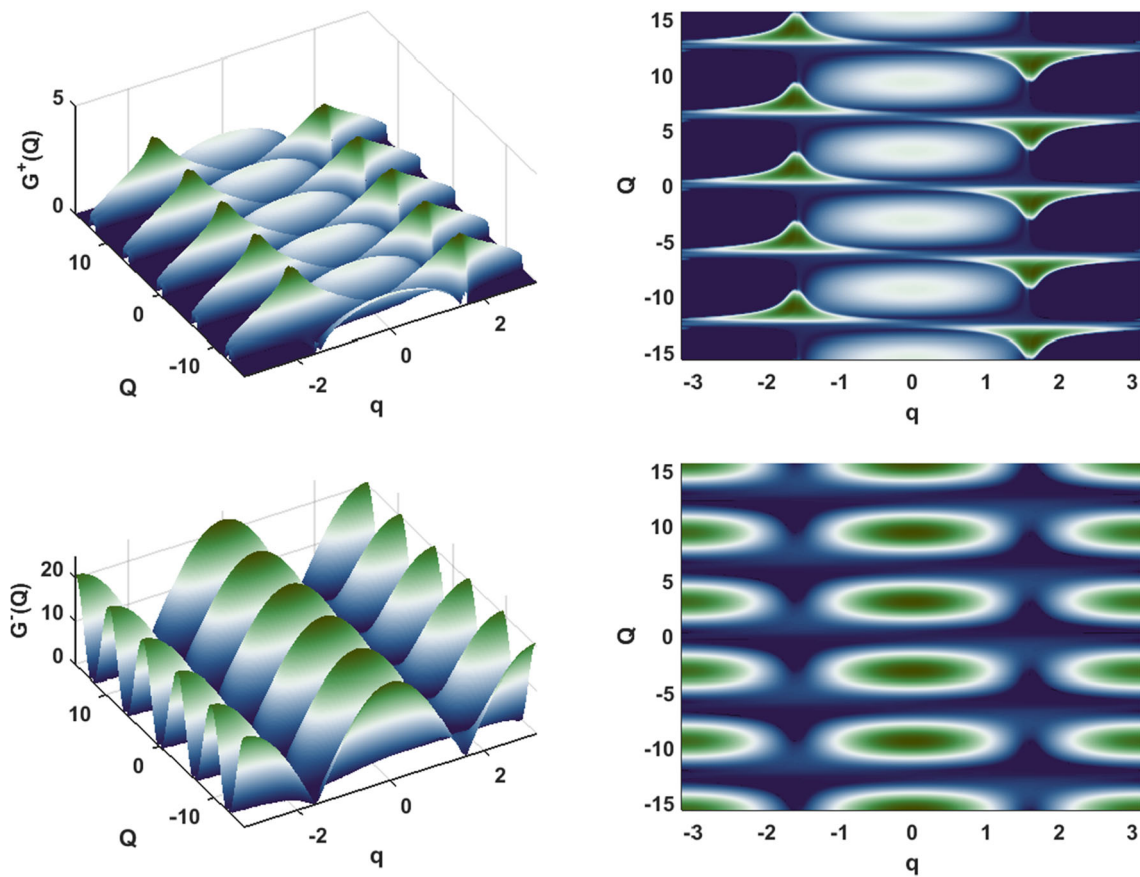
Fig. 3 (left panel): Growth rate of MI gain associated with solutions G^+ and G^- of Eq. (21) versus the wave numbers Q and q for the parameters $d = 0.5$, $c = 4$, and $\lambda_0 = 0.6$. (Right panel): Regions of stability in the (q, Q) plane are indicated by the dark bluish area(s), and the regions of modulational instability in the (q, Q) plane are indicated by the area(s) surrounded by bright greenish color

Fig. 4 Growth rate of MI gain for different values of the transverse coupling parameter d versus the wave number of the perturbation Q for $q = \frac{\pi}{100}$. Where the other parameters are: $c = 4$, $\lambda_0 = 0.6$. We observe that the MI gain spectrum is symmetric with respect to $Q = 0$
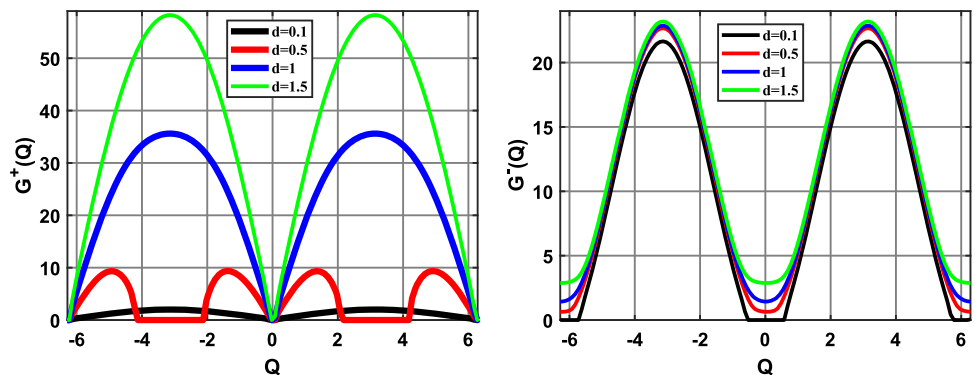

3.1 Linear instability

To proceed further, let the following exact plane wave solution of Eqs. (7) and (8) be the solutions of Eq. (6). That is

$$\psi_n = \lambda_0 e^{i(qn - \omega\tau)}, \tag{7}$$

$$\phi_n = \mu_0 e^{i(qn - \omega\tau)}, \tag{8}$$

where q is the wave number, ω the angular frequency, λ_0 and μ_0 are, respectively, the constant amplitudes of the vibrational angular displacements ψ_n and ϕ_n. Substituting Eqs. (7) and (8) into Eq. (6), we arrive to this relation

$$\begin{cases} \omega - 1 + c(2\cos(q) - 2) + d(\frac{\mu_0}{\lambda_0} - 1) + 2|\lambda_0|^2 = 0 \\ \omega - 1 + c(2\cos(q) - 2) + d(\frac{\lambda_0}{\mu_0} - 1) + 2|\mu_0|^2 = 0. \end{cases} \tag{9}$$
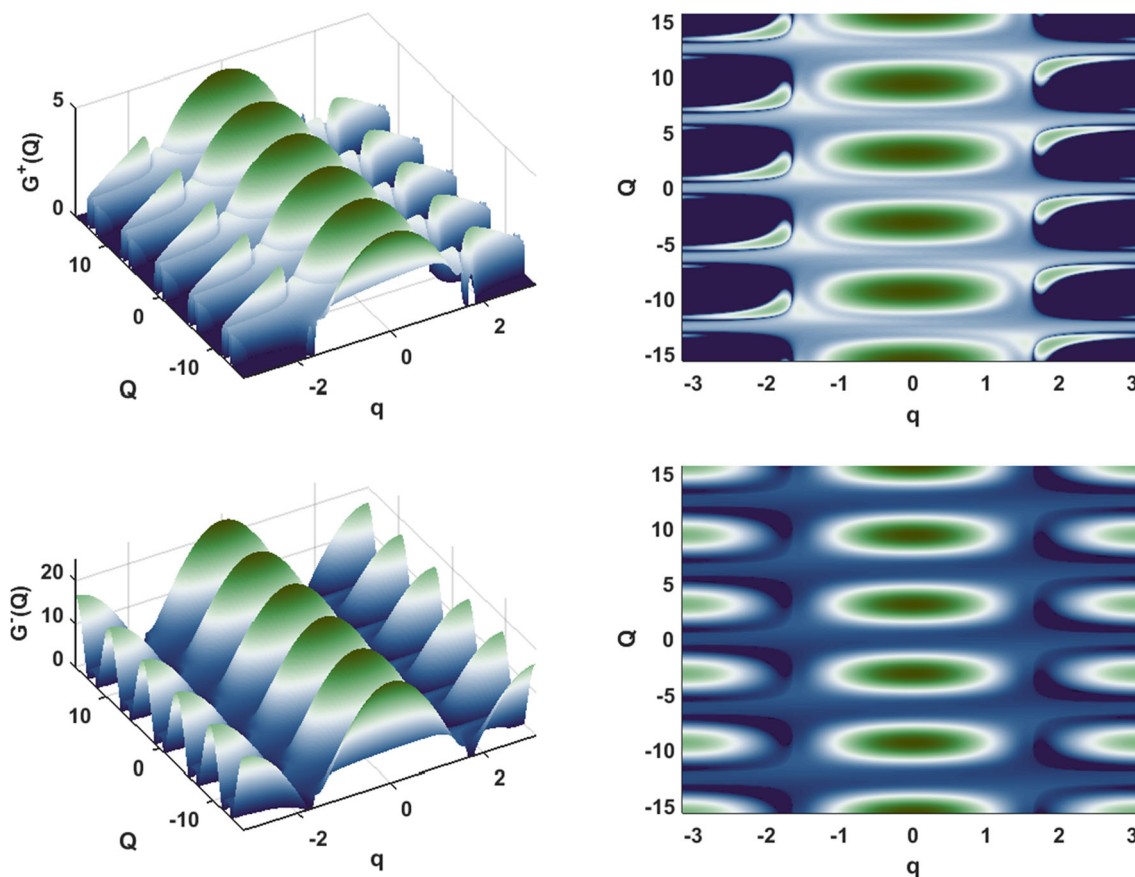
Fig. 5 (left panel): Growth rate of MI gain associated with solutions G^+ and G^- of Eq. (21) versus the wave numbers Q and q for the parameters $d = 1.5$, $c = 4$, and $\lambda_0 = 0.6$. (Right panel): Regions of stability in the (q, Q) plane are indicated by the dark bluish area(s), and the regions of modulational instability in the (q, Q) plane are indicated by the area(s) surrounded by bright greenish color

The two equations of Eq. (9) are compatible if $d(\frac{\mu_0}{\lambda_0} - 1) + 2|\lambda_0|^2 = d(\frac{\lambda_0}{\mu_0} - 1) + 2|\mu_0|^2$. By considering both λ_0 and μ_0 to be reals, one get a relation between the two amplitudes λ_0 and μ_0 as follows:

$$\mu_0 = \frac{d}{2\lambda_0}. \tag{10}$$

Thus, the nonlinear dispersion relation of the mode corresponding to the coupled chains is given as:

$$\omega = 1 + d - c(2\cos(q) - 2) - 2(\lambda_0{}^2 + \mu_0{}^2). \tag{11}$$

3.2 Modulational instability gain

MI is a mechanism from where soliton can form during confrontation between nonlinear and dispersions term. We employed the plane waves with small perturbations as follows:

$$\psi_n = (\lambda_0 + \lambda_n(\tau))e^{i(qn-\omega\tau)}, \tag{12}$$

$$\phi_n = (\mu_0 + \mu_n(\tau))e^{i(qn-\omega\tau)}. \tag{13}$$

Substituting Eqs. (12) and (13) into Eq. (6), making use of the dispersion relations (11), and after some mathematical computations, we obtain the following linearized set of coupled discrete differential equations for the perturbations λ_n and μ_n:

$$\begin{cases} i\frac{\partial\lambda_n}{\partial\tau} + ce^{iq}\lambda_{n+1} + ce^{-iq}\lambda_{n-1} + 2\lambda_0^2(\lambda_n + \lambda_n^*) + d\mu_n - (2c\cos(q) + 2\mu_0^2)\lambda_n = 0 \\ i\frac{\partial\mu_n}{\partial\tau} + ce^{iq}\mu_{n+1} + ce^{-iq}\mu_{n-1} + 2\mu_0^2(\mu_n + \mu_n^*) + d\lambda_n - (2c\cos(q) + 2\lambda_0^2)\mu_n = 0 \end{cases}, \tag{14}$$

where * denotes complex conjugate. Furthermore, the above simultaneous equation admits solutions of the form

$$\lambda_n = \alpha_1 \cos(Qn - \Omega\tau) + i\alpha_2 \sin(Qn - \Omega\tau), \tag{15}$$
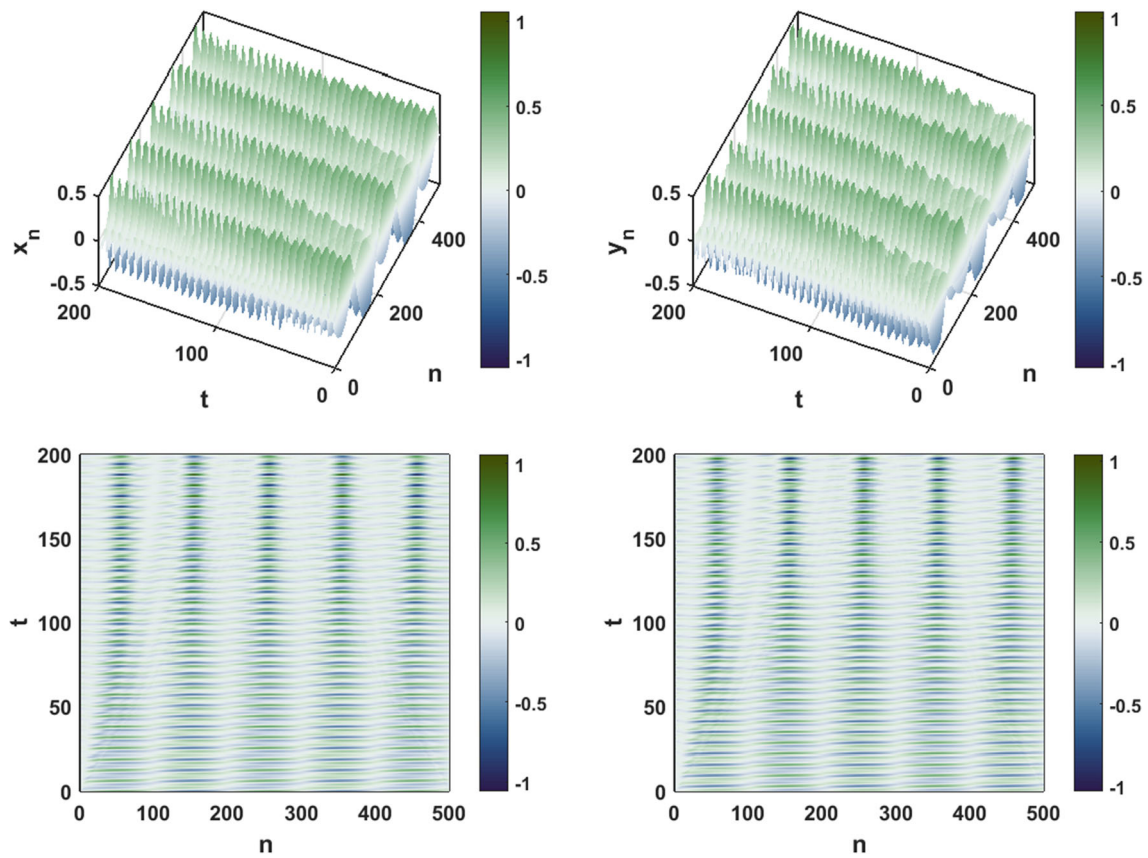
Fig. 6 Spatiotemporal evolution of the amplitudes of the initial plane waves which break into a wave train having the shape of a soliton due to the MI manifestation in a transversely connected nonlinear pendulum chains as predicted analytically, for $d = 0.1$, $c = 4$, $\lambda_0 = 0.6$, $q = \frac{\pi}{100}$ rad and $Q = 0.911\pi$ rad. (top panel): 3D representation, (down panel): 2D representation

$$\mu_n = \beta_1 \cos(Qn - \Omega\tau) + i\beta_2 \sin(Qn - \Omega\tau), \tag{16}$$

where Q and Ω are, respectively, the wave number of the perturbation and the corresponding propagation frequency of the modulation. Substituting Eqs. (15) and (16), into the coupled set, Eq. (14) yields a pair of coupled equations that can be written in matrix form as follows:

$$\begin{pmatrix} 4\lambda_0^2 + D_1 & \Omega - D_2 & d & 0 \\ \Omega - D_2 & D_1 & 0 & d \\ d & 0 & 4\mu_0^2 + D_3 & \Omega - D_2 \\ 0 & d & \Omega - D_2 & D_3 \end{pmatrix} \begin{pmatrix} \alpha_1 \\ \alpha_2 \\ \beta_1 \\ \beta_2 \end{pmatrix} = \begin{pmatrix} 0 \\ 0 \\ 0 \\ 0 \end{pmatrix}, \tag{17}$$

where

$$D_1 = 2c\cos(Q)\cos(q) - \rho,$$

$$D_2 = 2c\sin(Q)\sin(q),$$

$$D_3 = 2c\cos(Q)\cos(q) - \sigma, \tag{18}$$

$$\sigma = 2c\cos(q) + 2\lambda_0^2,$$

$$\rho = 2c\cos(q) + 2\mu_0^2.$$
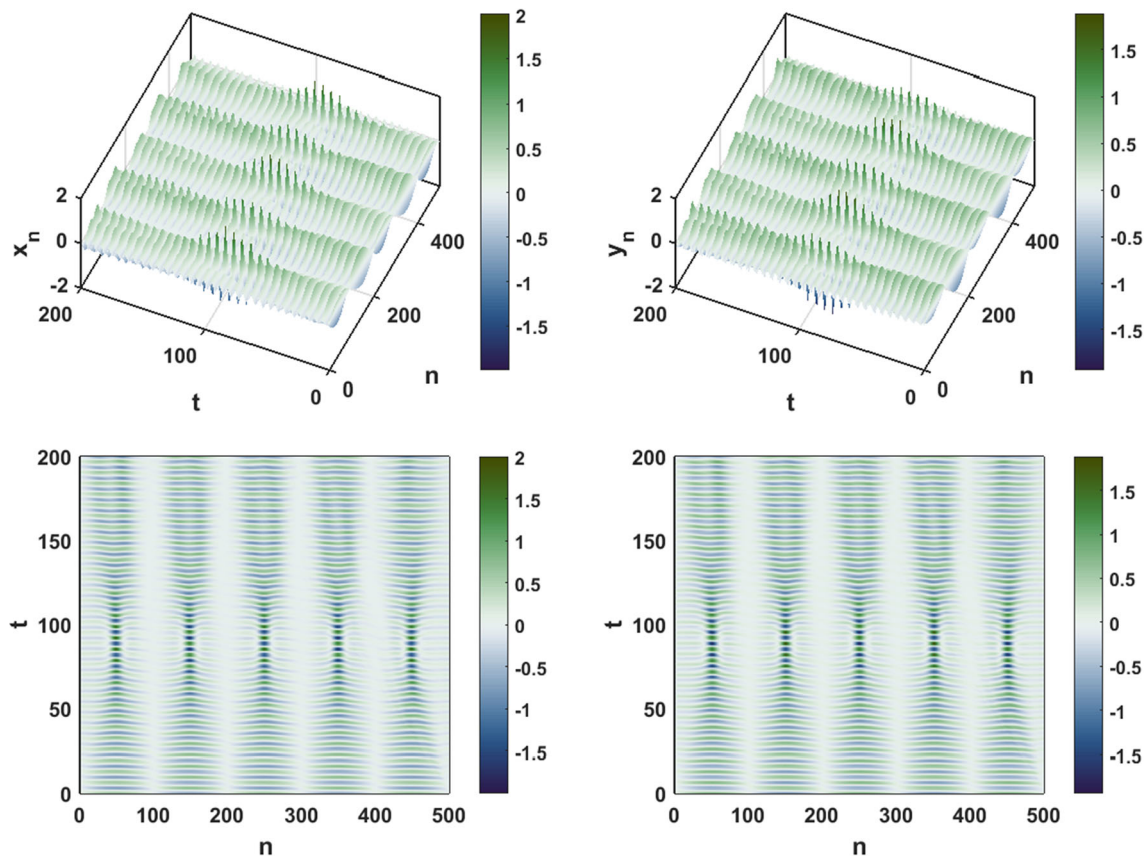
Fig. 7 Spatiotemporal evolution of the amplitudes of the initial plane waves which break into a wave train having the shape of a soliton due to the MI manifestation in a transversely connected nonlinear pendulum chains as predicted analytically, for $d = 1.0$, $c = 4$, $\lambda_0 = 0.6$, $q = \frac{\pi}{100}$ rad, and $Q = 0.911\pi$ rad. (top panel): 3D representation, (down panel): 2D representation

The solutions of the system of Eq. (17) are non-trivial. Given that the determinant of 4×4 matrix is zero, then, we obtain the dispersion relations given by:

$$\Omega^+_\pm = D_2 \pm \frac{1}{2}\sqrt{\chi_1 + 2\sqrt{16\chi_2 + 8\chi_3 + \chi_4}},$$

$$\Omega^-_\pm = D_2 \pm \frac{1}{2}\sqrt{\chi_1 - 2\sqrt{16\chi_2 + 8\chi_3 + \chi_4}},$$

(19)

with

$$\chi_1 = 8\,D_1\lambda_0{}^2 + 8\,D_3\mu_0{}^2 + 4\,d^2 + 2\,D_1{}^2 + 2\,D_3{}^2,$$

$$\chi_2 = 4\,d^2\mu_0{}^2\lambda_0{}^2 + D_1{}^2\lambda_0{}^4 - 2\,D_1 D_3\mu_0{}^2\lambda_0{}^2 + D_3{}^2\mu_0{}^4 + d^2 D_1\mu_0{}^2 + d^2 D_1\lambda_0{}^2,$$

$$\chi_3 = 2\,d^2 D_3\mu_0{}^2 + 2\,d^2 D_3\lambda_0{}^2 + D_1{}^3\lambda_0{}^2 - D_1{}^2 D_3\mu_0{}^2 - D_1 D_3{}^2\lambda_0{}^2 + D_3{}^3\mu_0{}^2,$$

$$\chi_4 = 4\,d^2 D_1{}^2 + 8\,d^2 D_1 D_3 + 4\,d^2 D_3{}^2 + D_1{}^4 - 2\,D_1{}^2 D_3{}^2 + D_3{}^4.$$

(20)

The dispersion relation of Eq. (19) determines the condition for stability of the plane waves with the wave number q in the network. However, our interest is the complex solutions of Ω. To have such result, $\chi_1 + 2\sqrt{16\chi_2 + 8\chi_3 + \chi_4}$ or $\chi_1 - 2\sqrt{16\chi_2 + 8\chi_3 + \chi_4}$ should be less than zero. MI occurs when wave number possesses a nonzero imaginary part leading to an exponential growth of the perturbed amplitudes $\lambda_n(\tau)$ and $\mu_n(\tau)$ which set off the generation of localized modes in the transversely coupled chains. Therefore, the MI gain is the imaginary part of the propagation frequency of the modulation. It is calculated using the formula

$$G(Q) = |\text{Im}(\Omega)|.$$

(21)

Now, we investigate the behavior of the MI gains G^+ and G^- or MI zones by playing on the values of the transverse coupling parameter d. The MI gains exhibit two bands, namely the stable band and the unstable band. It is worth noting that the unstable zone of the MI corresponds to the generation of modulated plane wave solutions. That is, in unstable regions, the plane waves are
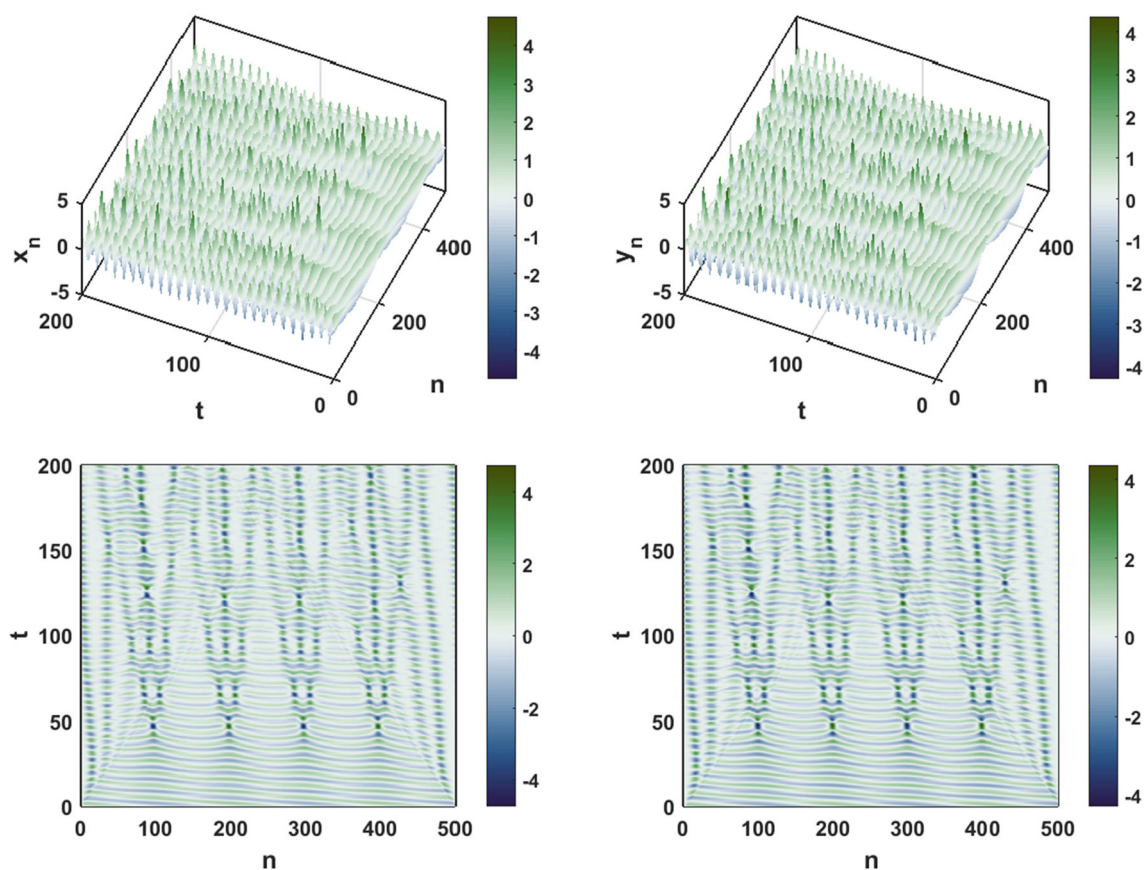
Fig. 8 Spatiotemporal evolution of the amplitudes of the initial plane waves which break into a wave train having the shape of a soliton due to the MI manifestation in a transversely connected nonlinear pendulum chains as predicted analytically, for $d = 1.5$, $c = 4$, $\lambda_0 = 0.6$, $q = \frac{\pi}{100}$ rad, and $Q = 0.911\pi$ rad. (top panel): 3D representation, (down panel): 2D representation

supposed to be broken up into trains of solitary waveforms or pulses, or it is considered as stable when the wave numbers q and Q belong to the stability bands.

In Figs. 2, 3 and 5, we have fixed $c = 4$, $\lambda_0 = 0.6$ and varied the transverse coupling parameter, respectively, as $d = 0.1$, $d = 0.5$, and $d = 1.5$. The transverse coupling parameter appears to dramatically impact the instability features. That is, it influences the stability and instability zones as well observed in the left panel of those figures. There, the regions surrounded by bright greenish areas represent the unstable band, while the dark bluish areas indicate the regions of stability. Thus, it is observed that for the instability growth rate G^+, when one increases the transverse coupling parameter, the amplitude of the gain increases as we can clearly observe on the left panel of Fig. 4, while the stable bands decrease and the MI regions increase as clearly shown in Fig. 5. Hence, the chances of observing MI in the lattice reduce with a decrease in the transverse coupling parameter. On the other hand, for the instability growth rate G^-, when one increases the transverse coupling parameter, the amplitude of the gain increases slightly as we can clearly observe on the right panel of Fig. 4, while the stable bands and the MI regions slightly change. Also, it can be clearly observed that the MI gains are symmetric with respect to $q = 0$. Therefore, it has been shown that the instability growth rate and MI band are dramatically affected by the transverse coupling parameter.

In Fig. 4, the behavior of the amplitude of MI growth rate for carrier waves versus the wave number of perturbation Q for the wave number $q = \frac{\pi}{100}$ with four values of transverse coupling parameter d has been displayed. It is observed in Fig. 4 that the instability growth rate G^+ is significantly sensitive to the transverse coupling term. For $d = 0.1$, the dynamics of the network displays a very weak growth rate amplitude, whereas the instability growth rate G^- does not change considerably with the transverse coupling term. Also, it is important to point out that for $Q = \pi$, the amplitude of MI gain is maximum.

In the left panel of Figs. 2, 3 and 5, the unstable regions of MI are clearly depicted; consequently, the plane wave solutions of the transversely coupled pendulum chains model become unstable. Hence, the dynamics of the generated unstable plane wave solutions will be studied numerically in the next section.

4 Numerical analysis of MI

In order to check the validity of the linear stability analysis which does not tell us anything about the behavior of the propagation of the slowly modulated waves when the instability grows, we perform in the present section some numerical investigations of the equation of motion (2). This numerical simulation is done in order to understand the dynamics of the transversely connected nonlinear pendulum chains under MI in the nonlinear regime.

To this end, it is carried out by integrating the full Eq. (2) using a fourth-order Runge–Kutta scheme with normalized time step $\Delta t = 10^{-8}$. We consider the number of sites N in the n direction to be equal to 501 with periodic boundary conditions such as to avoid the wave reflection at the end of the line. In accordance with Eqs. (12) and (13), the initial modulated plane waves with slightly modulated amplitudes introduced are in this form

$$
\begin{aligned}
x_n(t=0) &= \lambda_0[1 + 0.01\cos(Qn)]\cos(qn); \quad \dot{x}_n(t=0) = \lambda_0\omega[1 + 0.01\cos(Qn)]\sin(qn) \\
y_n(t=0) &= \mu_0[1 + 0.01\cos(Qn)]\cos(qn); \quad \dot{y}_n(t=0) = \mu_0\omega[1 + 0.01\cos(Qn)]\sin(qn)
\end{aligned}
\tag{22}
$$

with the set of wave numbers q and Q taken in a given unstable zones of Figs. 2, 3, and 5 obtained from the linear stability analysis and the wave frequency ω calculated from the dispersion relation of Eq. (11).

We introduce in the network the initial conditions of Eq. (22) by considering different values of the transverse coupling term. Firstly, for $d = 0.1$, we choose a wave with $q = \frac{\pi}{100}$ rad perturbed at wave number $Q = 0.911\pi$ rad belonging to the unstable region of Fig. 2. Using these parameters, we obtained Fig. 6 which illustrates the generation of localized pulses in the cause of the MI. We can clearly see that the initial solution tends to disintegrate during propagation, which leads to the breakup of the wave into a periodic localized pulses or envelope soliton train. It is important to point out that the wave displayed an oscillating and breathing behavior and each component of the train has the shape of a soliton-like object; this is due to the existence of MI in the network.

We display in Fig. 7 the spatiotemporal evolution of amplitudes for $d = 1.0$ by choosing a wave with $q = \frac{\pi}{100}$ rad perturbed at wave number $Q = 0.911\pi$ rad belonging to the unstable region (not shown here) where the envelope pulses also emerge due to the existence of MI. Thus, the localization in time is observed. For $d = 1.5$, the number of localization solution in time increases as illustrated in Fig. 8. Hence, transversely connected nonlinear pendulum pairs can be convenient tools for the study of wave propagation in nonlinear dispersive media.

5 Conclusion

In this work, we have investigated MI in transversely connected nonlinear pendulum pairs where each pendulum is connected to the nearest neighbors in the longitudinal and transverse directions. The equations describing the dynamics of the model are obtained from Hamilton's equations. Also, in order to study the existence of MI in the model, the multiple scale method was used to derive the coupled discrete nonlinear Schrödinger equation.

By carrying out the linear stability analysis, we have calculated and plotted the growth rate of the MI. It has been revealed that both the gain and the MI bands are sensitive to the transverse coupling parameter. Therefore, with the results obtained from MI analysis, we predicted the formation of the periodic localized solitons in the network. Thus, numerical simulations of MI have been carried out and let to the generation of periodic localized pulses in the system. We have observed that the transverse coupling term has an influence on the localization of envelope pulses. Finally, from the interesting results obtained in this work, we can say that transversely connected nonlinear pendulum chains can be convenient tools for studying wave propagation in dispersive nonlinear media.

References

1. T.B. Benjamin, J.E. Feir, The disintegration of wave trains on deep water. Part 1 Theory. J. Fluid Mech. **27**, 417–430 (1967)
2. N.F. Piliptetskii, A.R. Rustamov, Observation of self-focusing of light in liquids. JETP Lett. **2**, 55–56 (1965)
3. V.I. Bespalov, V.I. Talanov, Filamentary structure of light beams in nonlinear liquids. ZhETF Pisma Redaktsiiu **2**, 471–476 (1966)
4. P. Marquié, J.M. Bilbault, M. Remoissenet, Generation of envelope and hole solitons in an experimental transmission line. Phys. Rev. E **49**, 828 (1994)
5. P. Marquié, J.M. Bilbault, M. Remoissenet, Observation of nonlinear localized modes in an electrical lattice. Phys. Rev. E **51**, 6127 (1995)
6. M. Remoissenet, *Waves Called Solitons Concepts and Experiments* (Springer, Berlin, 1999)
7. A. Kenfack-Jiotsa, E. Tala-Tebue, Effect of Second-Neighbor Inductive Coupling on the Modulational Instability in a Coupled Line of Transmission. J. Phys. Soc. Jpn. **80**, 034003 (2011)
8. F. I.I. Ndzana, A. Mohamadou, T.C. Kofane, Modulated waves and chaotic-like behaviours in the discrete electrical transmission line. J. Phys. D: Apply. Phys. **40**, 3254 (2007)

9. R. Stearrett, L.Q. English, Experimental generation of intrinsic localized modes in a discrete electrical transmission line. J. Phys. D: Apply. Phys **40**, 5394 (2007)

10. Y. Doi, A. Nakatani, K. Yoshimura, Modulational instability of zone boundary mode and band edge modes in nonlinear diatomic lattices. Phys. Rev. E **79**, 026603 (2009)

11. B. Sadjo, C.B. Tabi, H. Edongue, A. Mohamadou, Coupled energy patterns in zigzag molecular chains. Wave Motion **17**, 30052–5 (2017)

12. S. Abbagari, A. Houwe, L. Akinyemi, Y. Saliou, T.B. Bouetou, Modulation instability gain and discrete soliton interaction in gyrotropic molecular chain. Chaos Solit. Fract. **160**, 112255 (2022)

13. R. Abouem, A. Ribama, Z.I. Djoufack, J.P. Nguenang, Breather-impurity interactions and modulational instability in a quantum 2D Klein-Gordon chain. Eur. Phys. J. B **95**, 86 (2022)

14. E. Tala-Tebue, G. Roger Deffo, S.B. Yamgoue, A. Kenfack-Jiotsa, F.B. Pelap, Monoatomic chain: modulational instability and exact traveling wave solutions. Eur. Phys. J. Plus **135**, 715 (2020)

15. F. Gounoko Mounouna, E. Wamba, A.S. Tchakoutio Nguetcho, I.A. Bhat, J.M. Bilbault, Modulational stability brought by cubic-quartic interactions of the nearest-neighbor in FK model subjected in a parametrized on-site potential. Commun. Nonlinear Sci. Numer. Simulat. **105**, 106088 (2022)

16. K. Ourabah, T. Yamano, Nonlinear Schrödinger equations involved in dark matter halos: modulational instability. Eur. Phys. J. Plus **135**, 634 (2020)

17. G. Fongang Achu, F.M. Moukam Kakmeni, A.M. Dikande, Breathing pulses in the damped-soliton model for nerves,. Phys. Rev. E **97**, 012211 (2018)

18. A.S. Foualeng Kamga, G. Fongang Achu, F.M. Moukam Kakmeni, P. Guemkam Ghomsi, F.T. Ndjomatchoua, C. Tchawoua, Continuous signalling pathways instability in an electromechanical coupled model for biomembranes and nerves. Eur. Phys. J. B **95**, 12 (2022)

19. M. Khalid, F. Hadi, A. ur Rahma, Modulation of multi-dimensional waves in anisotropic magnetized plasma. Eur. Phys. J. Plus **136**, 1061 (2021)

20. V.K. Sharma, Chirped soliton-like solutions of generalized nonlinear Schrödinger equation for pulse propagation in negative index material embedded into a Kerr medium. Indian J. Phys. **90**, 1271 (2016)

21. C.D. Bansi Kamdem, C.B. Tabi, A. Mohamadou, Dissipative Mayer's waves in fluid-filled viscoelastic tubes. Chaos Solit. Fract. **109**, 170 (2018)

22. F. Dalfovo, S. Giorgini, L.P. Pitaevskii, S. Stringari, Theory of Bose-Einstein condensation in trapped gases. Rev. Mod. Phys. **71**, 463 (1999)

23. F.S. Cataliotti, L. Fallani, F. Ferlaino, C. Fort, P. Maddaloni, M. Inguscio, Superfluid current disruption in a chain of weakly coupled Bose-Einstein condensates. New. J. Phys. **5**, 71 (2003)

24. B. Wu, Q. Nu, Landau and dynamical instabilities of the superflow of Bose-Einstein condensates in optical lattices. Phys. Rev. A **64**, 061603 (2001)

25. J.D. Tchinang Tchameu, C. Tchawoua, A.B. Togueu Motcheyo, Effects of next-nearest-neighbor interactions on discrete multibreathers corresponding to Davydov model with saturable nonlinearities. Phys. Lett. A **379**, 2984 (2015)

26. R.Y. Ondoua, J.C. Mimshe Fewu, D. Belobo Belobo, C.B. Tabi, H.P. Ekobena Fouda, Excitons dynamic in a three-stranded a-helix protein chains with diagonal and off-diagonal couplings: effects of strong long-range interactions. Eur. Phys. J. Plus **136**, 274 (2021)

27. H.C. Yuen, B.M. Lake, Instabilities of waves on deep water. Ann. Rev. Fluid Mech. **12**, 303–334 (1980)

28. P. Agrawal, *Govind, Nonlinear Fiber Optics*, 2nd edn. (Academic Press, San Diego (California), 1995)

29. E. Kenig, B.A. Malomed, M. Cross, R. Ifshitz, Intrinsic localized modes in parametrically driven arrays of nonlinear resonators. Phys. Rev. E **80**, 046202 (2009)

30. F. Palmero, J. Han, L.Q. English, T.J. Alexander, P.G. Kevrekidis, Multifrequency and edge breathers in the discrete sine-Gordon system via subharmonic driving: theory, computation and experiment. Phys. Lett. A **380**, 402–407 (2016)

31. L.M. Floria, J.J. Mazo, Dissipative dynamics of the Frenkel-Kontorova model. Adv. Phy. **45**, 505–598 (1996)

32. J. Wu, R. Keolian, I. Rudnick, Observation of a nonpropagating hydrodynamic soliton. Phys. Rev. Lett. **52**, 1421–1424 (1984)

33. B. Denardo, W. Wright, S. Putterman, A. Larraza, Observation of a kink soliton on the surface of a liquid. Phys. Rev. Lett. **64**, 1518–1521 (1990)

34. X. Wang, R. Wei, Dynamics of Multisoliton Interactions in Parametrically Resonant Systems. Phys. Rev. Lett. **78**, 2744–2747 (1997)

35. O.M. Braun, Y. Kivshar, *The Frenkel-Kontorova Model: Concepts, Methods, and Applications* (Springer-Verlag, Berlin, Heidelberg, 2004)

36. C. Vasanthi, M. Latha, Heisenberg ferromagnetic spin chain with the bilinear and biquadratic interactions in (2 + 1) dimensions. Commun. Nonlinear Sci. Numer. Simulat. **28**, 109–122 (2015)

37. I. Barashenkov, M. Bogdan, V. Korobov, Stability diagram of the phase-locked solitons in the parametrically driven, damped nonlinear Schrodinger equation. Eur. Phys. Lett. **15**, 113 (1991)

38. Y. Xu, T.J. Alexander, H. Sidhu, P.G. Kevrekidis, Instability dynamics and breather formation in a horizontally shaken pendulum chain. Phys. Rev. E **90**, 042921 (2014)

39. V.M. Burlakov, Interference of mode instabilities and pattern formation in anharmonic lattices. Phys. Rev. Lett. **80**, 3988 (1998)

40. J. Leon, M. Manna, Discrete instability in nonlinear lattices. Phys. Rev. Lett. **83**, 2324 (1999)

41. A.V. Gorbach, M. Johanson, Gap and out-gap breathers in a binary modulated discrete nonlinear Schrödinger model. EPJ D **29**, 77 (2004)

42. J. Meier, G.I. Stegeman, D.N. Christodoulides, Y. Silberberg, R. Morandotti, H. Yang, G. Salamo, M. Sorel, J.S. Aitchison, Experimental observation of discrete modulational instability. Phys. Rev. Lett. **92**, 163902 (2004)

43. N.V. Alexeeva, I.V. Barashenkov, A.A. Sukhorukov, Y.S. Kivshar, Optical solitons in $PT-symmetric$ nonlinear couplers with gain and loss. Phys. Rev. A **85**, 063837 (2012)

44. I.V. Barashenkov, S.V. Suchkov, A.A. Sukhorukov, S.V. Dmitriev, Y.S. Kivshar, Breathers in $PT-symmetric$ optical couplers. Phys. Rev. A **86**, 053809 (2012)

45. N.V. Alexeeva, I.V. Barashenkov, Y.S. Kivshar, Solitons in $PT-symmetric$ ladders of optical waveguides. New J. Phys. **19**, 113032 (2017)

46. E. Destyl, S.P. Nuiro, D.E. Pelinovsky, P. Poullet, Coupled pendula chains under parametric PT-symmetric driving force. Phys. Lett. A **381**, 3884–3892 (2017)

47. A. Chernyavsky, D.E. Pelinovsky, Breathers in Hamiltonian PT -symmetric chains of coupled pendula under a resonant periodic force. Symmetry **8**(7), 59 (2016). https://doi.org/10.3390/sym8070059

48. A. Chernyavsky, D.E. Pelinovsky, Long-time stability of breathers in Hamiltonian PT-symmetric lattices. J. Phys. A: Math. Theor. **49**, 475201 (2016)

49. A. Kamdoum Kuitche, A.B. Togueu Motcheyo, T. Kanaa, C. Tchawoua, Supratransmission in transversely connected nonlinear pendulum pairs. Chaos Solitons Fractals **160**, 112196 (2022)

50. A. Jallouli, N. Kacem, N. Bouhaddi, Stabilization of solitons in coupled nonlinear pendulums with simultaneous external and parametric excitations. Commun. Nonlinear Sci. Numer. Simulat. **42**, 1–11 (2017)

51. P.G. Kevrekidis, *The Discrete Nonlinear Schrödinger Equation: Mathematical Analysis, Numérical Computations and Physics Persective* (Springer-Verlag, Berlin/Heidelberg, Germany, 2009)

Bright soliton propagation with loss and gain phenomena in transversely connected nonlinear pendulum pairs

A. Kamdoum Kuitche [ID]*,‡, A. B. Togueu Motcheyo [ID]*,†,§, Zakari Yaou [ID]†,¶,
Thomas Kanaa [ID]†,‖ and C. Tchawoua [ID]*,**

*Laboratory of Mechanics, Department of Physics, Faculty of Science,
University of Yaounde I, P. O. Box 812, Yaounde, Cameroon

†Department of Mechanical Engineering,
Higher Technical Teacher's Training College,
University of Ebolowa, P. O. Box 886, Ebolowa-Cameroon
‡kamdoumkuitchealex@yahoo.com
§abtogueu@yahoo.fr; alain.togueu@univ-yaounde1.cm
¶zakariyaou@yahoo.com
‖t_kanaa@yahoo.fr
**ctchawa@yahoo.fr

In this work, we seek to investigate the dynamics of bright soliton in a chain of coupled pendulum pairs. After deriving the linear dispersion relation from the equation of the model, we find that among the obtained modes, the fast mode is the one on which we are going to be focused. Since the discrete simultaneous equation describing the dynamics of the model has not been extensively studied in the literature, we assume that the two lines of the model are proportional to each other. We use the rotating wave approximation method to derive a NLS equation governing the propagation of waves in the network. Depending on the choice of wave number, we deduce that the system supports bright and hole-soliton solutions. We use the obtained bright soliton as the initial condition for numerical computation, which demonstrates the significant role of the transverse coupling parameter in the system. That is, it affects the behavior of the forward-bright soliton generated in the system. The lattice allows gain and loss phenomena during the propagation of the waves.

Keywords: Solitons; coupled pendulum pairs; NLS equation; gain and loss phenomenon.

1. Introduction

Within the past two decades, wave propagation in dispersive nonlinear media has become an increasingly important research field. The concept of soliton discovered by Zabusky and Krustal[1] and the recurrence observation of wave propagation in the

---

§Corresponding author.

dynamics of a medium designed by Fermi–Pasta–Ulam[2] play a great role in understanding the phenomenon. The phenomenon has been studied in many dispersive discrete nonlinear media such as in nonlinear magnetic metamaterials,[3] in the nonlinear transmission lines,[4–7,9,11–14] in nonlinear acoustic meta material,[15] in dusty plasma crystals,[16,17] in molecular chains[18] and coupled cantilever array.[20–22] These systems bear many interesting features whose applications extend to different aspects of life,[23–25] nonlinear optics,[26–30] plasma physics,[31,32] biophysics.[34,36,37] One of the mostly used model was the chain of coupled pendulum.

Interestingly, from different points of view, the chain of coupled pendulums has been studied for more than three decades to investigate many interesting physical phenomena like the propagation of solitons.[38–40,43,41,42,44–46] For example, stabilization of solitons in coupled nonlinear pendulums with simultaneous external and parametric excitations was studied numerically.[47] Numerical approximations were employed in this paper in order to demonstrate that the use of external and parametric excitations simultaneously enables the transformation of a zero attractor soliton solution to a periodically stable one. In Ref. 48, the authors show that the pinning of the soliton on a "long" impurity expands dramatically its stability region, whereas "short" defects simply repel solitons, producing effective partition in arrays of parametrically driven pendulum chains. Another example of recent studies can be found in Refs. 49–51.

The previous underlying studies were interesting and worth investigating. However, the authors mostly considered single coupled pendulum chains, which limit the usability of their obtained results to only one-dimensional phenomena. Whereas there are many physical phenomena, such as the loss and gain phenomena found in Refs. 52–54, that cannot be properly understood within a one-dimensional framework. Recently, in Refs. 55–59, a chain of coupled pendulum pairs connected to the nearest neighbors in the longitudinal and transverse directions has been studied, but until now investigations that deal with the direction in which the bright soliton envelope will evolve in each line of the network have not yet shown to the best of our knowledge.

In this paper, our key goal is to widen the understanding of two-dimensional coupled pendulum networks as propagating media. Specifically, we will be investigating the dynamics of the transverse coupling parameter in a transversely coupled pendulum pairs. The outline of the paper is organized as follows: In Sec. 2, we present the mathematical model and the linear dispersion relation. In Sec. 3, we first show that the motion of modulated waves in the model can be governed by a nonlinear Schrödinger equation and, then, the bright soliton of that equation is derived. In Sec. 4, we use the bright soliton solution as initial conditions to numerically integrate the full governing equation of our model. Finally, Sec. 5 concludes.

2. Mathematical Description of the Model

The model under consideration is a chain of coupled pendula displayed in Fig. 1,[57] where each pendulum is connected to the nearest neighbors in the longitudinal and
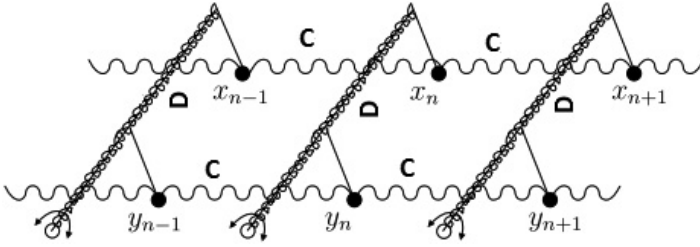
Fig. 1.   Schematic representation of the coupled pendulum pairs.[57] Each pendulum is connected to the nearest neighbors in the longitudinal and transverse directions. The positive parameters C and D describe couplings between the nearest pendula in the longitudinal and transverse directions, respectively.

Source: Courtesy of Prof D. E. Pelinovsky.

transverse directions. The parameters C and D represent, respectively, the longitudinal and transverse constant coupling.

By applying Euler–Lagrange's equations, the Newton's equations of motion for the nth pendulum in both directions take the following form:

$$\begin{cases} \ddot{x}_n - C(x_{n+1} - 2x_n + x_{n-1}) - D(y_n - x_n) + \sin(x_n) = 0, \\ \ddot{y}_n - C(y_{n+1} - 2y_n + y_{n-1}) - D(x_n - y_n) + \sin(y_n) = 0, \end{cases} \quad (1)$$

where (x_n, y_n) corresponds to the angles in each pair of the two pendula and the dots denote derivatives with respect to time t.

The linear dispersion relation corresponding to the Newton's equation (1) can be studied by linearizing the above equation with respect to (x_n, y_n) and assuming a sinusoïdal wave in the form $(x_n, y_n) = (\gamma, \delta)e^{i(kn-\omega t)}$, where ω and k are, respectively, the angular frequency and wave number, $|\gamma \ll 1|$ and $|\delta \ll 1|$ are small amplitudes of x- and y-chain, respectively. The phonon spectrum of the system is then given by

$$\omega_p^2 = 4C\sin^2\left(\frac{k}{2}\right) + (D+1) + (-1)^p D, \quad (p = 1, 2). \quad (2)$$

The lower and upper cutoff frequencies are given, respectively, at $k = 0$ by

$$\omega_{\min p} = \sqrt{(D+1) + (-1)^p D}, \quad (3)$$

and at $k = \pi$ by

$$\omega_{\max p} = \sqrt{4C + (D+1) + (-1)^p D}. \quad (4)$$

Due to the linear cross-coupling, an analogy can be found with the two electrical transmission lines coupled by a linear capacitor.[60–64] In the same spirit with Refs. 58, 60, 61, we can allow our model to exhibit slow and fast modes obtained by setting $p = 1$ and $p = 2$ at the cut-off frequencies. Therefore, the angular frequency ω of the slow- and fast-mode are within the intervals $\omega_{\min 1} \leq \omega \leq \omega_{\max 1}$ and $\omega_{\min 2} \leq \omega \leq \omega_{\max 2}$, respectively.
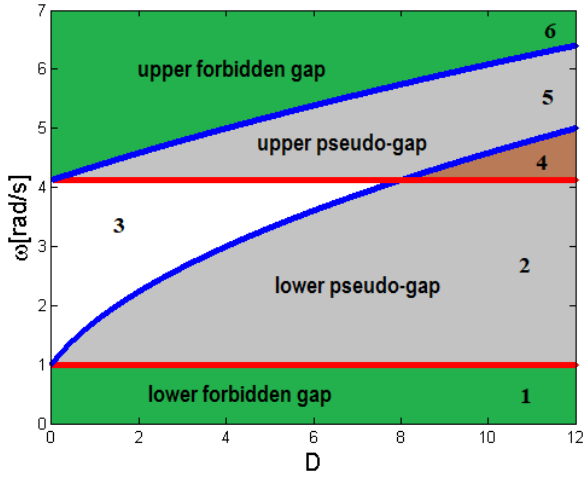
Fig. 2. (Color online) Linear dispersion law curve for $C = 4$. Blue lines represent the cut-off frequencies of the fast-mode and the red ones represent the cut-off frequencies of the slow-mode.

For values of k taken in the first Brillouin zone, Fig. 2 represents the evolution of the angular frequency for the two directions and for different values of the transverse coupling. At $D = 2C$, the intersection between the upper pseudo-gap and the lower pseudo-gap or the intersection between the lower forbidden gap of the fast-mode and the upper forbidden gap of the slow-mode starts (zone 4). In Fig. 2, it is seen that, the bandwidth of the allowed angular frequencies (zone 3) decreases as the coupling D between the nearest pendula in the transverse direction increases. This means that, the linear coupling parameter D contributes to increase the network effects on the wave during its motion. An important remark is that, the slow-mode remains equal to the case of uncoupled system i.e. a single chain. So, our attention will be focused only on the fast-mode which is related to the coupling between the two chains.

Also, due to the fact that Eq. (1) is up to now analytically intractable because of its discrete aspect, let us expand $\sin(x_n)$ and $\sin(y_n)$ in Taylor series up to the third order, and assume the angles are proportional: $y_n = \lambda x_n$ for some real number λ. The goal of this hypothesis is to solve simultaneously the equation governing the dynamics of the model by keeping both coupling parameters (C and D) i.e. the intrinsic physical design of the mechanical model. Therefore, one has from Eq. (1)

$$\begin{cases} \ddot{x}_n - C(x_{n+1} - 2x_n + x_{n-1}) - D(\lambda - 1)x_n + x_n - \frac{1}{6}x_n^3 = 0, \\ \lambda\ddot{x}_n - \lambda C(x_{n+1} - 2x_n + x_{n-1}) - D(1 - \lambda)x_n + \lambda x_n - \lambda^3\frac{1}{6}x_n^3 = 0. \end{cases} \tag{5}$$

The above two equalities are compatible if and only if λ satisfies $\lambda(\lambda - 1) = (1 - \lambda)$ and $\lambda^2 = 1$, which has solutions $\lambda = \pm 1$. When $\lambda = 1$, the two lines are in phase i.e. the system reduces to an uncoupled one or to a single chain as the Klein–Gordon chain found in Ref. 65: this corresponds to the slow-mode. In the case where $\lambda = -1$, the two lines become coupled, and the angles oscillate in the opposite

phases: This corresponds to the fast-mode on which our attention is paid. Thus, Eq. (5) yields

$$\ddot{x}_n - C(x_{n+1} - 2x_n + x_{n-1}) + \omega_g^2 x_n - \beta x_n^3 = 0, \tag{6}$$

where $\omega_g^2 = 2D + 1$ and $\beta = \frac{1}{6}$.

In order to derive the linear dispersion relation of Eq. (6), we can seek for a solution in the form of plane waves

$$x_n = A_0 e^{i(kn - \omega t)} + \text{c.c.}, \tag{7}$$

where c.c. stands for complex conjugate, ω and k are, respectively, the angular frequency and wave number. Substituting Eq. (7) into the linearized form of Eq. (6), we get a linear dispersion relation in the following form

$$\omega^2 = \omega_g^2 + 4C \sin^2\left(\frac{k}{2}\right). \tag{8}$$

The obtained dispersion relation of Eq. (8) corresponds to the fast mode of the one of Eq. (2) which admits the same lower cutoff frequency at $k = 0 (\omega_{\min} = \omega_g)$ and the same upper cutoff frequency at $k = \pi$ ($\omega_{\max} = \sqrt{\omega_g^2 + 4C}$). Hence, Eq. (6) will be used to investigate wave propagation.

The group velocity relation associated with the wave packet is defined by

$$v_g = \frac{d\omega}{dk} = \frac{C}{\omega} \sin(k). \tag{9}$$

The graphical representation of Eq. (8) shows the increase in the frequency when the wave number increases. This involves the positive values of the group velocity given by Eq. (9) in the first Brillouin zone [see Fig. 3] which shows the variation of group velocity in terms of wave number for some fixed values of transverse coupling
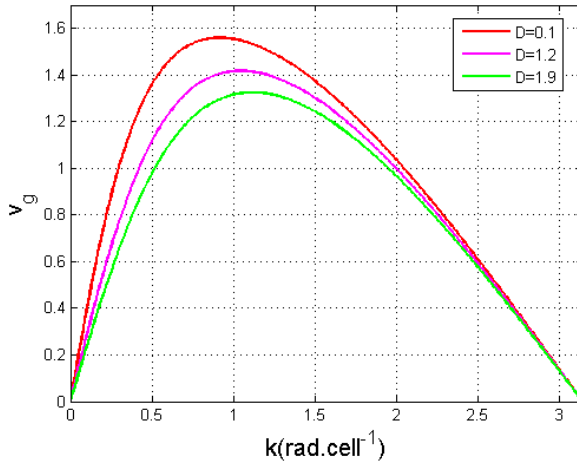

Fig. 3.   (Color online) Curve of group velocity relation.

parameters. The group velocity decreases when the transverse coupling parameter D increases. So, this transverse coupling parameter can be used to control the magnitude of generated waves.

3. The Nonlinear Schrödinger Model and Solutions

The mathematical model of Eq. (6) is less straightforward to tackle directly. For this reason, we are going to use the rotating wave approximation to derive the nonlinear Schrödinger equation describing the motion of modulated waves in the network of Fig. 1. This approximation allows us to consider the solution of Eq. (6) in the following form

$$x_n = \varepsilon[\psi(X, \tau)\exp(-i\theta_n) + \psi^*(X, \tau)\exp(i\theta_n)], \tag{10}$$

where the asterisk denotes complex conjugation, $\theta_n = \omega t - kn$ is the rapidly varying phase, ε is a positive small parameter ($0 < \varepsilon \le 1$), ψ is an unknown (continuous) slowly varying envelope function depending on the slow scale $X = \varepsilon(n - v_g t)$, and $\tau = \varepsilon^2 t$. In the following, we are going to use this expansion

$$x_{n\pm1} = \varepsilon\left(\psi \pm \varepsilon\frac{\partial\psi}{\partial X} + \varepsilon^2\frac{\partial^2\psi}{\partial X^2}\right)\exp(\pm ik)\exp(-i\theta_n) + \text{c.c.}, \tag{11}$$

where c.c. stands for the complex conjugate.

Inserting Eqs. (10) and (11) into Eq. (6) yield to different equations as power series of ε. First, by keeping the terms proportional to $\varepsilon\exp(-i\theta_n)$ and $\varepsilon^2\exp(-i\theta_n)$, we obtain, respectively, the dispersion relation and group velocity related to the fast-mode studied above. Finally, by keeping the terms proportional to $\varepsilon^3\exp(-i\theta_n)$, we obtain the following one-dimensional nonlinear Schrodinger evolution equation for $\psi(X, \tau)$

$$i\frac{\partial\psi}{\partial\tau} + P\frac{\partial^2\psi}{\partial X^2} + Q|\psi|^2\psi = 0, \tag{12}$$

with the dispersion coefficient (P) and nonlinear coefficient (Q) defined by

$$P = \frac{C\cos k - v_g^2}{2\omega}, \tag{13}$$

$$Q = \frac{1}{4\omega}. \tag{14}$$

Actually, we focus our attention on the analytical computation of the exact representation of the solution of Eq. (12). In fact, it is well known in Ref. 66 that NLS equation supports different types of solution depending on the sign of the product of the nonlinear coefficient Q and the linear dispersion coefficient P. That is, if $PQ > 0$, the NLS equation admits a bright soliton solutions, whereas for $PQ < 0$, it supports a dark or hole soliton solutions. Figure 4 depicts the dependence of the product of dispersive and nonlinear coefficients in terms of the wave number for some fixed
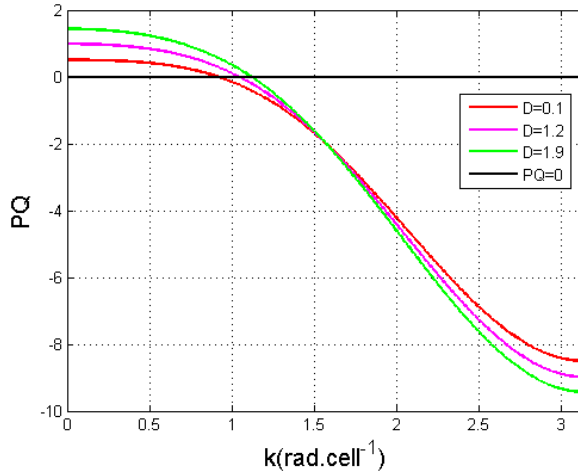
Fig. 4. (Color online) Dependence of the product PQ in term of the wave number and for $D = 0.1$, $D = 1.2$ and $D = 1.9$.

values of transverse coupling parameter D. It appears that, in the first Brillouin zone, the increase of D leads to the expansion of the width of wave numbers for which bright soliton prevails and to the reduction of the one for which dark solitons occur. Merely, the increase of the transverse coupling parameter extends the domain of existence of bright solitons. In the following, we will be focused on the case where $PQ > 0$ i.e. on the bright soliton solutions of Eq. (12). This solution is given as in Refs. 3, 16, 66 by

$$\psi(X, \tau) = \gamma \text{sech}[\rho(X - V\tau)]\exp i(KX - \Omega\tau). \tag{15}$$

Based on the above equation, the expression of the solution of Eq. (6) can easily be written as follows:

$$x_n \simeq x_0 \text{sech}[\varepsilon\rho(n - v_g t)]\cos(kn - \Omega_0 t), \tag{16}$$

where $\rho = \gamma\sqrt{|\frac{Q}{2P}|}$, $\Omega = \frac{K^2-\rho^2}{2}$, $x_0 = 2\varepsilon\rho\sqrt{|\frac{2P}{Q}|}$ and $\Omega_0 = \omega + 2\varepsilon^2\Omega P$. Equation (16) is a modulated bright pulse signal solution of the network equation (6) whose characteristic parameters, namely the amplitude, the velocity, the inverse width and the frequency are x_0, V, ρ and Ω_0.

The bright soliton solution of Eq. (6) will be used in the next section as initial condition for the full numerical integration of Eq. (1) to investigate the behavior of the solitary wave during its propagation while moving from one line to another.

4. Numerical Experiments

Now, to consolidate the validity of analytical results, let us proceed to study numerically the evolution of the previous bright soliton in the network of Fig. 1. In this

section, we report the results of the numerical experiments performed on the exact discrete equation (1) of the network. We use the Ode45 solver of Matlab with periodic boundary conditions using the following parameters $\gamma = 1$, $\varepsilon = 0.02$ and $C = 4$.

For a given value of wave number k depending on the domain of each soliton (see Fig. 4), we evaluate the angular frequency ω using the dispersion relation of Eq. (8), the nonlinear coefficient Q, the dispersion coefficient P and other soliton's parameters given just after Eq. (16). Similarly, the number of cells for both lines is chosen to be equal to 1001.

For the effectiveness of the investigations, we consider different values of the transverse coupling parameter so as to examine its effect on the progression of the solitary wave from one line to another. For this purpose, let us consider two cases depending on the input signal or initial conditions applying on each line.

- First, as initial condition, we take as the input signal the profile of the bright soliton for the x-line such that

$$x_n(0) \simeq x_0 \text{sech}(\varepsilon \rho n) \cos(kn), \tag{17}$$

and consider that at $t = 0$, y-line is at rest, that is

$$y_n(0) \simeq 0. \tag{18}$$

With zero velocity ($k = 0\,\text{rad/cell}$), we obtain Fig. 5. The case where the transverse coupling parameter is zero ($D = 0$) is depicted on the first line: One can observe the localization of the wave in the x-line while no wave is propagating in the y-line. For the transverse coupling term different from zero (second and third line of Fig. 5), we observe the localization in both x-line and y-line.

The remarkable phenomenon here is the fact that, for a given time, the wave exists in the x-line while there is no wave in the y-line. This is similar to the gain and loss phenomenon observed in the optical waveguide arrays.[67] Despite the fact that only one chain is excited, there is an alternative transfer of energy between both lines. Additionally, what is the behavior of the lattice for the nonzero group velocity? Figure 6 displays the spatiotemporal evolution of the wave for $k = 0.5\,\text{rad/cell}$. It is well seen on the first line of this figure for $D = 0$ that, no wave is propagating in the y-line as expected. For $D = 0.01$ (second line), the energy is transferred from the x-line to the y-line and the gain and loss phenomenon is observed. The same phenomenon is obtained for $D = 0.1$. This is in agreement with the first idea of the construction of the lattice of Fig. 1 by Destyl et al.[57] For a large value of the transverse coupling constant as can be seen in Fig. 7, we observe that, the wave introduced at the origin at $t = 0$ exhibits some nonlinear distortions of the envelope when time grows. Then, the fission of the initial wave occurs with time as shown in that figure.
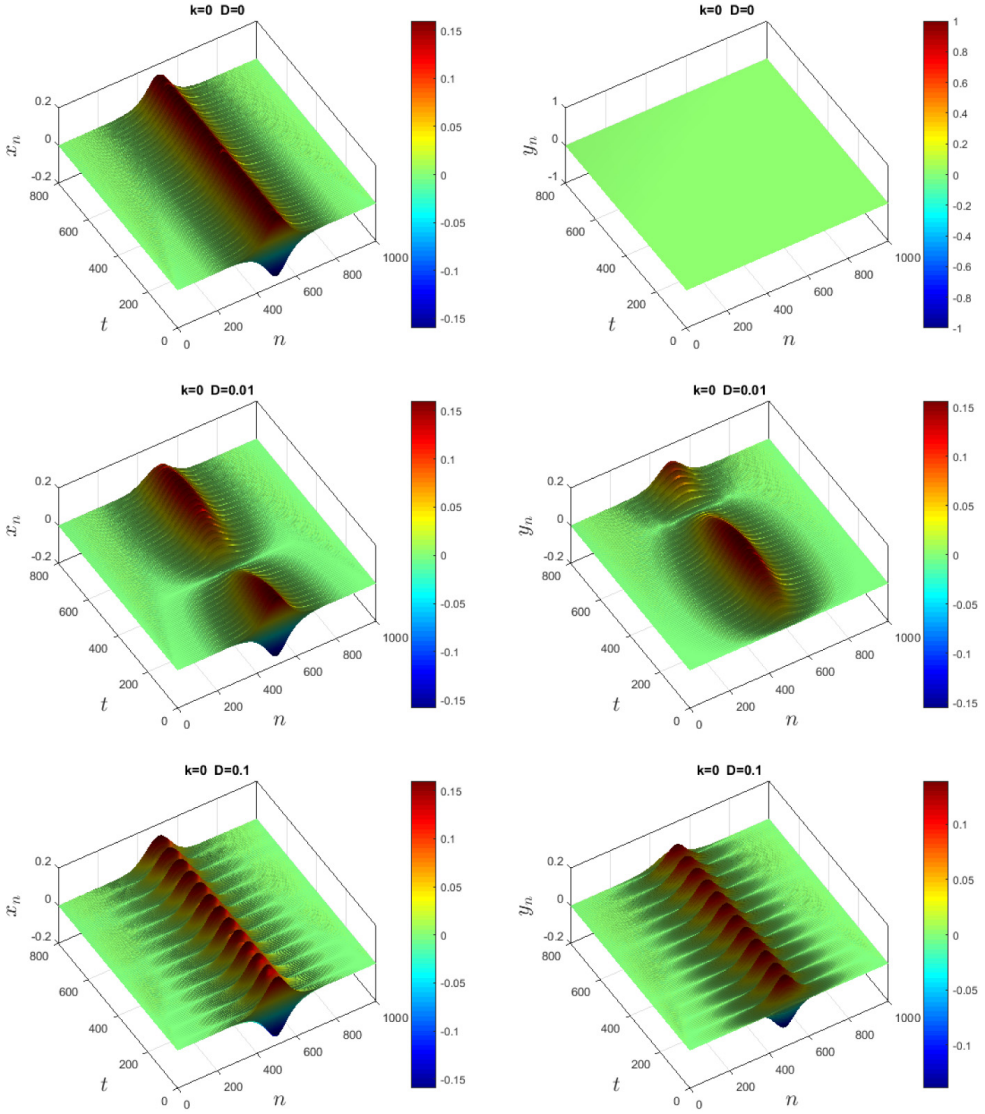
Fig. 5.   (Color online) Space-time evolution plot of angles x_n (left panel) and y_n (right panel) showing the behavior of the bright soliton with zero velocity ($k = 0$) in the network.

- Second, considering the fact that $y_n = -x_n$ (as shown in Sec. 2 i.e. the two lines are out of phase), as initial condition, we take as the input signal the profile of the bright soliton for the x-line such that

$$x_n(0) \simeq x_0 \text{sech}(\varepsilon \rho n) \cos(kn), \tag{19}$$
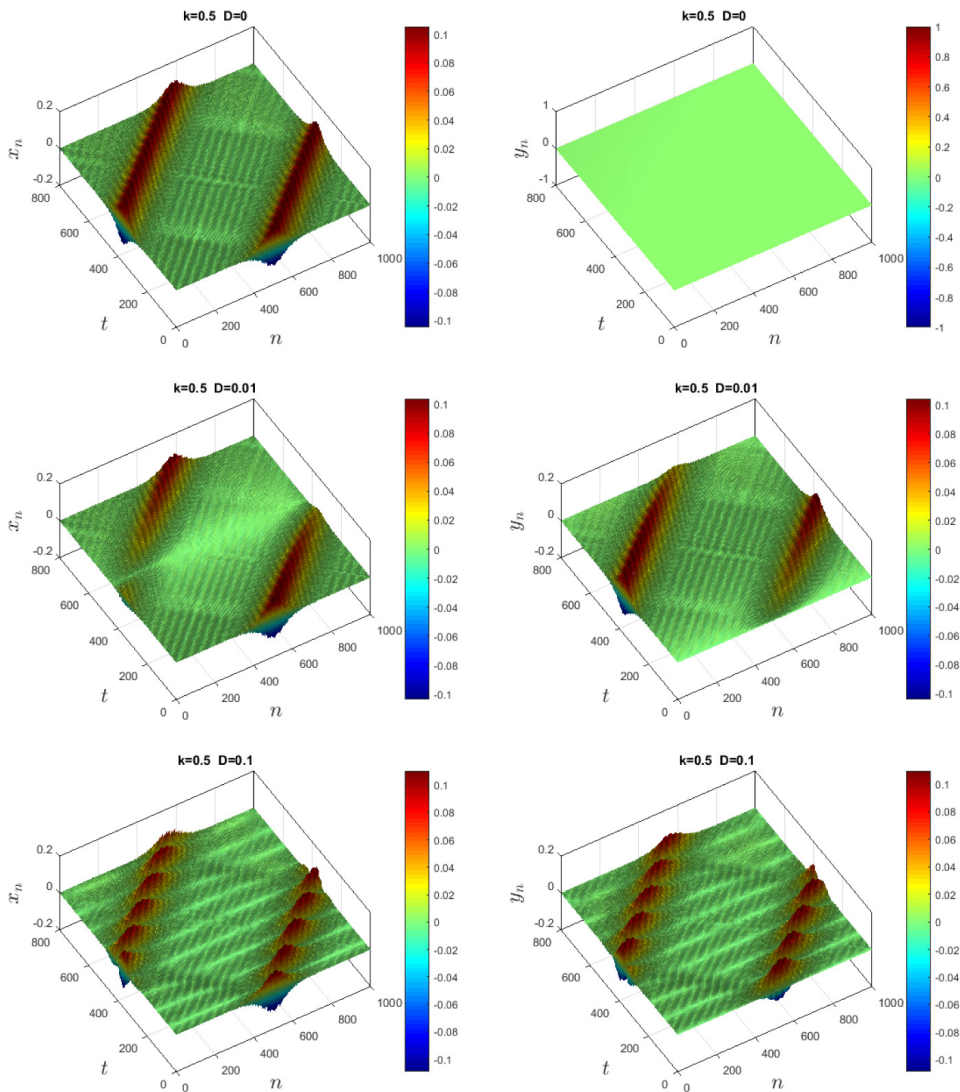
Fig. 6.   (Color online) Space-time evolution plot of angles x_n (left panel) and y_n (right panel) showing the propagation of the bright soliton with nonzero velocity ($k = 0.5$) in the network.

and consider that at $t = 0$, the input signal of the y-line is the opposite of that of x-line, that is

$$y_n(0) \simeq -x_0 \mathrm{sech}(\varepsilon \rho n) \cos(kn). \tag{20}$$

Following the initial conditions of Eqs. (19) and (20), we obtain Fig. 8. We observe the propagation of the wave on the right-hand side. As both chains are excited, the loss in the x-line is compensated by the gain of the y-line and vice versa.
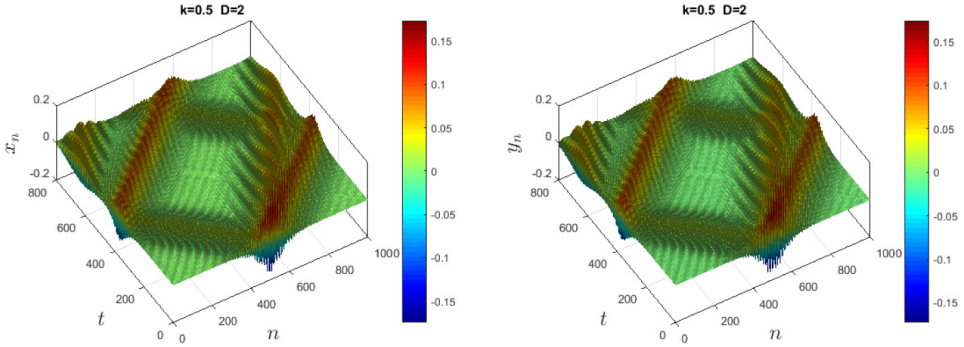
Fig. 7. (Color online) Space-time evolution plot of angles x_n (left panel) and y_n (right panel) showing the propagation of the bright soliton in the network with large transverse coupling parameter.
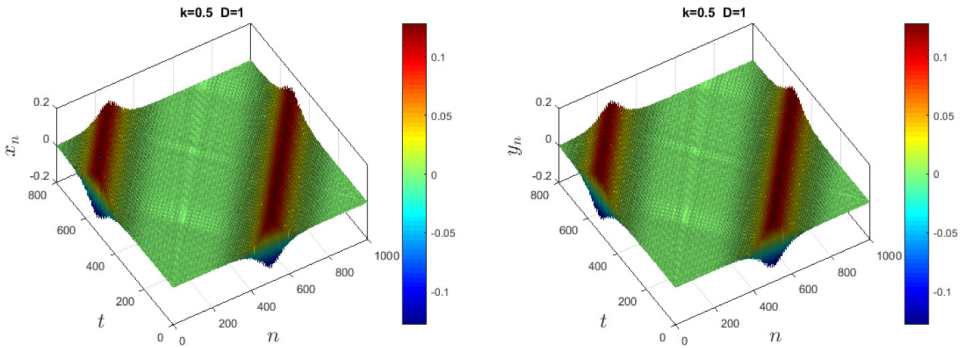

Fig. 8. (Color online) Space-time evolution plot of angles x_n (left panel) and y_n (right panel) showing the propagation of the bright soliton in the network with the initial conditions given by Eqs. (19) and (20).

The compensation of the loss by the gain in both chains induces the coherency of the waves during its propagation.

5. Conclusion

In this work, we were called upon to study wave propagation in a nonlinear discrete coupled pairs of pendulum chains connected to the nearest neighbors in the longitudinal and transverse directions. We derived from the Euler–Lagrange's equation the simultaneous equation governing the dynamics of the model. We obtained the corresponding linear dispersion law describing the small amplitude waves of the network. We allowed our model to exhibit two modes of propagation of waves namely; the fast- and the slow-mode. The slow-mode was equivalent to the case of a single chain whereas the fast one was not. This lets our attention to be focused only on the fast-mode. Moreover, by considering the fact that the two chains of the model

are proportional, we obtained a single equation which obeyed the linear dispersion relation of the fast mode.

Afterwards, applying the rotating wave approximation method on the obtained single equation, we have shown that the generalized coordinate of the system is governed by a nonlinear Schrödinger equation. We deduced that, the obtained NLS equation supports bright and dark or hole solitons as solutions. Due to the fact that the transverse coupling parameter had the same effects on each soliton, we focused our attention only on bright soliton. We used the obtained bright soliton as initial conditions for numerical investigation to follow the progression of the generated waves in the network from one line to the other when varying the transverse coupling parameter.

From the interesting results obtained in this work, we saw clearly that, the transverse coupling plays a significant role in the model of the nonlinear coupled pendulum lines and could be used to generate the gain and loss phenomenon. It is important to notice that, our study can be useful to the better understanding of wave propagation in discrete multicomponent systems. Also, this work opens up the possibility of additional mathematical analysis on discrete simultaneous equation describing the dynamics of discrete multicomponent systems.

ORCID

A. Kamdoum Kuitche ⬡ https://orcid.org/0009-0007-5504-1853

A. B. Togueu Motcheyo ⬡ https://orcid.org/0000-0002-6918-9281

Zakari Yaou ⬡ https://orcid.org/0009-0000-2089-9234

Thomas Kanaa ⬡ https://orcid.org/0009-0009-7058-4607

C. Tchawoua ⬡ https://orcid.org/0009-0006-5375-6452

References

1. N. J. Zabusky and M. D. Kruskal, *Phys. Rev. Lett.* **15** (1965) 240.
2. E. Fermi, J. Pasta and S. Ulam, *Nonlinear Wave Motion*, Lectures in Applied Mathematics, Vol. 15, ed. A. C. Newell (American Mathematical Society, Providence, 1974).
3. A. B. Togueu Motcheyo, T. Kanaa and S. Ndjakomo Essiane, *J. Superconduct. Novel Magn.* 34 (2021) 2619.
4. J. B. Gonpe Tafo, F. Kenmogne, A. Mando Kongne, R. Eno and D. Yemélé, *Results Phys.* **50** (2023) 106532.
5. A. Yokus, *Mod. Phys. Lett. B* **35** (2021) 32.
6. G. P. Veldes, J. Cuevas, P. G. Kevrekidis and D. J. Frantzeskakis, *Phys. Rev. E* **88** (2013) 013203.
7. A. B. Togueu Motcheyo, J. D. Tchinang Tchameu, S. I. Fewo, C. Tchawoua and T. C. Kofane, *Commun. Nonlinear Sci. Numer. Simul.* **17** (2017) 8.
8. A. B. Togueu Motcheyo and J. E. Macías-Díaz, *Waves Random Complex Media* **32**(6) (2022) 2718.
9. G. R. Deffo, S. B. Yamgoué and F. B. Pelap, *Phys. Rev. E* **98** (2018) 062201.
10. P. A. Simo Motcheyo, R. L. Woulache, E. Tchomgo Felenou and T. C. Kofane, *Phys. Lett. A* **483** (2023) 129047.
11. S. El-Ganaini and H. Kumar, *Math. Methods Appl. Sci.* **46**(2) (2023) 2746.

12. S. M. Ngounou and F. B. Pelap, *Chin. Phys. B* **30**(6) (2021) 060504.

13. N. Raza and Z. A. Alhussain, *Mod. Phys. Lett. B* **35**(33) (2021) 2150498.

14. A. S. Tchakoutio Nguetcho, G. M. Nkeumaleu and J. M. Bilbault, *Appl. Math. Comput.* **403** (2021) 126136.

15. A. V. Porubov, *Int. J. Non-Linear Mech.* **137** (2021) 103788.

16. A. B. Togueu Motcheyo, E. Nkendji Kenkeu, J. Djako and C. Tchawoua, *Phys. Plasmas* **25** (2018) 123701.

17. E. Nkendji Kenkeu, A. B. Togueu Motcheyo, T. Kanaa and C. Tchawoua, *Phys. Plasmas* **29** (2022) 043702.

18. S. Sabari, O. T. Lekeufack, S. B. Yamgoue, R. Tamilthiruvalluvar and R. Radha, *Int J. Theor. Phys.* **61** (2022) 222.

19. Z. I. Djoufack, A. Kenfack-Jiotsa and J.-P. Nguenang, *Int. J. Mod. Phys. B* **31**(20) (2017) 1750140.

20. M. Kimura and T. Hikihara, *Phys. Lett. A* **373**(14) (2009) 1257.

21. M. Kimura and T. Hikihara, *Procedia IUTAM* **5** (2012) 288.

22. M. Kimura, Y. Matsushita and T. Hikihara, *Phys. Lett. A* **380** (2016) 2823.

23. C. J. McKinstrie and R. Bingham, *Phys. Fluids B: Plasma Phys.* **1** (1989) 230.

24. C. L. Gninzanlong, F. T. Ndjomatchoua and C. Tchawoua, *Phys. Rev. E* **102** (2020) 052212.

25. J. D. Tchinang Tchameu, C. Tchawoua and A. B. Togueu Motcheyo, *Wave Motion* **65** (2016) 112–118.

26. A. B. Aceves, G. Fibich and B. Ilan, *Physica D* **189** (2004) 277.

27. M. Alidou, A. Kenfack-Jiotsa and T. C. Kofane, *Chaos, Solitons Fractals* **27** (2006) 914.

28. R. Nath, P. Pedri and L. Santos, *Phys. Rev. Lett.* **101** (2008) 210402.

29. H. N. Chan and K. W. Chow, *Commun. Nonlinear Sci. Numer. Simul.* **18** (2018) 30171-0.

30. L. Ouahid, M. A. Abdou and S. Kumar, *Mod. Phys. Lett. B* **36**(7) (2022) 2150603.

31. E. Lorin, M. Lytova, A. Memarian and A. D. Bandrauk, *J. Phys. A: Math. Theor.* **48** (2015) 105201.

32. J. F. R. Archilla, S. M. M. Coelho, F. D. Auret, V. I. Dubinkoc and V. Hizhnyakov, *Physica D* **297** (2015) 56.

33. J. D. Tchinang Tchameu, C. Tchawoua and A. B. Togueu Motcheyo, *Phys. Lett. A* **379** (2015) 2984.

34. S. Issa, C. B. Tabi, H. P. Ekobena and T. C. Kofane, *Int. J. Mod. Phys. B* **29** (2015) 1550244.

35. N. Oma Nfor, P. Guemkam Ghomsi and F. M. Moukam Kakmeni, *Chin. Phys. B* **32** (2023) 020504.

36. Y. Hanif and U. Saleem, *Mod. Phys. Lett. B* **34**(5) (2020) 2050070.

37. E. H. M. Zahran and A. Bekir, *Mod. Phys. Lett. B* **37**(13) (2023) 2350027.

38. J. Wu, R. Keolian and I. Rudnick, *Phys. Rev. Lett.* **52** (1984) 1421.

39. B. Denardo, W. Wright, S. Putterman and A. Larraza, *Phys. Rev. Lett.* **64** (1990) 1518.

40. X. Wang and R. Wei, *Phys. Rev. Lett.* **78** (1997) 2744.

41. E. Kenig, B. A. Malomed, M. Cross and R. Ifshitz, *Phys. Rev. E* **80** (2009) 046202.

42. F. Palmero, J. Han, L. Q. English, T. J. Alexander and P. G. Kevrekidis, *Phys. Lett. A* **380** (2016) 402.

43. L. M. Floria and J. J. Mazo, *Adv. Phys.* **45** (1996) 505.

44. O. M. Braun and Y. Kivshar, *The Frenkel-Kontorova Model: Concepts, Methods, and Applications* (Springer-Verlag, Berlin, Heidelberg, 2004).

45. C. Vasanthi and M. Latha, *Commun. Nonlinear Sci. Numer. Simul.* **28** (2015) 109.

46. I. Barashenkov, M. Bogdan and V. Korobov, *EPL* **15** (1991) 113.

47. A. Jallouli, N. Kacem and N. Bouhaddi, *Commun. Nonlinear Sci. Numer. Simul.* **42** (2015) 1.

48. N. V. Alexeeva and I. V. Barashenkov, *Phys. Rev. Lett.* **14** (2017) 48.
49. H. Susanto, Q. E. Hoq and P. G. Kevrekidis, *Phys. Rev. E* **74** (2006) 067601.
50. M. Syafwan, H. Susanto and S. M. Cox, *Phys. Rev. E* **81** (2010) 026207.
51. J. Cuevas, L. Q. English, P. G. Kevrekidis and M. Anderson, *Phys. Rev. Lett.* **102** (2009) 224101.
52. N. V. Alexeeva, I. V. Barashenkov, A. A. Sukhorukov and Y. S. Kivshar, *Phys. Rev. A* **85** (2012) 063837.
53. I. V. Barashenkov, S. V. Suchkov, A. A. Sukhorukov, S. V. Dmitriev and Y. S. Kivshar, *Phys. Rev. A* **86** (2012) 053809.
54. N. V. Alexeeva, I. V. Barashenkov and Y. S. Kivshar, *New J. Phys.* **19** (2017) 113032.
55. A. Chernyavsky and D. E. Pelinovsky, *Symmetry* **8**(7) (2016) 59, https://doi.org/10.3390/sym8070059.
56. A. Chernyavsky and D. E. Pelinovsky, *J. Phys. A: Math. Theor.* **49** (2016) 475201.
57. E. Destyl, S. P. Nuiro, D. E. Pelinovsky and P. Poullet, *Phys. Lett. A* **381** (2017) 3884.
58. A. Kamdoum Kuitche, A. B. Togueu Motcheyo, T. Kanaa and C. Tchawoua, *Chaos, Solitons Fractals* **160** (2022) 112196.
59. A. Kamdoum Kuitche, A. B. Togueu Motcheyo, T. Kanaa and C. Tchawoua, *Eur. Phys. J. Plus* **138** (2023) 142.
60. B. Z. Essimbi, L. Ambassa and T. C. Kofane, *Physica D* **106** (1997) 207.
61. B. Z. Essimbi, T. C. Kofane and J. M. Ngundam, *Phys. Scr.* **67** (2003) 157.
62. A. Kenfack-Jiotsa and E. Tala-Tebue, *J. Phys. Soc. Jpn.* **80** (2011) 034003.
63. K. Narahara, *Wave Motion* **51** (2015) 935.
64. K. Narahara, *Wave Motion* **58** (2015) 13.
65. F. Geniet and J. Leon, *Phys. Rev. Lett.* **89** (2002) 134102.
66. G. P. Veldes, J. Cuevas, P. G. Kevrekidis and D. J. Frantzeskakis, *Phys. Rev. E* **83** (2011) 046608.
67. R. El-Ganainy, K. G. Makris, M. Khajavikhan, Z. H. Musslimani, S. Rotter and D. N. Christodoulides, *Nat. Phys.* **14** (2018) 11.